SYNTHETIC ANTIGEN-PRESENTING VESICLES FOR SELECTIVE IMMUNOMODULATION

Thesis by

Blade A. Olson

In Partial Fulfillment of the Requirements for

the degree of

Doctor of Philosophy

CALIFORNIA INSTITUTE OF TECHNOLOGY

Pasadena, California

2026

Defended August 19th, 2025

Blade A. Olson
ORCID: 0000-0002-1526-1399

ACKNOWLEDGEMENTS

Thank you to my PhD advisors, Dr. Stephen L. (Steve) Mayo and Dr. Richard M. Murray, for their advice, leniency, mentorship, patience, and pragmatism. Whether we were discussing the co-advisement relationship or picking my PhD project, I've never had meetings be so productive in such a short amount of time—and I always walked out of the meetings feeling better than when I walked in! Thank you for giving me a home and for letting me take a shot at being a scientist.

Thank you to Kathryn "Beth" Huey-Tubman, Priyanthi "Pri" Gnanapragasam, and Dr. Magnus Hoffmann for graciously training me and bestowing the core wet lab skills that enabled this PhD thesis. Magnus, thank you for letting me shadow you, for your advice, and for sharing your personal journey with me. Magnus' dogged pursuit of experimental results was a major inspiration for my own work ethic that has essentially resulted in me being still unmarried while I put the finishing touches on this PhD thesis. I'll never forget his words as I was walking home from Caltech one afternoon to eat a late lunch: "Blade!" Magnus yelled from across the street, pointing back to Caltech's campus, "Where are you going? Success is *that* way!"

Lastly, I would like to thank my family: my brother Logan, who remained congratulatory and excited about my scientific progress despite his own runaway career successes, my dad Ted, who must have passed down his disposition for engineering to me and continues to mentor me as my spiritual advisor, and most especially my mom Jo Marie, a PhD scientist herself who has been a tremendous source of emotional and intellectual guidance leading up to and during my time at Caltech. I called my mom almost every day of my PhD, and on the worst days, when my experimental results were just awful, she had this incredible ability to talk me into a great mood—thanks, mom!

ABSTRACT

The rapid advancement of generative artificial intelligence has enabled unprecedented progress for the field of computational protein design. A forthcoming challenge for generative protein design algorithms is the immunocompatibility of these de novo designed molecules with organism physiology, namely humans. A separate, but related, aspirational goal for synthetic biology is to perform cellular reprogramming *in vivo* so that cell-based therapies and biologics are generated endogenously by patients rather than being externally manufactured or expanded before delivery, as is the case with biologics, T cell therapies, and stem cell therapies; again, a major hurdle for the *in vivo* production of these therapies and *in vivo* cellular reprogramming is immunogenicity.

To address these challenges, we first demonstrate a cell-like, cell-free approach for *in vivo* cellular reprogramming with the induced release of pMHCI and pMHCII-loaded synthetic antigen-presenting vesicles that are secreted from non-immune cells by DNA and mRNA transfection to facilitate the selective expansion or silencing of immune responses. Next, we show initial results for the use of human tonsil organoids as a quantitative assay for adenoviral vector immunogenicity, enabling future directed evolution approaches for immunogenicity reduction as well as generation of an immunogenicity dataset to tailor modern computational protein design algorithms for human immunocompatibility. Together, these projects represent complementary methods to control protein immunogenicity, either through rationally engineered or directedly evolved modifications identified by physiologically-relevant *in vitro* models, or with an administered mRNA therapeutic that selectively modifies the immune response to a protein that cannot be computationally redesigned.

PUBLISHED CONTENT AND CONTRIBUTIONS

Chapter 2:

Olson, B. A., Huey-Tubman, K. E., Mao, Z., Hoffmann, M. A. G., Murray, R. M., & Mayo, S. L. (2025). Recruiting ESCRT to single-chain heterotrimer peptide-MHCI releases antigen-presenting vesicles that stimulate T cells selectively. *bioRxiv*, 2025.2001.2017.633600. https://doi.org/10.1101/2025.01.17.633600

B.A.O. designed experiments, generated reagents, performed experiments, wrote the first draft of the manuscript, and participated in the editing of the manuscript.

Chapter 3:

Olson, B. A., Mellody, M., Soemardy, C., Mao, Z., Mei, A., Lippert, K., Hoffmann, M. A. G., Carlo, D. D., & Mayo, S. L. (2025). Functionalizing hydrogel nanovials with vesicles mimicking antigen-presenting vesicles and cancer exosomes improves T cell capture and activation. *bioRxiv*, 2025.2006.2024.661128. https://doi.org/10.1101/2025.06.24.661128

B.A.O. designed experiments, generated reagents, performed experiments, wrote the first draft of the manuscript, and participated in the editing of the manuscript.

TABLE OF CONTENTS

Chapter 1

INTRODUCTION

1.1 Overview of cellular immunity

Cellular immunity requires the involvement of peptide, major histocompatibility complex (MHC), and T cell receptors (TCR). All nucleated cells of the human body present intracellular proteins on their surface as digested 9-11mer peptides bound to class I major histocompatibility complexes (MHCI); when a peptide is bound to MHCI, the complex is referred to as peptide:MHCI (pMHCI), and the T cell receptors (TCRs) of CD8+ T cells recognize the presence of infection or cancer if the binding pocket of the T cell's TCR stably binds to the epitope presented by pMHCI, which typically occurs when the peptide presented by MHCI is of pathologic origin.[1] Professional antigen-presenting cells (APCs), such as dendritic cells, are specialized cells of the immune system that are efficient at presenting antigens from a foreign pathogen, virus-infected cell, or cancer cell along with immunostimulatory molecules to initiate a focused downstream adaptive immune response that will eliminate a target containing the presented antigen.[1,2] APCs internalize antigens, process the antigen into peptide fragments, and then display the digested peptides on their membrane as pMHCI or, unique to APCs, as peptide bound to class II major histocompatibility complex (pMHCII) which binds to TCRs on CD4+ T cells.[1]

T cells initially recognize and interact with pMHC on the membrane of an APC. However, to further activate the T cell, professional antigen-presenting cells need to provide two more additional signals: a costimulatory signal from a membrane protein such as CD80/CD86 and a differentiation signal such as IL-12. When a T cell has received all three signals from a professional antigen-presenting cell, the T cell will differentiate into an immune effector cell capable of eliminating targets presenting the antigenic peptide presented by pMHCI.[1,2] However, in the absence of these costimulatory signals and in relatively sterile environments devoid of molecular patterns of cellular lysis, antigen recognition by pMHC-TCR

interactions induces a nonresponsive (anergic) state in lymphocytes that supports peripheral self-tolerance of autoantigens.[1]

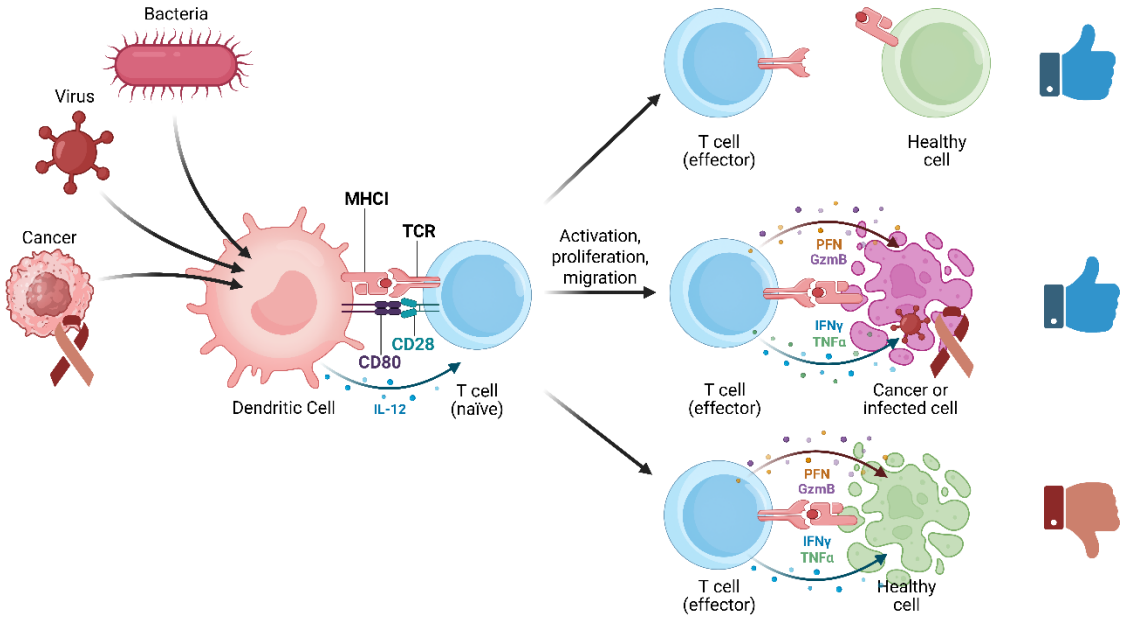

Figure 1.1 Professional antigen-presenting cells activate T cells

Professional antigen-presenting cells, such as dendritic cells, engulf, process, and subsequently present bacterial, viral, or cancer-relevant peptide-MHC complexes on their cell surface to bind the specific, cognate T cell receptor (TCR) on T cells. TCR binding by pMHC represents the first of three signals needed for T cell activation and proliferation: (1) peptide-MHC binding to TCR, (2) a costimulatory signal from a membrane protein such as CD80/CD86 binding to CD28, and (3) a differentiation signal such as IL-12. Activated, cytotoxic T cells are primed to attack cancerous or virally infected T cells and spare healthy cells presenting pMHC for which the T cell does not have a relevant TCR. However, in pathological scenarios, T cells will bind pMHC presenting endogenous, autogenic peptides presented on healthy cells, initiating the destruction of healthy cells and tissue as seen in cell-mediated autoimmune diseases. *MHCI: major histocompatibility complex I, TCR: T cell receptor, IL-12: interleukin-12, PFN: perforin, GzmB: granzyme B, IFNγ: interferon gamma, TNFα: Tumor Necrosis Factor alpha*

Self-tolerance is primarily maintained by four mechanisms: peripheral deletion or inactivation of autoreactive thymic T-cell or bone marrow-derived B-escapees as was just described; central deletion of high-avidity autoreactive T- or B-cell clones; export of mature regulatory T (Treg) cells from the thymus that are developed in response to stimulation by autoantigen that is too weak to cause deletion, but above the threshold for positive selection; and de novo generation of induced Treg or regulatory B (Breg) cells in the periphery when naïve self-reactive cells recognize their cognate antigen in the presence of TGF-B. Treg cells can suppress autoreactive lymphocytes that recognize a variety of different self-antigens, as long as the antigens are from the same tissue or are presented by the same APC.[1] Traditionally, Treg cells were largely considered a subset of CD4+ T cells, but recent advancements have recognized the significance of CD8+ Treg cells in regulating autogenic self-tolerance.[3,4] As a result, APCs, or more specifically pMHCI and pMHCII, are capable of selectively inducing regulatory T cells and highly specific tolerization of autoantigens.

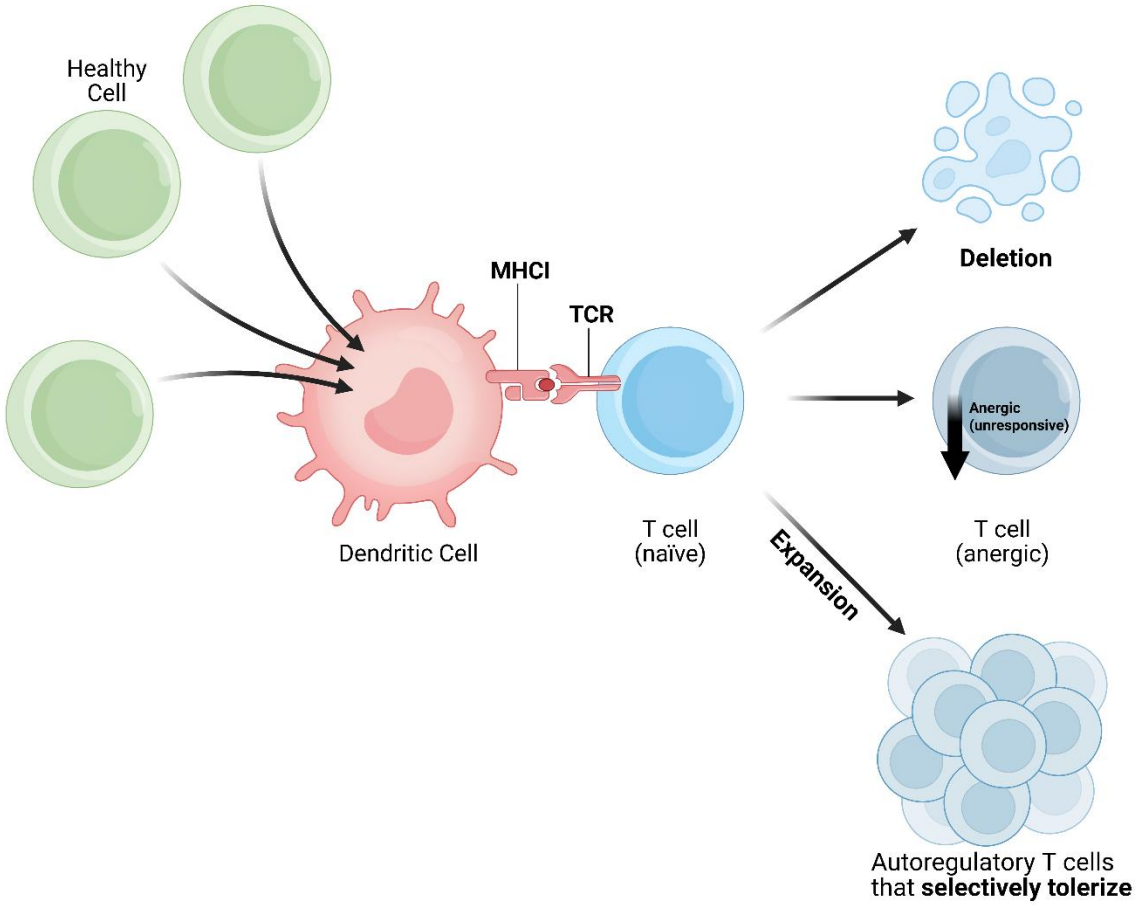

Figure 1.2 Professional antigen-presenting cells help maintain self-tolerance

Professional antigen-presenting cells, such as dendritic cells, can engulf healthy cells and present the digested proteins as peptides on MHC to the TCRs of T cells without costimulatory signals. The lack of costimulation during peptide-MHC presentation causes potentially autoinflammatory T cells to become anergic, perform apoptosis, or differentiate into autoregulatory T cells that selectively tolerize the body to these self-antigens. *MHCI: major histocompatibility complex I, TCR: T cell receptor*

Because of their critical ability to both initiate a protective immune response against pathogens and cancer as well as induce self-tolerance to commensal microbiota and autoantigens, APCs are intensely studied for their role as key linchpins in activating or dampening the immune system. Dendritic cell-based vaccination for cancer and infectious disease has seen considerable development over recent decades in parallel with the more

widespread attention chimeric T-cells have seen for immunotherapy.[5-8] Even before the crystal structure of the human MHCI was resolved, researchers had tried to recreate the functionality of antigen-presenting cells by incorporating HLA-A and HLA-B pMHCI antigens into phospholipid vesicles to induce cytotoxic T lymphocytes.[9]

Research teams have since ventured to engineer more complex versions of these vesicles that can direct the immune system to attack a target of interest, deeming them "artificial antigen-presenting cells" (aAPCs).[10] Initial rudimentary aAPCs were designed by conjugating MHC together as tetramers using biotin and streptavidin, which is still used today to capture and identify T cells with high affinity for a specific pMHC.[11,12] Later designs for aAPCs included mammalian cells conjugated with immunostimulatory molecules,[13-17] polymer nanoparticles conjugated with APC effector proteins,[18-23] nanoparticles coated with dendritic cell membranes via extrusion or sonication,[24,25] or engineered extracellular blebs produced by the exosome pathway[26-30]. While the direct manipulation of dendritic cells through gene therapy or targeted antigen delivery has shown promising results, the generation of sufficient autologous DCs to prepare exosomes or artificial APCs from dendritic cell lysates remains a barrier to the broad utility of DC-based therapies as dendritic cell copy numbers in blood are relatively low;[31] what's more, artificial APC publications have previously cited better T cell activation from their nanoparticle artificial APCs than from actual dendritic cells, possibly due in part to the low copy number and activation potential of the autologous dendritic cells and the added benefit afforded by 'cross-dressing' of nearby cells by the nano-sized aAPCs.[16,32] At the nanometer scale, these synthetic artificial APCs, either intentionally or not, are recreations of the immunomodulatory extracellular vesicles that already exist in the human body: antigen-presenting vesicles.

1.2 Antigen-presenting vesicles and the ESCRT and ALIX-Binding Region

After decades of what was commonly identifed as cellular "debris", the designation 'extracellular vesicles' (EVs) was suggested in 2011 as a collective term for the lipid bilayer-enclosed, cell-derived nanoparticles that were being isolated from biological fluids.[33] EVs are produced and secreted by all cell types in all animal species, are present in all human

body fluids, and seem to be involved in nearly all biological processes, including adaptive immunity.[34] Almost thirty years ago, Raposo, G. et al. first reported on the release of B cell-derived extracellular vesicles (EVs) with functional peptide:MHC (pMHC) complexes on their surface[35] and subsequent publications have elaborated on the immunomodulatory potential of these antigen-presenting vesicles (APVs).[33] Typically ranging between 50-150nm in diameter, APVs can present pMHC directly to T cells; APVs can attach and become concentrated on the surface of dendritic cells for efficient immune synapse formation; APVs can be endocytosed by APCs and their presenting peptides re-presented on the APC surface; and APVs can act as synaptic vesicles that transfer between migratory dendritic cells and conventional dendritic cells in lymph nodes.[33]

Because of their biocompatibility,[36,37] prolonged blood circulation,[38] multivalency,[39] protective encapsulation of their contents,[40,41] immunomodulatory potential, and ubiquity in biological fluids, cell-secreted EVs and APVs have emerged as promising therapeutic vehicles.[42,43] Despite their many advantages, however, the application of EVs for immunotherapeutic contexts has been limited because of difficulties scaling manufacturing,[44] the heterogeneity of the harvested exosomal population,[45] and cell-targeting that is often defined by the vesicle's original cell source,[46] which is typically low in number resulting in low EV yield.[40] *In vivo* production of APVs from a patient's own somatic cells would address the problems of copy number and workflow complexity stated above. "Immunosomes" generated from virus-like particles were demonstrated nearly two decades ago by fusing lipid-raft targeting sequences to the immune-activating membrane proteins of professional APCs to generate antigen-presenting virus-like particles.[32] These authors surmised that the HIV gag/pol proteins naturally assembled at lipid rafts and would carry the lipid-raft-associated pMHC along with the virus-like particle as it buds from the cell. However, expressing viral coat proteins to induce budding would unavoidably lead to inflammatory immune activation in patients, and the expression of multiple structural proteins would be difficult to encode in an mRNA-LNP therapeutic for downstream *in vivo* immune cell reprogramming.

In 2023, Dr. Magnus Hoffmann published his work pioneering the use of an ESCRT- and ALIX-binding region (EABR) sequence, taken from the human proteome, to generate enveloped virus-like particles (eVLPs) *in vivo* by mRNA-LNP vaccination.[47] Appending an endosomal sorting complex required for transport (ESCRT)- and ALG-2-interacting protein X (ALIX)- binding region (EABR) to the cytoplasmic tail of membrane proteins directly recruits the ESCRT machinery and induces the release of vesicles displaying the EABR-tagged protein. This EABR sequence was subsequently found to be universally applicable to nearly every membrane protein in which it was tested, and thus could be used to produce synthetic EABR-mediated antigen-presenting vesicles if the EABR sequence was appended to MHC. pMHCI and pMHCII, however, are complexes, and thus export of a complete pMHC on the surface of EABR-mediated antigen-presenting vesicles might benefit from structural linkers that guarantee pMHC complex formation before EABR-mediated export from the cell.

1.3 Major Histocompatibility Complex

1.3.1 MHCI

MHCI is composed of two protein subunits, an α "heavy chain" and β chain referred to as "β_2-Microglobulin" (β2m), which bind an 9-11-mer presenting peptide to form the complete pMHCI complex. MHC class I's β chain (β2m) is conserved throughout the human species and has no direct interaction with the presenting peptide. The α heavy chain, typically referred to by its class I allele (e.g. human leukocyte antigen-A*02:01 or HLA-A*0201 or, more simply, HLA-A2), is the sole determinant of the peptide binding groove. Once synthesized and present in the endoplasmic reticulum, MHCI's α chain is stabilized by calnexin until β2m binds. Calnexin is released, and calreticulin and ERp57 bind to help stabilize the MHCI α:β heterodimer for Tapasin. Tapasin forms a bridge between MHCI and TAP, allowing for peptides to be loaded into the MHC's peptide-binding groove. Peptide editing and pMHCI quality control can occur throughout this process: Tapasin ensures that the groove remains open until a peptide of sufficient affinity is bound, and glucosidase II (GlsII) and TAPBPR ensure proper folding of the pMHCI complex before the stabilized complex is transported to the cell surface.[1]

This intricate series of steps can be bypassed, however, when the pMHCI complex is expressed as a single, uninterrupted amino acid chain termed a "single-chain heterotrimer" or "single-chain trimer" (SCT) pMHCI.[48] In work published in 2023,[49] William Chour in the lab of James Heath extensively characterized the thermostability of rationally-engineered, highly-stable variants of SCT pMHCI as well as their binding affinity for their respective TCRs. Covalent linkage of the pMHCI complex subunits into a SCT dramatically improves the diffusion kinetics required for complex formation, and some SCT variants have even been shown to circumvent the cell's quality control mechanisms during transport to the cell surface.[50] As a result, these SCT variants expedite pMHCI complex formation, even when the presenting peptide has poor binding efficiency to MHCI, and could thus enable the efficient production of APVs harboring therapeutically-relevant pMHCI.

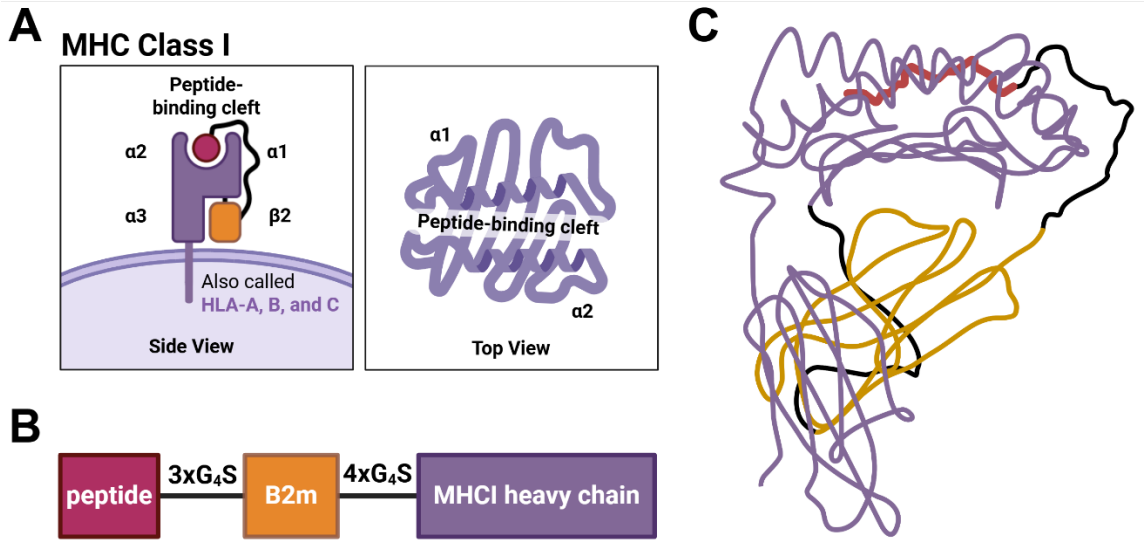

Figure 1.2 Single-chain heterotrimer pMHCI

Single-chain heterotrimer (SCT) peptide-MHCI is composed of an α "heavy chain" and a β chain, referred to as "β2-Microglobulin" (β2m), which bind an 9-11-mer presenting peptide to form the complete pMHCI complex. The presenting peptide is connected to the N-terminus of β2m by a glycine-serine linker, and the C-terminus of β2m is connected to the N-terminus of the α "heavy chain" by a second glycine-serine linker.

(A) Cartoon schematic diagram depicting a side view (left) and top view (right) of the peptide-binding cleft of SCT pMHCI

(B) Sequence map describing the connection between peptide, β2m, and the α "heavy chain" using glycine-serine linkers.

(C) Cartoon ribbon diagram of a side-view of SCT pMHCI drawn using the structure provided by Mitaksov et al.[51]

1.3.2 MHCII

Similar to MHCI, MHCII is composed of two protein subunits, an α chain and β chain, which together bind and present peptides that are typically between 13-17 amino acids, though shorter or longer lengths are not uncommon. Unlike MHCI, though, both the α chain and β chain of MHCII are involved in forming the peptide binding groove. The MHCII α:β heterodimer is initially synthesized and assembled in mammalian cells as part of a nine-chain complex of three α chains, three β chains, and three "invariant" chains (li) that are stabilized by calnexin. Once this complex is formed, calnexin releases the stable nine-chain complex as it departs the endoplasmic reticulum toward acidified endosomal vesicles. The MHCII complex is retained for 2-4 hours in endosomal vesicles while the li chain is proteolytically cleaved to generate a CLIP:α:β complex. HLA-DM, a complex similar to the MHCII α:β heterodimer, binds to and stabilizes the CLIP:α:β complex to catalyze the release of CLIP and the binding of antigenic peptides. Peptides rapidly bind to and release from this open α:β MHCII heterodimer, but only high-affinity peptides can induce HLA-DM dissociation from pMHCII to generate the final pMHCII complex that will traffic to the cell surface.[1] Similar to MHCI, SCT variants of pMHCII, such as those designed by Thayer et al.,[52] have previously been explored to circumvent this lengthy process and increase the stability of low-affinity presenting peptides.[48]

1.4 Adeno-Associated Viruses

Cell-based therapies would naturally seem to be the best approach for modulating cellular immunity, but adoptive cell therapies are both expensive[53] to manufacture and difficult to control,[54] leading to a growing list of complicated receptors that bioengineers have designed

to shepherd cell therapies away from healthy cells and to include "kill-switches" to shut down lethal, unpredictable adverse events that are still occurring in clinical trial and therapeutic settings.[55] On the other end of the therapeutic spectrum, soluble protein biologics have already been deployed in clinical settings as immunomodulators[56-59], but previous work has demonstrated the importance of molecular avidity and the presence of a fluid lipid membrane on membrane receptor clustering that is critical for the formation of an "immunological synapse" and immune cell activation.[60] In this context, EVs and EV-forming sequences encoded by relatively short-acting mRNA-LNP therapies may be especially relevant as a form of cell-free, cell-like immunotherapy that improves upon the potency of soluble biologics and the safety of adoptive cell therapies. However, if a long-term form of immunotherapy is required, *in vivo* cellular programming may require the application of gene therapy vectors such as AAVs.

Adeno-associated virus (AAV) is a non-enveloped ssDNA parvovirus that transduces both dividing and non-dividing cells, but doesn't integrate into the host genome. Rather, the genes flanked by inverted terminal repeats (ITRs) encoded within an AAV form concatemers that persist in the nucleus of transduced cells,[61] resulting in stable long-term gene expression without integration in host DNA. The virus is not associated with disease in humans and is replication-deficient.[62] These characteristics make AAVs an ideal delivery vehicle for gene therapy applications. To date, 11 wild-type AAV serotypes have been identified, each with distinct tropism for specific tissue and organs.[63] The different serotypes arise from variations in the virus capsid, which is made up of three structural proteins. Recently, researchers aiming to capitalize on this feature have shown that using directed evolution and other methods to engineer the viral capsid can produce more specific tropism for desired target tissue.[64-67]

One of the most significant obstacles for the clinical translation of AAV therapy is the immune response against the viral capsid and the delivered transgene. Due to prior exposure to wild-type AAVs, many individuals possess pre-existing adaptive immunity, characterized by neutralizing antibodies (NAbs) and T cells against AAV serotypes. This can lead to the

loss of transgene expression or the elimination of transduced cells, severely undermining clinical efficacy and preventing re-administration. The prevalence of pre-existing NAbs varies between AAV serotypes, with estimates ranging from 34.8% for anti-AAV5 to as high as 74% for anti-AAV2, the current most commonly used variant in clinical applications.[68,69] In addition to hindering therapeutic efficacy, immune response from the host triggered by the viral capsid can result in immune-mediated toxicities, most commonly hepatotoxicity and thrombotic microangiopathy, which presents a significant safety concern for patients. While most patients respond to steroid therapy, there have been a few cases of fatal immune-mediated adverse events occurring post-AAV-administration.[70,71]

Like any therapeutic that leads to anti-drug antibodies (ADAs), broadly acting immunosuppressants, such as steroids, mTOR inhibitors, or B-cell-depleting monoclonal antibodies, have been used to improve the efficacy of AAV administration and potentially allow for repeat dosing. However, systemic immunosuppression may increase the risk of opportunistic bacterial or viral infections and is not effective in complete remission of high titer NAbs.[70,72,73] AAV-specific plasmapheresis columns and bacteria-derived antibody-degrading proteases, such as the Immunoglobulin G-degrading enzyme of S.pyogenes (IdeS), have been used to deplete anti-AAV NAbs in plasma, but these methods may not completely eradicate NAbs nor antibody-producing cells.[74] Further, plasmapheresis and IdeS proteases remove total antibody content and thus can also increase the risk of infection in patients. Chemical modification of AAV capsids, including PEGylation and polymer encapsulation, can potentially decrease transduction efficiency, alter biodistribution of AAV vectors, and result in anti-polymer antibody formation.[75,76] Exosome-enveloped AAVs can transduce the target cells in the presence of pre-existing immunity, but encapsulating AAVs with exosomes can alter tropism and transduction efficiency, as well as introduce nucleic acid or protein contaminants that ultimately lead to ADAs.[77-79] Shielding AAVs from NAbs via encapsulation in vaults, endogenous proteinaceous organelles recognized as self by the immune system, has also been proposed as a method for evading the immune system.[80] AAVs packaged inside vaults have been shown to transduce cells in the presence of anti-AAV neutralizing serum, however this method has yet to be tested *in vivo*. Most recently, T

cell epitopes were identified and removed by rational design to reduce the immunogenicity of an AAV capsid, but the authors noted certain epitopes that they could not eliminate or "silence" in their chimeric design.[81] A significant limitation in all of these studies is the evaluation of capsid immunogenicity by using animal models or *in vitro* T cell assays, which cannot accurately recapitulate the human adaptive immune response seen during clinical trials.[82,83] An ideal AAV capsid for gene therapy would retain highly specific tissue tropism and transfection efficiency while avoiding an ADA response that would preclude repeat dosing in patients.

1.5 Thesis Overview

Chapter 2 describes the synthetic production of EABR-mediated antigen-presenting vesicles and characterizes the benefit of linking the three subunits of pMHC into a single protein chain for the purpose of releasing fully formed pMHC complexes on extracellular vesicles. Synthetic pMHCI APVs are shown to stimulate their cognate T cells selectively as a demonstration of their therapeutic immunomodulatory potential. Chapter 3 extends the work of Chapter 2 by showing these APVs can be engineered to include costimulatory signals or full-length membrane-bound cancer antigen for improved single-cell T cell capture and activation within hydrogel nanovials. Hydrogel functionalization with EABR-mediated vesicles could improve high-throughput screening of T cell populations for cell-based therapies, support future high-throughput studies investigating the membrane protein composition of EVs and their effect on immunomodulation, or improve the immunogenicity of patient-implanted biomaterials. Chapter 4 describes nascent work involving the use of human tonsil organoids to study the immunomodulatory potential of antigen-presenting vesicles and the immunogenicity of AAVs in a more physiologically-relevant context than previous *in vitro* studies. Lastly, some of my other PhD work, which was largely divorced from my immunology-focused work, is added as a set of appendices to share the range of translational applications in which Dr. Hoffmann's vesicle-forming EABR sequence can be applied.

Chapter 2

RECRUITING ESCRT TO PEPTIDE-MHC GENERATES ANTIGEN-PRESENTING VESICLES THAT STIMULATE T CELLS SELECTIVELY

Adapted from:

Olson, B. A., Huey-Tubman, K. E., Mao, Z., Hoffmann, M. A. G., Murray, R. M., & Mayo, S. L. (2025). Recruiting ESCRT to single-chain heterotrimer peptide-MHCI releases antigen-presenting vesicles that stimulate T cells selectively. *bioRxiv*, 2025.2001.2017.633600. https://doi.org/10.1101/2025.01.17.633600

2.1 Abstract

Immune cells naturally secrete extracellular antigen-presenting vesicles (APVs) displaying peptide:MHC complexes to facilitate the initiation, expansion, maintenance, or silencing of immune responses. Previous work has sought to manufacture and purify these vesicles for cell-free immunotherapies. In this study, APV assembly and release is achieved in non-immune cells by transfecting a single-chain heterotrimer (SCT) peptide/major histocompatibility complex I (pMHCI) construct containing an ESCRT- and ALIX-binding region (EABR) sequence appended to the cytoplasmic tail; this EABR sequence recruits ESCRT proteins to induce the budding of APVs displaying SCT pMHCI. A comparison of multiple pMHCI constructs shows that inducing the release of APVs by the addition of an EABR sequence generalizes across SCT pMHCI constructs. Purified pMHCI/EABR APVs selectively stimulate IFN-γ release from T cells presenting their cognate T cell receptor, demonstrating the potential use of these vesicles as a form of cell-free immunotherapy.

2.2 Introduction

Almost thirty years ago, Raposo, G. et al. first reported on the release of B cell-derived extracellular vesicles (EVs) with functional peptide:MHC (pMHC) complexes on their surface.[35] Since then, EVs that were previously labeled as simple cellular "debris" have been increasingly recognized for their immunoregulatory potential as a simpler, cell-free alternative to cell-based immunotherapies.[33,84] Naturally occurring pMHC-displaying

antigen-presenting vesicles (APVs) in particular have been demonstrated to orchestrate immune responses either directly or with the aid of antigen-presenting cells (APCs).[9] Research teams have ventured to engineer more complex versions of these antigen-presenting vesicles: whole mammalian cells conjugated with immunostimulatory molecules,[13-17] nanoparticles coated with APC-derived membranes via extrusion or sonication,[24,25] or engineered extracellular blebs from dendritic cells.[26-30] These previous approaches demonstrated the therapeutic potential of APVs, but production is often low yield or requires the patient's own cells to be harvested and processed before treatment can be administered. Significant attention has been given to manufacturing APVs via microfluidics,[85] but existing microfluidic vesicles suffer from short half-lives and are susceptible to rupture due to osmotic changes and the turbulent flow of the lymphatic and cardiovascular systems. Polymer-coated iron-oxide nanoparticles conjugated with pMHCI have shown remarkable therapeutic potential for autoimmune diseases such as type 1 diabetes, but the stiff spherical structure of the nanoparticle scaffold reduces the potential surface area for ideal pMHC:T cell receptor (TCR) interactions;[86-88] additionally, pMHC complexes are rigidly adhered to the nanoparticle surface, limiting pMHC movement and clustering considered important for the formation of a T cell stimulating immunological synapse.[89] Optimal, engineered APVs would ideally recreate the endogenous form of APVs, while maximizing the concentration of proteins that are critical for immunoregulation.

Here, we describe the engineered assembly and budding of peptide/MHCI-displaying APVs from the cell surface of non-immune cells by DNA transfection of an engineered single-chain heterotrimer (SCT) peptide/MHCI (pMHCI). Building on a recently described method for generating enveloped virus-like particles displaying the SARS-CoV-2 spike protein,[47] we fused an endosomal sorting complex required for transport (ESCRT)- and ALG-2-interacting protein X (ALIX)- binding region (EABR) to the cytoplasmic tail of SCT pMHCI to directly recruit the ESCRT machinery and induce the release of pMHCI-displaying vesicles. Immuno-electron microscopy (immuno-EM) of the supernatant from transfected cells showed halos of black punctae surrounding exosome-like vesicles, confirming the presence of SCT pMHCI on APVs. ELISPOT assays show that SCT pMHCI/EABR APVs are capable

of stimulating IFN-γ release from T cells at a level equivalent to refolded pMHCI tetramer, and that the APVs selectively stimulate T cells presenting their cognate TCR. Altogether, these results demonstrate a new method for generating synthetic, native-like APVs in high copy number and valency with the therapeutic potential for improved cell-free immunoregulation.

2.3 Results

2.3.1 EABR addition to the cytoplasmic tail of SCT pMHCI promotes APV release

To generate APVs from non-immune cells, we attached an EABR sequence from the human CEP55 protein[90] to the cytoplasmic tail of MHCI (Fig. 2.1A). To ensure each APV presented the same, intended peptide on MHCI, the complete peptide:MHCI complex was formed into a single-chain heterotrimer; the N-terminus of the HLA-A*02:01 α chain was extended with a 4xG_4S linker connecting to the C-terminus of beta-2 microglobulin (β2M), which was itself extended at its N-terminus by a 3xG_4S linker connecting to either the 10-mer MART-1 (MART1) or 9-mer NY-ESO-1(C165V)$_{157\text{-}165}$ (NYESO1) cancer-related peptides.[91] The EABR sequence used here was identical to the sequence used by Hoffmann et al.[47] to create enveloped virus-like particles (eVLPs) displaying the SARS-CoV-2 spike protein, and was attached to the cytoplasmic tail of the HLA-A*02:01 α chain by a G_3S linker (Fig. 2.1B). Adopting the nomenclature of Chour et al.'s thermostability studies[48,49] on previous SCT pMHCI designs, our first SCT pMHCI construct was named "D1/EABR" to denote a "D1" SCT design with an "EABR" sequence appended to the end of its cytoplasmic tail. A second "D9" variant of SCT pMHCI, containing Y84C and A139C substitutions, was also tested given its reported improvements in thermostability and T cell receptor binding compared to the D1 design (Table S2.1).[50]

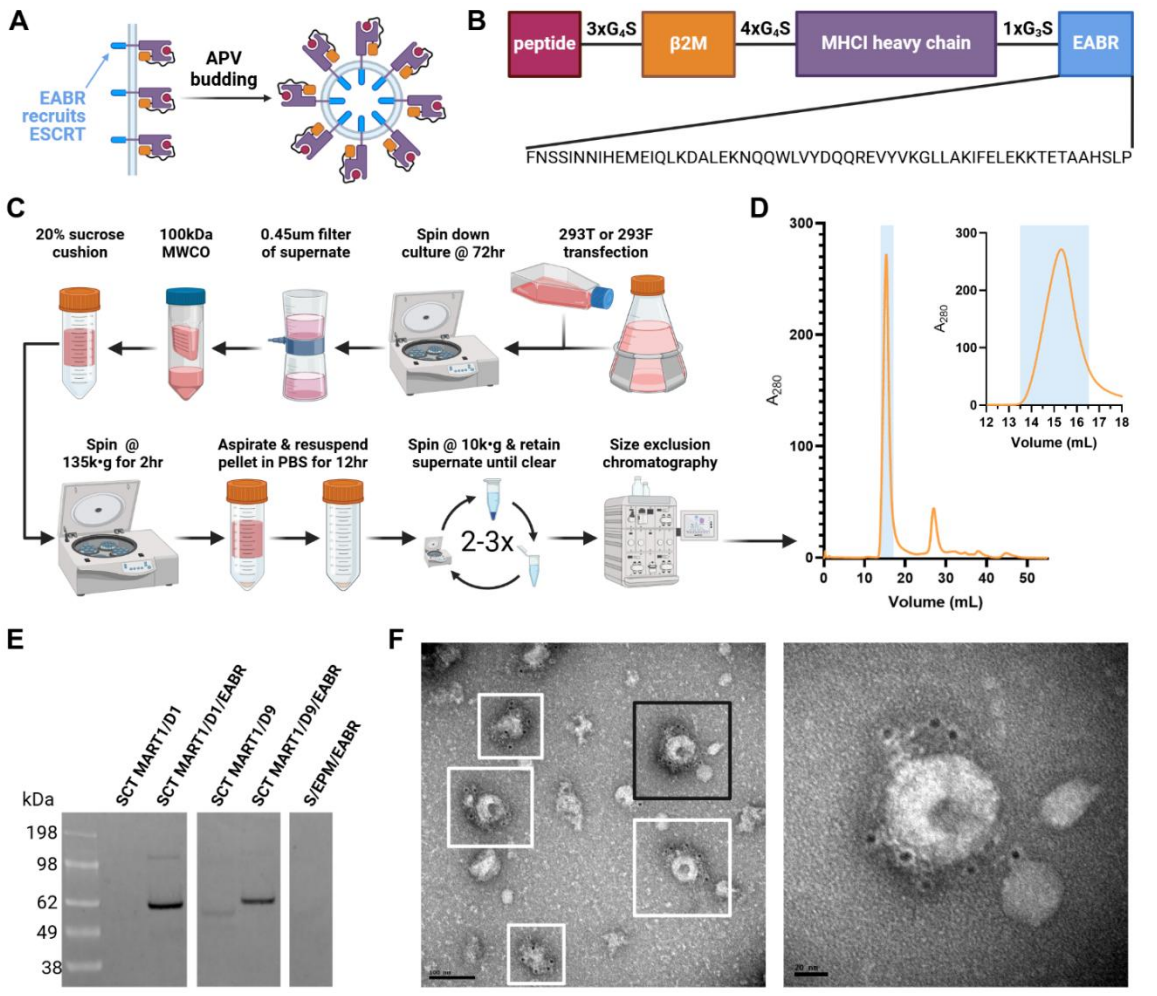

Figure 2.1. EABR addition to the cytoplasmic tail of SCT pMHCI promotes APV budding and release

(A) Schematic of membrane-bound SCT pMHCI proteins on a cell surface containing cytoplasmic tail EABR additions that induce budding of an APV comprising a lipid bilayer with embedded SCT pMHCI proteins.

(B) SCT pMHCI/EABR construct. Top: the SCT pMHCI protein is composed of a peptide fused to a 3x(Gly_4Ser) linker, β2M, a 4x(Gly_4Ser) linker, HLA-A*02:01 α chain, a Gly_3Ser spacer, and an EABR sequence. Bottom: EABR sequence.

(C) Schematic showing production and purification of APVs.

(D) Chromatogram representative of the typical yield of SCT pMHCI APVs from a 100 mL transfection of Expi293F cells. Inset highlights void volume peak.

(E) Western blot analysis detecting SCT pMHCI protein from APVs purified by ultracentrifugation on a 20% sucrose cushion from transfected HEK293T cell culture supernatants. Cells were transfected with SCT MART1/D1, SCT MART1/D1/EABR, SCT MART1/D9, SCT MART1/D9/EABR, and SARS-CoV-2 spike(S)/EPM/EABR (S/EPM/EABR) constructs. Rabbit anti-HLA-A primary antibody and Alexa488-conjugated anti-rabbit secondary antibody were used to detect SCT pMHCI protein.

(F) Immuno-EM images of SCT MART1/D1/EABR APVs purified from transfected Expi293F cell culture supernatants by ultracentrifugation and SEC. Primary rabbit anti-HLA-A antibody identical to primary antibody used in (E). Secondary 6 nm gold-conjugated anti-rabbit antibody appears as black punctate in image. Left: representative APVs are highlighted in boxes. Scale bar, 100 nm. Right: close up of black-boxed APV. Scale bar, 20 nm.

APVs were expressed by transfecting HEK293T or Expi293F cells with DNA plasmids encoding the SCT pMHCI constructs. Vesicles were purified by ultracentrifugation of cell culture supernatant on a 20% sucrose gradient as is typical for the purification of viral particles and exosomes[92] (Fig. 2.1C). Ultracentrifuged product was resuspended in pH 7.4 phosphate-buffered saline (PBS) and optionally further purified by size exclusion chromatography (SEC) to yield a high concentration of product in the void volume (Fig. 2.1D). Western blot analysis of the purified product showed that the addition of the EABR sequence to the cytoplasmic tails of both the MART1/D1/EABR and MART1/D9/EABR constructs generated higher levels of MHCI compared to their non-EABR counterparts (Fig. 2.1E). Because pMHCI is difficult to resolve with cryo-EM or cryo-ET, we prepared immuno-electron microscopy grids of the purified product to confirm the presence of pMHCI-displaying APVs, which presented as cup-like, collapsed spheres resembling the canonical shape of exosomes that partially collapse upon paraformaldehyde fixation and negative staining[93] (Fig. 2.1F and S2.1). Sandwich ELISAs of these pMHCI vesicles showed that pMHCI co-presented with the hallmark exosomal tetraspanin proteins CD81 and CD63 (Fig. S2.2), which was further confirmed by mass spectrometry showing enrichment of pMHCI and exosomal tetraspanin proteins in the purified product (Document S1). As a

result, the vesicles have been denoted as pMHCI-displaying "antigen-presenting vesicles" resembling natural immunoregulatory extracellular vesicles or "exosomes".

Table S2.1. Description of tested pMHCI constructs

CONSTRUCT NAME	ORIGIN	DESCRIPTION
MART1/D1	Human	I.e. D1 SCT MART1/HLA-A*02:01 – the complete peptide:MHCI complex was formed into a single-chain heterotrimer (SCT); the N-terminus of the human HLA-A*02:01 α chain was extended with a 4xG_4S linker connecting to the C-terminus of human beta-2 microglobulin (β2M), which was itself extended at its N-terminus by a 3xG_4S linker connecting to the human 10-mer MART-1 (MART1) cancer-related peptide.
MART1/D1/EABR	Human	I.e. D1 SCT MART1/HLA-A*02:01/EABR – identical to MART1/D1 above, but with the "EABR" sequence appended to the cytoplasmic tail with a 1xG_3S glycine-serine spacer.
MART1/D9	Human	I.e. D9 SCT MART1/HLA-A*02:01 – identical to MART1/D1 construct, but with A84C and Y139C mutations to resemble the "D9" variant of MHCI
MART1/D9/EABR	Human	I.e. D9 SCT MART1/HLA-A*02:01/EABR – identical to MART1/D9 construct, but with the "EABR" sequence appended to the cytoplasmic tail with a 1xG_3S glycine-serine spacer.
NYESO1/D1	Human	I.e. D1 SCT NYESO1(C165V)$_{157-165}$/HLA-A*02:01 – identical to MART1/D1 above, but the MART1 cancer-related peptide was replaced with the human 9-mer NY-ESO-1(C165V)$_{157-165}$ (NYESO1) cancer-related peptide.
NYESO1/D1/EABR	Human	I.e. D1 SCT NYESO1(C165V)$_{157-165}$/HLA-A*02:01/EABR - identical to NYESO1/D1 above, but with the "EABR" sequence appended to the cytoplasmic tail with a 1xG_3S glycine-serine spacer.
NYESO1/D9	Human	I.e. D9 SCT NYESO1(C165V)$_{157-165}$/HLA-A*02:01/MHCI - identical to NYESO1/D1 above, but with A84C and Y139C mutations to resemble the "D9" variant of MHCI
NYESO1/D9/EABR	Human	I.e. D9 SCT NYESO1(C165V)$_{157-165}$/HLA-A*02:01/EABR - identical to NYESO1/D9 above, but with the "EABR" sequence appended to the cytoplasmic tail with a 1xG_3S glycine-serine spacer.
NYESO1/β2M	Human	I.e. NYESO1(C165V)$_{157-165}$/β2M – the human HLA-A*02:01 α chain and the associated 4xG_4S linker was removed from the MART/D1 single-chain trimer (SCT) construct described above to generate a construct encoding only the NY-ESO-1(C165V)$_{157-165}$ (NYESO1) cancer peptide connected to the N terminus of human β2M by a 3xG_4S glycine-serine linker.
D1HC	Human	The human HLA-A*02:01 α chain

D1HC/EABR	Human	The human HLA-A*02:01 α chain appended with the "EABR" sequence by a 1xG_3S glycine-serine linker.
D1SCD	Human	The N-terminus of the human HLA-A*02:01 α chain was extended with a 4xG_4S linker connecting to the C-terminus of human beta-2 microglobulin (β2M).
D1SCD/EABR	Human	Identical to D1SCD, but with the "EABR" sequence appended to the cytoplasmic tail of the HLA-A*0201 α heavy chain by a 1xG_3S glycine-serine linker.
D9HC	Human	I.e. D9 HLA-A*02:01 HC - identical to the D1HC construct, but with A84C and Y139C mutations to resemble the "D9" variant of MHCI
D9HC/EABR	Human	I.e. D9 HLA-A*02:01 HC/EABR – identical to the D9HC construct, but with the "EABR" sequence appended to the cytoplasmic tail with a 1xG_3S glycine-serine spacer.
D9SCD	Human	I.e. D9 SCD β2M/ HLA-A*02:01 - identical to the D1SCD construct, but with A84C and Y139C mutations to resemble the "D9" variant of MHCI
D9SCD/EABR	Human	I.e. D9 SCD β2M/ HLA-A*02:01/EABR - identical to the D9SCD construct, but with the "EABR" sequence appended to the cytoplasmic tail with a 1xG_3S glycine-serine spacer.
NRP-V7/H-2K^d	Murine	NRP-V7/H-2K^d features the NRP-V7 mimotope for $IGRP_{206-214}$ connected by a glycine-serine linker to murine β2M followed by a glycine-serine linker connecting to the complete H-2K^d α heavy chain. The "EABR" sequence can optionally be added to the cytoplasmic tail of the H-2K^d α heavy chain by a glycine-serine linker.
IGRP/H-2K^d	Murine	IGRP/H-2K^d or $IGRP_{206-214}$/H-2K^d features the islet-specific glucose-6-phosphatase catalytic subunit related protein ($IGRP_{206–214}$) connected by a glycine-serine linker to murine β2M followed by a glycine-serine linker connecting to the complete H-2K^d α heavy chain. The "EABR" sequence can optionally be added to the cytoplasmic tail of the H-2K^d α heavy chain by a glycine-serine linker.
NRP-V7/D9_H-2K^d	Murine	NRP-V7/H-2K^d construct with A84C and Y139C mutations to resemble the "D9" variant of MHCI, a.k.a. NRP-V7/D9_H-2K^d.
IGRP/D9_H-2K^d	Murine	$IGRP_{206-214}$/H-2K^d construct with A84C and Y139C mutations to resemble the "D9" variant of MHCI, a.k.a. $IGRP_{206-214}$/D9_H-2K^d or IGRP/D9_H-2K^d.
NYESO1/D9/H-2D^b	Chimeric	The human NY-ESO-1(C165V)$_{157-165}$ (NYESO1) cancer-related peptide (NYESO1) is connected by a 3xG_4S glycine-serine linker to human β2M followed by a 4xG_4S glycine-serine linker connecting to the N-terminus of the human HLA-A*02:01 α heavy chain. The α_3 region and subsequent transmembrane and cytoplasmic regions of the human HLA-A*02:01 heavy chain are removed and replaced with the murine H-2D^b α_3 heavy chain, including the H-2D^b transmembrane and cytoplasmic regions.

NYESO1/D9/H-2K^b	Chimeric	Identical to NYESO1/D9/H-2D^b above, but replacing all murine H-2D^b regions with the murine H-2K^b α_3, transmembrane, and cytoplasmic regions.

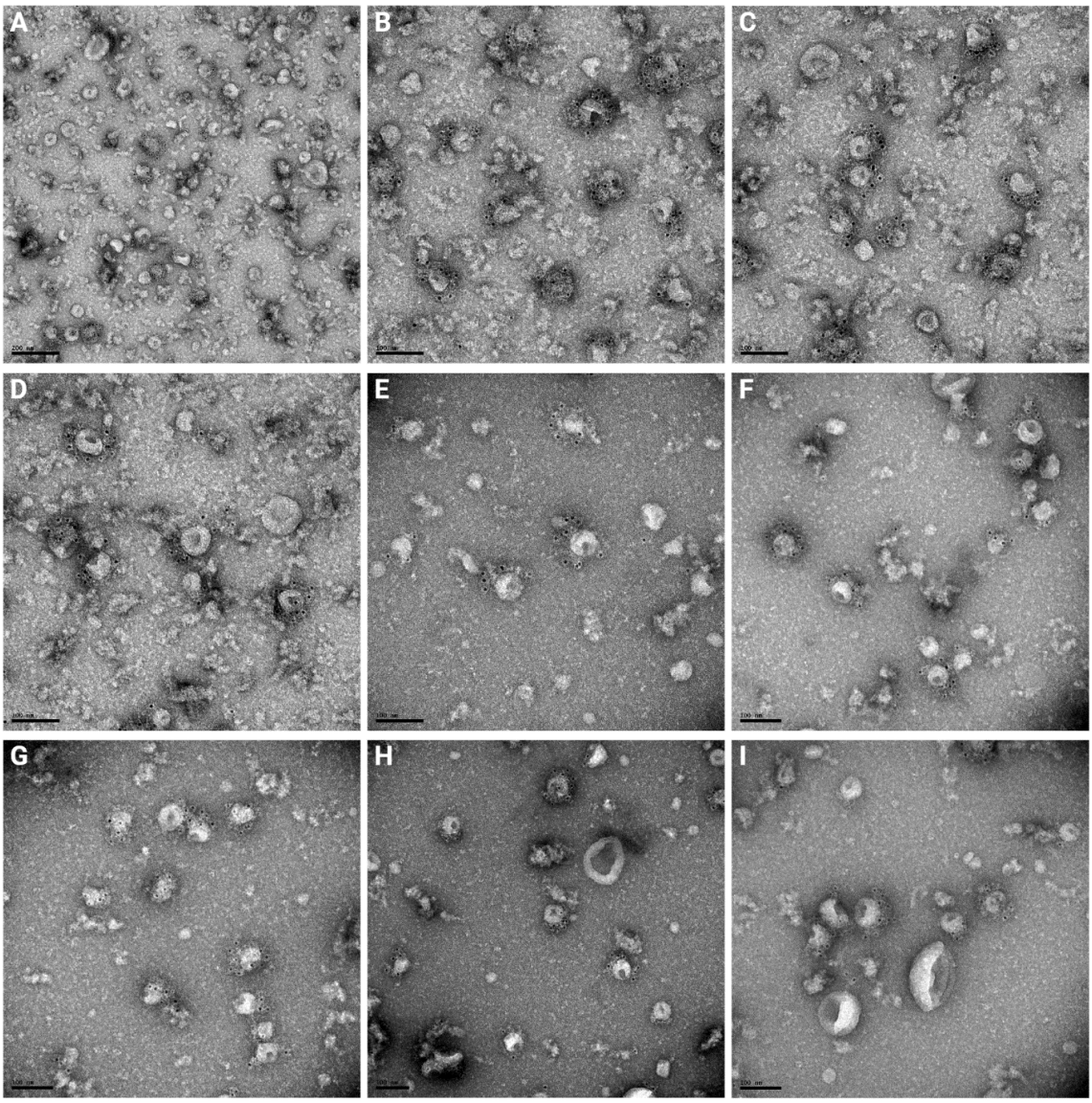

Figure S2.1. Additional micrographs of pMHCI/EABR grids prepared by immuno-EM show APVs

All micrographs show Expi293F cell culture supernatant after transfection with a SCT MART1/D1/EABR construct and purified by ultracentrifugation and SEC as outlined in Figure 1C. (A-D): 50 mL of purified Expi293F cell culture supernatant. (E-I) 200 mL of

purified Expi293F cell culture supernatant further diluted in pH 7.4 PBS after purification. All grids were prepared using the identical protocol as in Figures 1F and 2D-F. Secondary 6 nm gold-conjugated anti-rabbit antibody bound to primary rabbit anti-HLA-A antibody appears as black punctate in the image. (A) Scale bar, 200 nm. (B-I) Scale bar, 100 nm.

2.3.2 EABR addition to SCT pMHCI promotes budding of the complete, intended pMHCI complex on APVs

To better quantify the relative improvement in APV formation with EABR addition, we performed ELISA of SCT MART1 and SCT NYESO1 constructs. Both showed over 100-fold improvements in APV formation with the addition of the EABR sequence (Fig. 2.2A). Subsequent ELISAs showed that appending EABR to MHCI heavy chain (HC) alone (i.e., without covalently linked β2M and presenting peptide) still boosted MHCI yield in the purified transfection product relative to HC without an EABR tag, and an even greater concentration of MHCI resulted from transfection with EABR-tagged single-chain heterodimer (SCD) constructs comprised of MHCI heavy chain covalently linked to β2M without a presenting peptide (Table S2.1 and Fig. S2.3). Consequently, we next investigated whether the SCT form of pMHCI was necessary to assemble the intended pMHCI complex on released APVs.

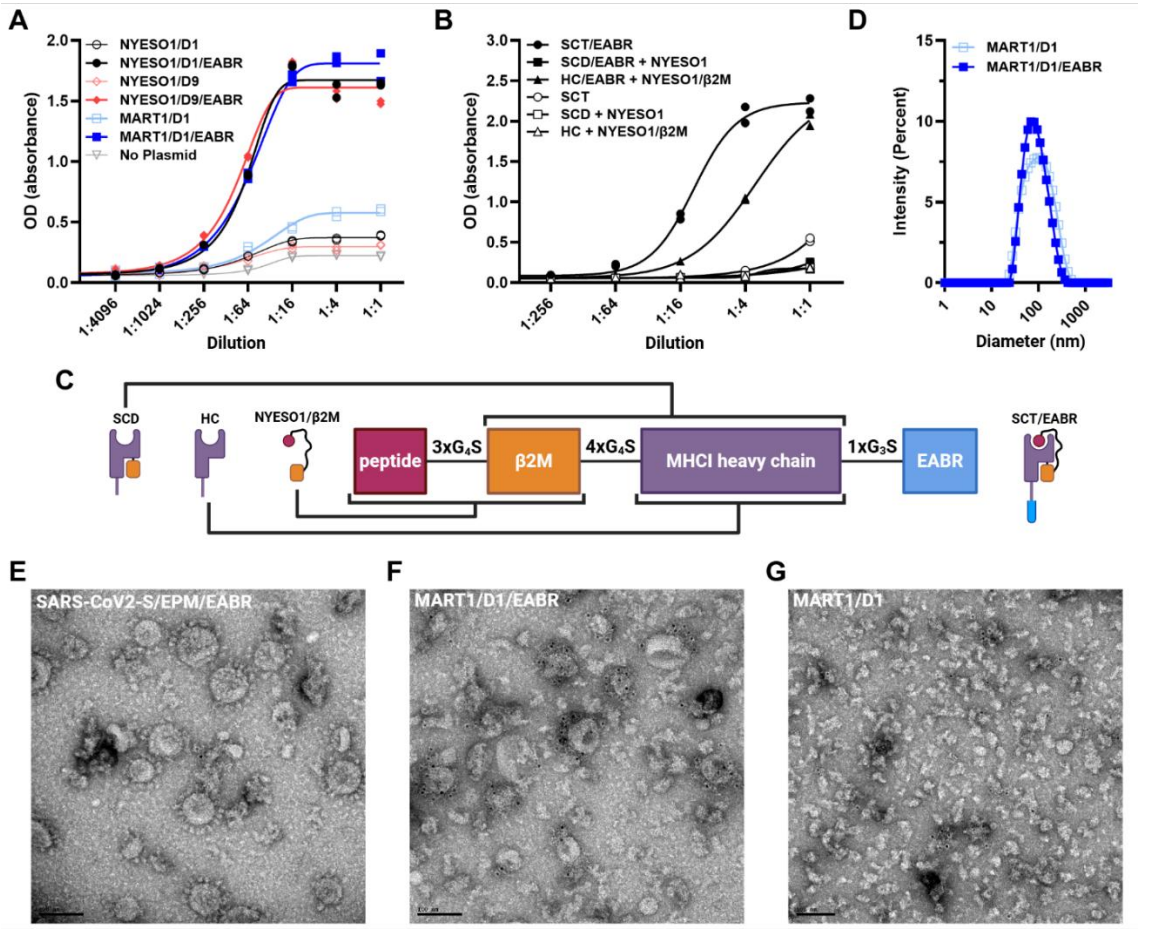

Figure 2.2. EABR addition to SCT pMHCI promotes budding of the complete, intended pMHCI complex on APVs

(A) Indirect ELISA of APVs purified by ultracentrifugation from transfected HEK293T cells with a primary rabbit anti-HLA-A antibody and secondary HRP-conjugated anti-rabbit antibody. Cells were transfected with SCT NYESO1/D1, SCT NYESO1/D1/EABR, SCT NYESO1/D9, SCT NYESO1/D9/EABR, SCT MART1/D1, and SCT MART1/D1/EABR constructs (2 replicates per dilution).

(B) Sandwich ELISA of APVs purified by ultracentrifugation from transfected HEK293T cells using anti-NYESO1:HLA-A*02:01 (3M4E5) for capture, biotinylated 3M4E5 for detection, and HRP-conjugated streptavidin secondary. Cells were transfected with SCT NYESO1/D9/EABR, SCD D9/EABR and NYESO1 peptide (SCD/EABR + NYESO1)), HC D9/EABR and NYESO1/β2M (HC/EABR + NYESO1/β2M), SCT NYESO1/D9 (SCT),

SCD D9 and NYESO1 peptide (SCD + NYESO1), HC D9 and NYESO1/β2M (HC + NYESO1/β2M) constructs (2 replicates per dilution).

(C) Schematic showing full SCT pMHCI/EABR construct (SCT/EABR) and various alternative constructs used for the ELISA in (B): NYESO1/β2M, HC, and SCD.

(D) Dynamic light scattering measurement of SCT MART1/D1 and SCT MART1/D1/EABR APVs represented as a probability mass function of the expected diameter values for each sample. Points are connected by a simple interpolating spline.

(E-G) Immuno-EM micrographs of different EABR vesicles purified from transfected Expi293F cell culture supernatants by ultracentrifugation and SEC. Samples were stained with a primary rabbit anti-HLA-A antibody and a secondary 6 nm gold-conjugated anti-rabbit antibody that appears as black punctate in image. Scale bars, 100 nm. (E) SARS-CoV2-S/EPM/EABR. Spike protein coronas are visible around the edges of the spherical vesicles. A single gold nanoparticle from a secondary antibody is visible in the middle of the image. (F) SCT MART1/D1/EABR gold particles from secondary antibody can be seen as halos of black punctate around deflated vesicles. (G) SCT MART1/D1 scattered gold particles from secondary antibody can be seen as non-specific staining without the presence of vesicles.

To compare the impact of different NYESO1/MHCI construct designs on APV assembly and release, we selectively removed the Gly_4Ser linkers from the SCT NYESO1/D9 construct—either removing the $3xG_4S$ linker between the peptide and β2M yielding SCD, or the $4xG_4S$ linker between β2M and the MHCI heavy chain yielding NYESO1/β2M—and performed ELISAs with a TCR-like antibody specific for the fully formed NYESO1:HLA-A*02:01 complex (Fig. 2.2B & 2.2C).[94] Decoupling the NYESO1 peptide from the EABR-tagged SCD MHCI complex led to an over 10-fold reduction in the detected level of expression of NYESO1/MHCI APVs in HEK293T cells to the extent that it was nearly undetectable by sandwich ELISA (Fig. 2.2B). Even in the higher-expressing Expi293F cell line, an exhaustive search of every possible combination of MHCI α heavy chain, β2M, and either the full-length NY-ESO-$1_{1\text{-}165}$ or 9-mer NYESO1 peptide did not produce measurable pMHCI product in the purified APVs when these constructs were assembled without glycine-

serine linkers between the 9-mer NYESO1 peptide and β2M (Fig. S2.4). Co-transfecting two separate constructs of HC/EABR and NYESO1/β2M, however, generated APVs detectable by sandwich ELISA, and the fully connected SCT form of NYESO1/D9/EABR further improved the expression of pMHCI-displaying APVs out of all constructs tested (Fig. 2.2B); in addition, because EABR-tagged MHCI heavy chain is capable of generating APVs without transfection of a presenting peptide such as NYESO1 (Fig. S2.3), the SCT form of pMHCI is the only design that ensures the APVs are presenting the transfection constructs' intended peptide.

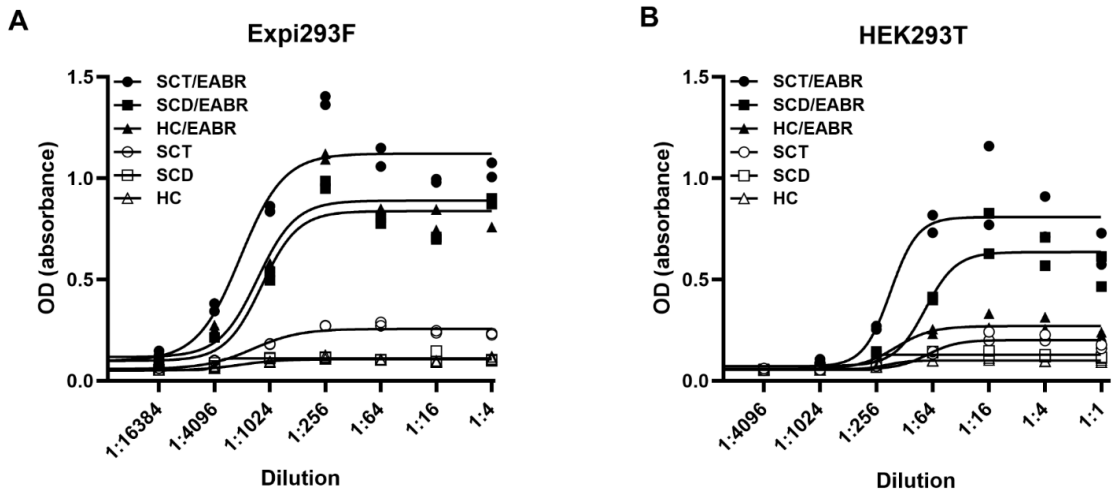

Figure S2.3. Indirect ELISA of purified Expi293F and HEK293T transfection supernatant suggests complete pMHCI not required for release of vesicles harboring MHCI α heavy chain

Indirect ELISA of purified Expi293F (A) and HEK293T (B) supernatant transfected with SCT MART1/D1/EABR (SCT/EABR), SCD D1/EABR (SCD/EABR), D1 HC-EABR (HC/EABR), and the non-EABR versions of the three constructs just described: SCT MART1/D1 (SCT), SCD D1 (SCD), and HC D1 (HC). See Figure 2C for diagrams of SCT, SCD, and HC. All supernatant was purified by ultracentrifugation and resuspended in pH 7.4 PBS. Polyclonal rabbit anti-HLA-A was used for the primary antibody, and HRP-conjugated goat anti-rabbit was used for the secondary antibody (2 replicates per dilution).

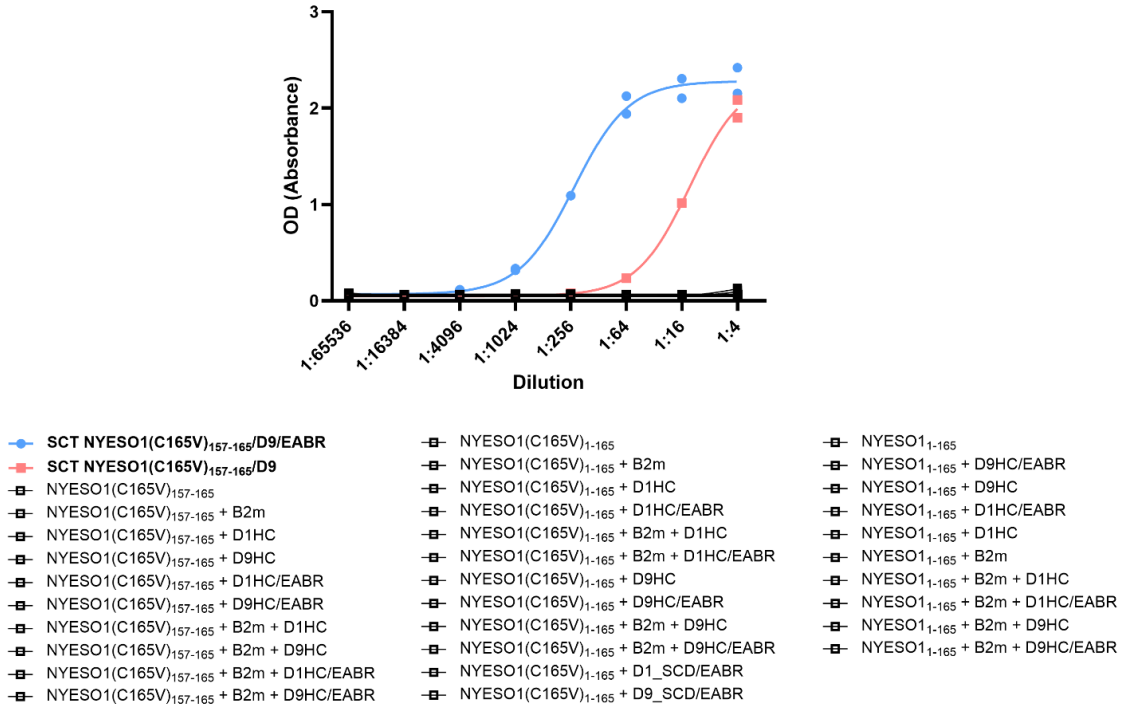

Figure S2.4. Sandwich ELISA of purified Expi293F transfection supernatant shows heterotrimer form of pMHCI optimizes APV release

Sandwich ELISA of purified Expi293F supernatant transfected with exhaustive permutations of pMHCI complex domains that are either linked covalently by glycine-serine linkers (denoted "/") or separated across plasmids (denoted "+") (Table S1). All supernatant was purified by ultracentrifugation and resuspended in pH 7.4 PBS. Monoclonal human anti-NYESO1:HLA-A*02:01 complex was used for the initial capture antibody. Biotinylated monoclonal human anti-NYESO1:HLA-A*02:01 complex was used for the primary detection antibody and secondary strep-HRP was then incubated in each well before developing with HRP substrate (2 replicates per dilution).

Interestingly, we still recovered low levels of MHCI protein after purification of non-EABR SCT pMHCI from transfected HEK293T supernatant, an effect that was amplified by expressing the same constructs in the higher-expressing Expi293F cell line that has been used previously for exosome production[95] (Fig. 2.2A & S2.4). Dynamic light scattering (DLS) of both the purified SCT MART1/D1 and SCT MART1/D1/EABR constructs showed similar

median particle diameters of 60-80 nm (range 30-250 nm) with the SCT MART1/D1/EABR construct exhibiting a slightly narrower distribution compared to the non-EABR SCT MART1/D1 construct (Fig. 2.2D). This particle size distribution is consistent with the vesicle sizes seen in immuno-EM images of the EABR constructs. We were unable, however, to observe pMHCI vesicles when imaging immuno-EM grid preparations of the non-EABR SCT MART1/D1 construct purified from Expi293F supernatant. Instead, the non-EABR SCT MART1/D1 grids showed what appeared to be pMHC aggregates or blebbing of sparsely populated membrane, which was less frequently observed in the grids prepared for the EABR-tagged vesicles (Fig. 2.2F, 2.2G, & S2.1). As a direct contrast, identically prepared EM grids for both SARS-CoV-2 S/EPM/EABR and SCT MART1/D1/EABR constructs were densely populated with vesicles displaying their respective proteins, and only the MART1/D1/EABR vesicles stained positively with a halo of anti-HLA-A antibody around each vesicle (Fig. 2.2E & 2.2F). Altogether, our results show that SCT pMHCI promotes the display of complete pMHCI complexes on APVs, and that addition of the EABR sequence increases APV release.

2.3.3 EABR-mediated APV release generalizes to mRNA transfection and across pMHCI variants

To further explore the generalizability of EABR sequence addition and heterotrimerization of pMHCI on APV release, we tested whether EABR-tagged SCT constructs of murine MHCI and chimeric human/mouse MHCI would also generate APVs displaying pMHCI relevant for *in vivo* studies of immunoregulation. Chimeric human/mouse SCT MHCI HLA-A2/H-2D^b and HLA-A2/H-2K^b were designed according to the D9 SCT design, with an NYESO1 presenting peptide fused to a 3x(Gly$_4$Ser) linker, human β2M, a 4x(Gly$_4$Ser) linker, and a chimeric MHCI α heavy chain composed of the extracellular α1 and α2 domains of human Y84A,A139C HLA-A*02:01 heavy chain and the α3, transmembrane, and cytoplasmic domains of murine H-2K^b or H-2D^b heavy chain, i.e., NYESO1/D9/H-2D^b and NYESO1/D9/H-2K^b, respectively (Figure 2.3A and Table S1). D1 SCT constructs of murine MHCI H-2K^d were prepared with either an NRP-V7 or IGRP$_{206\text{-}214}$ type 1 diabetes-relevant presenting peptide fused to a 3x(Gly$_4$Ser) linker, murine β2M, a 4x(Gly$_4$Ser) linker, and the

H-2K^d α chain, i.e., NRP-V7/H-2K^d and IGRP/H-2K^d, respectively; "D9" designs were further generated by introducing Y84A,A139C mutations in the H-2K^d α heavy chain to make NRP-V7/D9_H-2K^d and IGRP/D9_H-2K^d (Figure 2.3A and Table S2.1).

For the chimeric human/mouse SCT NYESO1/D9/H-2D^b and NYESO1/D9/H-2K^b, addition of an EABR sequence to the cytoplasmic tail of MHCI α heavy chain amplified the production of APVs as detected by sandwich ELISA (Fig. 2.3B). Similar to the previous SCT MART1/D1, NYESO1/D1, and NYESO1/D9 pMHCI constructs, the SCT NYESO1/D9/H-2D^b pMHCI construct showed evidence of substantial vesicle production in HEK293T cells regardless of the addition of the EABR sequence. Swapping the α3, transmembrane, and cytoplasmic domains to a different MHC haplotype, NYESO1/D9/H-2K^b, led to comparatively reduced APV expression (Fig. 2.3B), a phenomenon that could be attributed to increased cell surface presentation of the H-2D^b haplotype due to differences in the MHCI α3 domain which has been observed previously.[96]

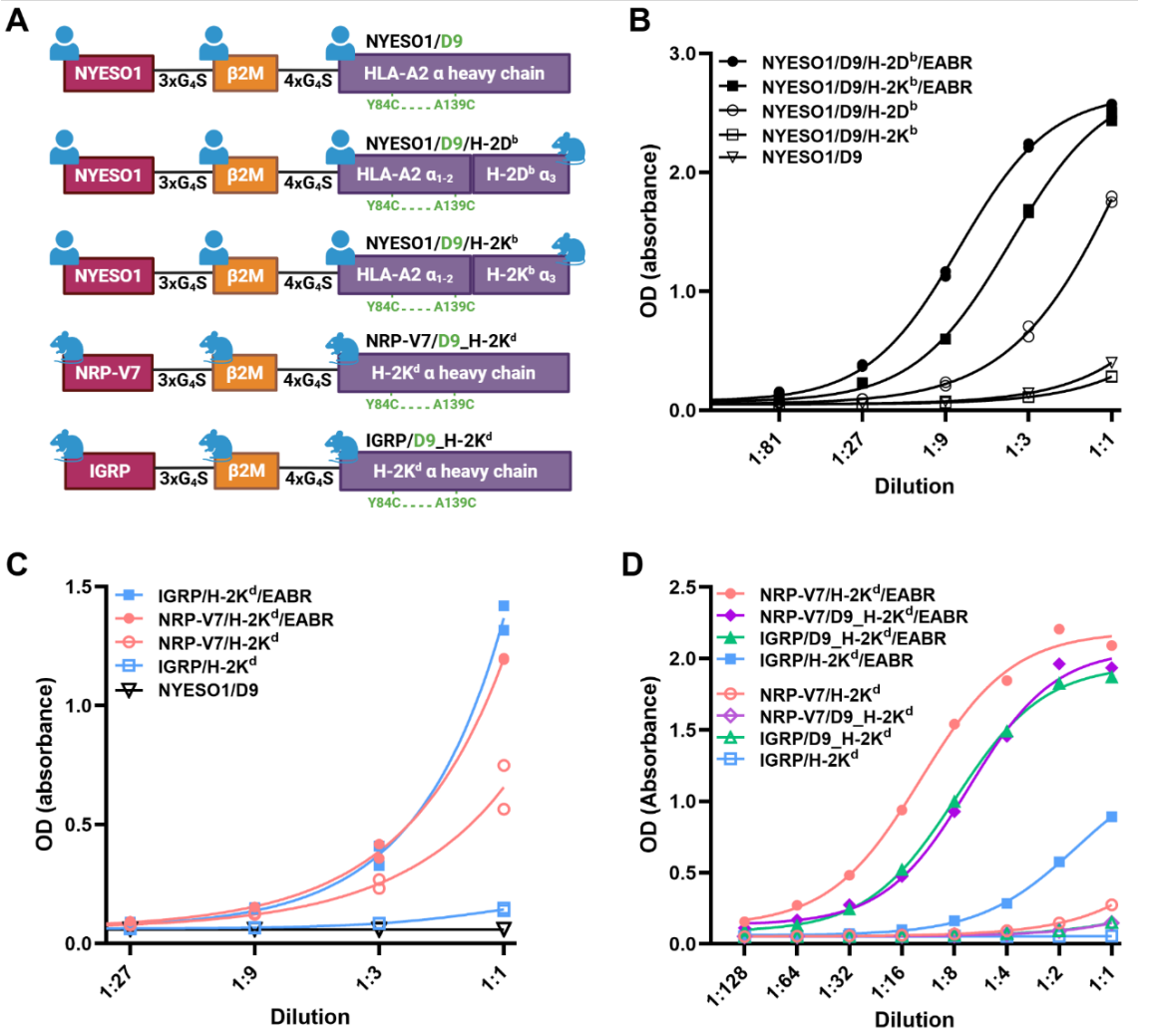

Figure 2.3. EABR-mediated APV release generalizes to mRNA transfection and across pMHCI variants

(A) Schematic of pMHCI constructs used in (B-D) showing which domains are sequences of human or murine origin. Further descriptions of constructs and domains can be found in Table S1.

(B) Sandwich ELISA of chimeric human/mouse SCT pMHCI protein on APVs purified by ultracentrifugation from transfected HEK293T cell culture supernatants (2 replicates per dilution). Mouse anti-NYESO1:HLA-A*02:01 capture antibody, biotinylated mouse anti-NYESO1:HLA-A*02:01 primary antibody, and HRP-conjugated streptavidin secondary antibody.

(C) Sandwich ELISA of murine SCT pMHCI of APVs purified by ultracentrifugation from DNA transfected HEK293T cells (2 replicates per dilution). Mouse anti-H-2K^d capture antibody, biotinylated mouse anti-H-2K^d primary antibody, and HRP-conjugated streptavidin secondary antibody.
(D) Sandwich ELISA of murine SCT pMHCI of APVs purified by ultracentrifugation from mRNA transfected NMuMG mammary epithelial cells (1 replicate per dilution). Mouse anti-H-2K^d capture antibody, biotinylated mouse anti-H-2K^d primary antibody, and HRP-conjugated streptavidin secondary antibody.

In a similar fashion, the fully murine SCT NRP-V7/H-2K^d and SCT IGRP/H-2K^d constructs showed amplified APV formation upon addition of an EABR sequence to the cytoplasmic tail of MHCI α heavy chain (Fig. 2.3C). While NRP-V7/H-2K^d was capable of measurable vesicle formation without the addition of EABR, IGRP/H-2K^d vesicle production was comparatively undetectable despite the only sequence difference being a change in the presenting peptide, likely reflecting differences in pMHCI stability based on changes in the presenting peptide[50,97,98]; mRNA transfection with murine-optimized sequences of the murine NRP-V7/H-2K^d and IGRP/H-2K^d constructs using the lower-expressing murine NMuMG mammary epithelial cell line generated a much more pronounced improvement in vesicle formation, as high as 50-fold, upon addition of the EABR sequence, highlighting the vesicle-forming potential of the EABR sequence in a more translationally-relevant context involving mRNA delivery.

Collectively, these results suggest that MHC haplotype and the loaded presenting peptide can influence vesicle production for SCT constructs. As shown previously by immuno-EM of the MART1/D9 and MART1/D9/EABR constructs (Fig. 2.2F, 2.2G), the increased yield of pMHCI product observed by ELISA in the non-EABR NRP-V7/H-2K^d and NYESO1/D9/H-2D^b constructs may be an artifact of pMHCI aggregation or indiscriminate membrane blebbing rather than intact APV formation. Further, vesicle formation by SCT pMHCI without EABR may be a result of improved protein stability or protein over-expression in the relatively higher-expressing HEK293T and Expi293F cell lines.[99]

Regardless of this intrinsic vesicle-forming potential, addition of the EABR sequence consistently increased APV release across these different pMHCI variants, and was shown to be further amplified in the context of mRNA transfection, demonstrating the generalizability of the EABR sequence for inducing APV production.

2.3.4 pMHCI/EABR APVs stimulate their cognate T cells selectively *in vitro*

Having confirmed that the EABR sequence reliably produces pMHCI-displaying APVs, we next asked whether EABR-induced pMHCI-displaying APVs were functional as T cell stimulators. SCT NYESO1/D9/EABR APVs were purified from transfected cell supernatants by ultracentrifugation and SEC, and the MHCI protein concentrations in purified APVs were determined by quantitative western blot analysis (Fig. S2.5). An equivalent concentration of MHCI for MART1/D9/EABR, NYESO1/D9/EABR, and NYESO1:HLA-A*02:01 tetramers was mixed with human donor T cells that were transduced with the 1G4 TCR specific for the NYESO1:HLA-A*02:01 epitope (Fig. S2.6), and T cell stimulation was evaluated using ELISPOT assay (Fig. 2.4A).

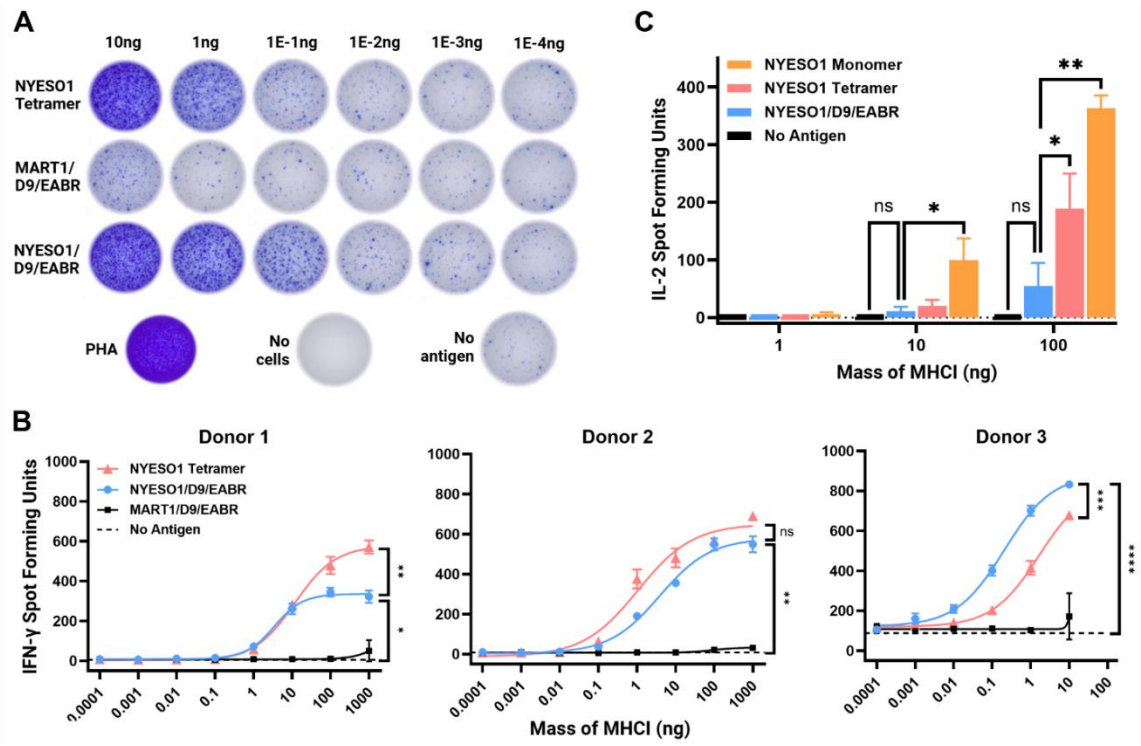

Figure 2.4. pMHCI/EABR APVs stimulate their cognate T cells selectively *in vitro*

(A) Top: Scans of ELISPOT wells detecting IFN-γ release from one replicate test of Donor 3's T cells after being dosed with serial dilutions of NYESO1:HLA-A*02:01 tetramers (NYESO1 Tetramer), SCT NYESO1/D9/EABR APVs, and SCT MART1/D9/EABR APVs. Bottom: Scans of ELISPOT wells detecting IFN-γ release from T cells dosed with 1.5% PHA as a positive control, wells without cells as a negative control (No cells), and T cells plated without antigen challenge (No antigen).

(B) ELISPOT spot forming units for IFN-γ from 1G4 T cells of three different donors dosed with SCT NYESO1/D9/EABR APVs, SCT MART1/D9/EABR APVs, NYESO1:HLA-A*02:01 tetramers (NYESO1 Tetramer), or no antigen challenge. Each data point is the response per $1x10^5$ cells. Baseline stimulation (i.e., "No antigen" – plated T cells without stimulation by antigen) was measured in triplicate for each donor and presented as a single mean in each plot with standard deviation. Because the NYESO1:HLA-A*02:01 tetramers generated larger spot sizes on average compared to the APVs, Donor 3's spot forming units were too numerous to count when dosed with more than 10 ng of NYESO1:HLA-A*02:01 tetramer, preventing direct comparison between antigen conditions at higher concentrations for this donor.

(C) ELISPOT spot forming units for IL-2 from 1G4 T cells of "Donor 3" in (B). T cells were dosed with SCT NYESO1/D9/EABR APVs, NYESO1:HLA-A*02:01 tetramers (NYESO1 Tetramer), NYESO1:HLA-A*02:01 monomers (NYESO1 Monomer), or no antigen challenge (3 replicates per dilution).

Significant differences between conditions linked by vertical lines are indicated by asterisks: ns > 0.05; *p < 0.05; **p < 0.01; ***p < 0.001; ****p < 0.0001.

Analysis of ELISPOT assay spot forming units (SFUs) from three different human T cell donors showed that both refolded NYESO1:HLA-A*02:01 tetramers and NYESO1/D9/EABR APVs significantly stimulated 1G4 T cells above background (Fig. 2.4B). This level of activation was specific to the NYESO1 peptide, as 1G4 T cells dosed with MART1/D9/EABR APVs demonstrated a statistically similar response to 1G4 T cells without antigen challenge. Interestingly, the elevated baseline of T cell activation without

antigen challenge in "Donor 3" coincided with an increase in the potency of NYESO1/D9/EABR APVs relative to NYESO1:HLA-A*02:01 tetramers for this donor. The possible association between the baseline activation level of a donor's T cells and the potency of the NYESO1/D9/EABR APVs is also seen in the relatively weakly activated "Donor 1" and moderately activated "Donor 2" T cells, which demonstrate correspondingly weak and moderate receptiveness, respectively, to NYESO1/D9/EABR APV stimulation as compared to NYESO1:HLA-A*02:01 tetramers (Fig. S2.7). Notably, soluble tetramers and monomers of natural, refolded pMHCI can activate pools of T cells by the release and subsequent representation of the pMHCI presenting peptide on T cell surfaces containing costimulatory signals, which then act as antigen-presenting cells for their T cell neighbors.[100] Thus, T cell stimulation by these SCT pMHCI APVs may be altogether different than stimulation by refolded tetramer or monomer, which is further supported by our subsequent assay of IL-2 release from the strongly responding "Donor 3" (Fig. 2.4C); at an equivalent mass of pMHCI, both monomer and tetramer forms of pMHCI induced significantly more IL-2 release than the EABR-mediated pMHCI. A dampened IL-2 release despite the substantial release of IFN-γ would coincide with *in vitro* studies of pMHCI-loaded extracellular vesicles in the context of Type 1 diabetes[84], which showed limited IL-2 release when co-cultured alone with human T1D-relevant T cells, and pMHCI nanoparticles, which showed a substantial release of IFN-γ when co-cultured with murine T1D-relevant T cells and were therapeutic when administered *in vivo*.[86,101]

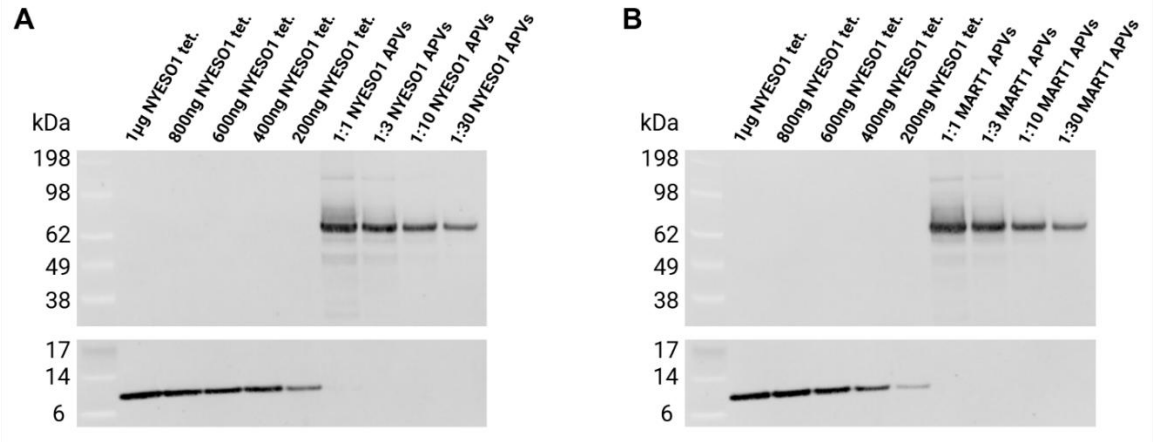

Figure S2.5. Quantitative Western Blots of purified Expi293F transfection supernatant in preparation for ELISPOT assays

Quantitative western blots of NYESO1:HLA-A*02:01 tetramer (NYESO1 tet.) and either NYESO1/D9/EABR APVs (NYESO1 APVs) (A) or MART1/D9/EABR APVs (MART1 APVs) (B) using mouse anti-B2m primary and goat Alexa488 anti-mouse secondary.

(A) Quantitative western blot comparing known amounts of NYESO1:HLA-A*02:01 tetramer (NYESO1 tet.) standards (lanes 1–5) with various dilutions of purified NYESO1/D9/EABR APVs (NYESO1 APVs) (lanes 6–9).

(B) Quantitative western blot comparing known amounts of NYESO1:HLA-A*02:01 tetramer (NYESO1 tet.) standards (lanes 1–5) with various dilutions of purified MART1/D9/EABR APVs (MART1 APVs) (lanes 6–9).

Overall, these data confirm that the presence of pMHCI/EABR APVs is sufficient to stimulate IFN-γ release from T cells harboring their cognate TCR, and that their stimulation is specific to those T cells that feature their cognate TCR. Future studies will explore whether the observed difference in IL-2 release induced by APVs, and their seemingly dynamic potency for inducing IFN-γ release, is consistent across *in vitro* T cell clonal types and *in vivo* models of disease.

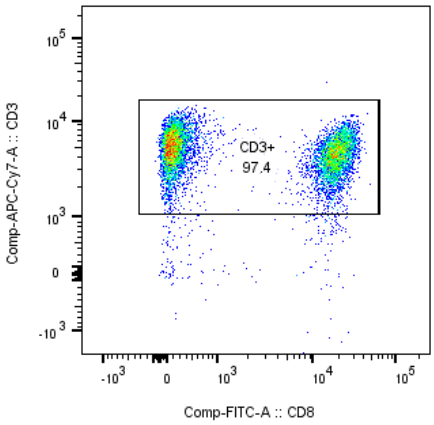

3095772_1G4_017.fcs
Single Cells
8126

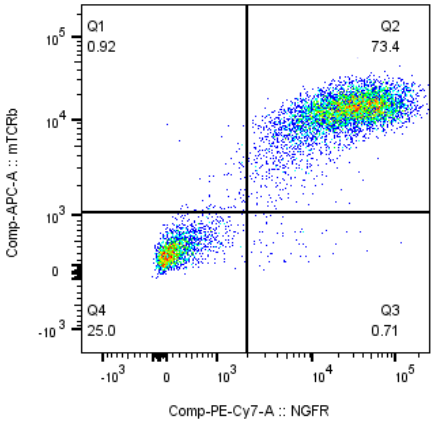

3095772_1G4_017.fcs
CD3+
7915

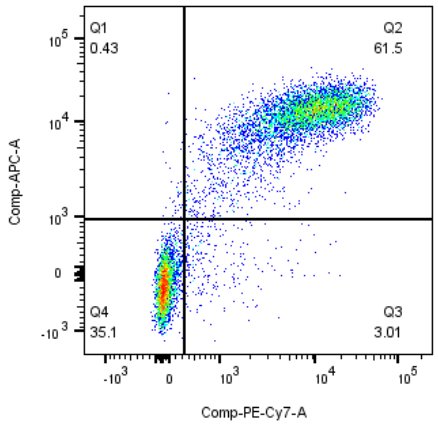

1G4_3108618_001.fcs
CD3+
8932

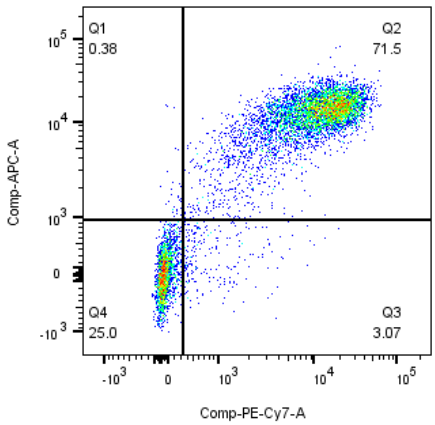

1G4_3112710_002.fcs
CD3+
8202

Figure S2.6. Flow cytometry of PBMCs after TCR transduction

Total PBMCs from healthy donors were retrieved, thawed, and activated using CD3/CD28 dynabeads to facilitate TCR overexpression through retroviral infection. The PBMCs were cultured in AIM V media supplemented with human AB serum, human IL-2, and human IL-15. Left: at the end of the 7 to 10-day culture period, we observed that over 90% of the cells were CD3+. The proportion of CD4+ and CD8+ cells varies depending on the individual donor. Right: transduction efficiency (NGFR) and TCR membrane trafficking (murine TCRβ or mTCRb) were assessed using flow cytometry on day 7. The three donors from Fig. 4B are shown here.

A

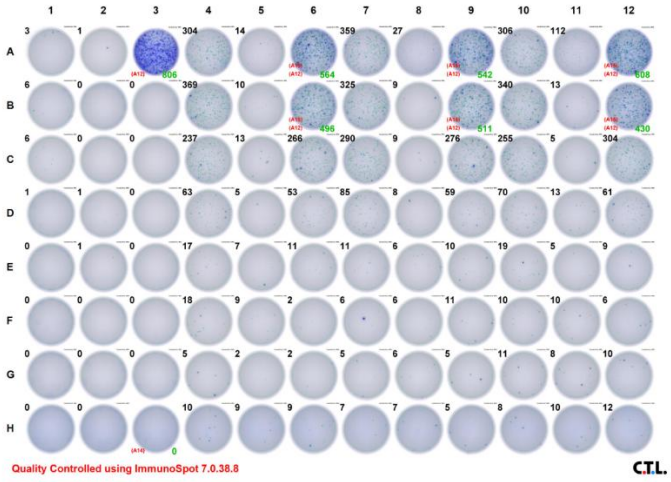
Quality Controlled using ImmunoSpot 7.0.38.8
C.T.L.

B

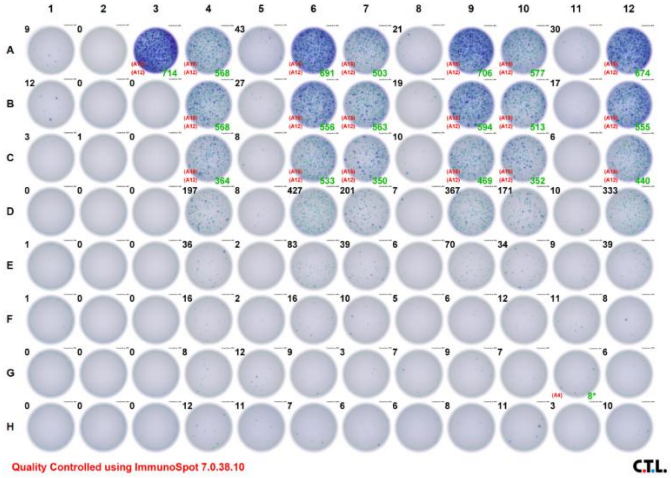
Quality Controlled using ImmunoSpot 7.0.38.10
C.T.L.

C

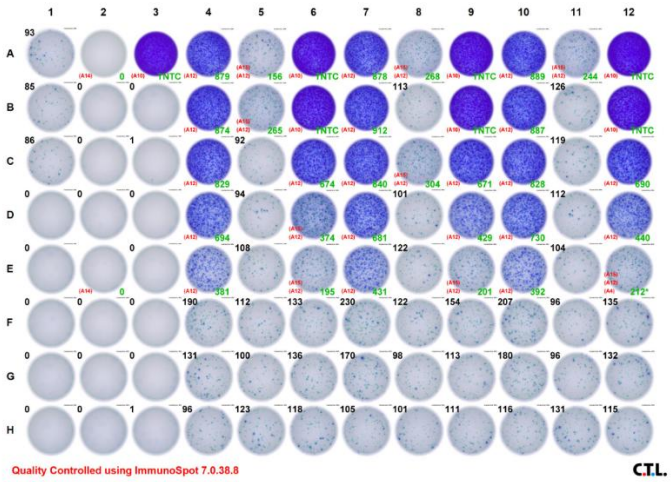
Quality Controlled using ImmunoSpot 7.0.38.8
C.T.L.

Figure S2.7. Scans of ELISPOT plates detecting IFN-γ release from donor T cells after APV co-incubation

(A-C) Scans of ELISPOT wells detecting IFN-γ release from donor T cells after being dosed with serial dilutions of SCT NYESO1/D9/EABR APVs (lanes 4,7,10), SCT MART1/D9/EABR APVs (lanes 5,8,11), and NYESO1:HLA-A2 tetramers (lanes 6,9,12); 1.5% PHA (lane 3, row A); without cells or antigen challenge (lane 2, rows A); and cells without antigen challenge (lane 1, rows A-C). (A) Donor 1; (B) Donor 2; (C) Donor 3.

2.3.5 EABR addition to MHCII α chain promotes budding of the complete pMHCII complex on APVs

Class I and class II pMHC nanoparticles have been previously demonstrated to generate similar, selective immunosuppressive therapeutic outcomes in animal models. However, whereas pMHCI nanoparticles *expanded* pre-existing, disease-generated memory-like autoregulatory $CD8^+$ T cells that arise spontaneously from low-avidity precursors,[86] pMHCII nanoparticles induced the *differentiation* of pathogenic antigen-experienced CD4+ T cells into disease-suppressing TR1 cells, which further induced the formation and recruitment of regulatory B cells.[102] Many cell-mediated autoimmune diseases are based on pMHCII epitopes, and a method for synthetically generating pMHCII APVs may improve the therapeutic potency of mRNA-based immunomodulation. Potentially more significant is that *differentiation* of pathogenic antigen-experienced CD4+ T cells by pMHCII nanoparticles would imply that pMHCII APVs may be useful as a general immunomodulator capable of reducing anti-drug antibodies or rescuing biologics or gene therapy vectors that fail in human trails due to unpredictable immunogenicity.

To generate pMHCII APVs from non-immune cells, we attached the EABR sequence[47] from the human CEP55[90] protein to either, or both, of the cytoplasmic tails of the α and β chains of MHCII (Fig. 2.5A). Further, to promote pMHCII formation with the intended peptide presented on the complete peptide:MHCII complex, the N-terminus of the α and β chains were optionally extended with a $3xG_4S$ linker connecting to the $E\alpha_{52\text{-}68}$ peptide (Fig. 2.5B).[103] Like pMHCI, SCT variants of pMHCII have been explored in previous work, and we

recreated the design from Thayer et al.[52] to compare against co-expression of the α and β chains without covalent glycine-serine linkers. Complete pMHCII complex formation on APVs purified by ultracentrifugation were assessed by immunoassays using the Y-Ae antibody specific for the complete $E\alpha_{52\text{-}68}$:I-A^b complex.

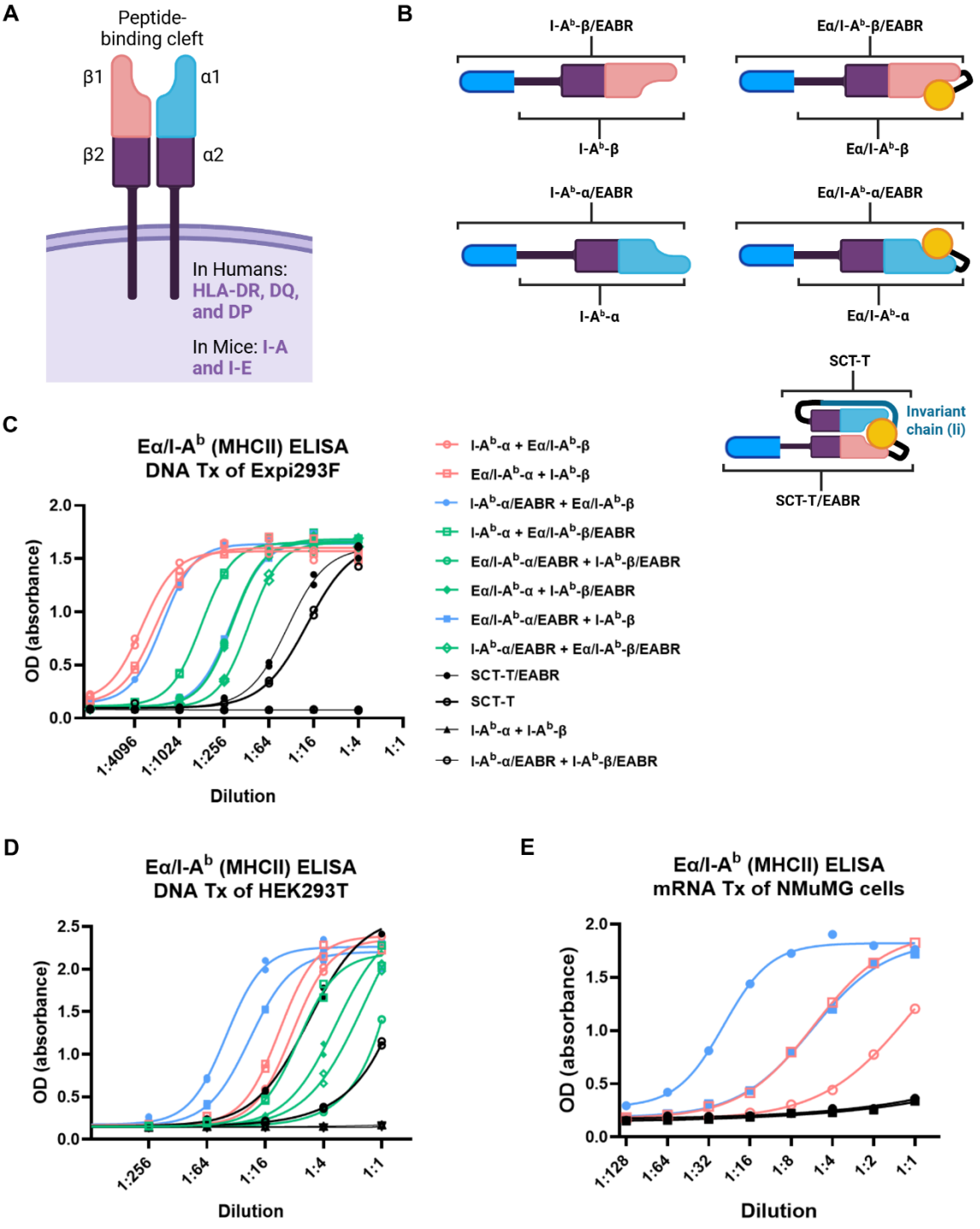

Figure 2.5. EABR addition to MHCII α chain promotes budding of the complete pMHCII complex on APVs

(A) Schematic of MHCII complex α chain and β chain forming the peptide binding cleft, and the naming scheme for MHCII in mice and humans.

(B) Naming convention for the different engineered MHCII α and β chains that include either the EABR vesicle-forming sequence appended to the cytoplasmic tail or the addition of an $Ealpha_{52\text{-}68}$ (Eα) presenting peptide appended to the N-terminal of the sequence with a Gly_3Ser spacer. The "SCT-T" variant uses the invariant chain to connect the α chain, presenting peptide, and β chain in a single-chain heterotrimer format first described in Thayer et al.[52]

(C-E) Sandwich ELISA of APVs purified by ultracentrifugation from transfected Expi293F, HEK293T, or NMuMG cells using anti-$Ea_{52\text{-}68}$:I-A^b (Y-Ae) for capture, biotinylated Y-Ae for detection, and HRP-conjugated streptavidin secondary (2 replicates per dilution). The Y-Ae antibody is specific for the complete Ea/I-A^b complex; the MHCII α chain, the MHCII β chain, and the Eα presenting peptide must all be present in a fully formed complex for Y-Ae to bind.

(C) Sandwich ELISA after DNA transfection of Expi293F cells.

(D) Sandwich ELISA after DNA transfection of HEK293T cells.

(E) Sandwich ELISA after mRNA transfection of murine NMuMG cells.

Interestingly, ELISA of pMHCII APVs that were generated from DNA transfection of Expi293F cells showed that addition of the EABR sequence, or covalently linking the subunits of pMHCII into a single-chain heterotrimer, did not improve upon the natural tendency of pMHCII to form APVs (Fig. 2.5C). Similar to pMHCI, we hypothesized that improved protein stability or protein over-expression in the relatively higher-expressing Expi293F cell lines might be leading to vesicle formation regardless of EABR addition.[99] Supporting this hypothesis is that our subsequent DNA transfection of the same constructs in lower-expressing HEK293T cells showed an improvement in the potency of EABR (Fig. 2.5D), a phenomenon that persisted upon mRNA transfection of NMuMG cells (Fig. 2.5E). While these early results support the conclusion that addition of EABR to the α chain of MHCII improves pMHCII APV release, ongoing work will seek to further improve pMHCII

yield and thermostability while we assay the relative immunological significance of APV formation for mRNA-based immunotherapies.

2.4 Discussion

Here, we present a new approach for generating immunomodulatory pMHCI-displaying APVs from non-immune cells. SCT pMHCI/EABR constructs containing a cytoplasmic EABR sequence[47] from the human centrosomal protein CEP55 recruit ESCRT proteins involved in cell division and viral budding to drive efficient assembly and release of pMHCI-displaying APVs. The lipid bilayer of the APV is expected to allow for pMHCI reorganization in the membrane and pMHCI clustering, both of which are considered important for the formation of a T cell stimulating immunological synapse. Purified pMHCI/EABR APVs elicited IFN-γ release from T cells, and the response was specific to T cells harboring the cognate TCR.

Unlike previous methods that have used viral coat proteins to induce budding,[32] the pMHCI/EABR construct does not require accessory proteins for vesicle release. Consequently, these pMHCI/EABR APVs could prove to be less immunogenic compared to other APV production methods as the pMHCI/EABR vesicles are composed of protein sequences already found in the human proteome. Thus, these T cell-targeting APVs, with putatively reduced immunogenicity and reduced potential for inducing release of IL-2 known for T cell proliferation and survival, could be applicable as a targeted immunosuppressive therapeutic for autoimmune diseases. As an example, the presenting peptides that were tested for SCT murine pMHCI H-2Kd in this study—NRP-V7 and $IGRP_{206-214}$—are two therapeutically relevant epitopes for a murine type 1 diabetes (T1D) model that showed promise as a T1D therapeutic *in vitro* when formulated as SCT IGRP/H-$2K^d$ tetramers[104]; these pMHCI complexes have also been conjugated to iron-oxide polymer nanoparticles and demonstrated *in vivo* efficacy as a targeted T1D therapy by selectively expanding the pool of antidiabetogenic memory-like autoregulatory CD8+ T cells,[86] suggesting a potential clinical application for the APVs described here.

As we demonstrated in this study, another advantage of using the EABR sequence for APV budding is that pMHCI APV assembly requires expression of only a single pMHCI/EABR protein and the corresponding gene construct could be delivered as an mRNA therapeutic. Previous work has explored the use of mRNA therapeutics for multiple sclerosis by delivering a mRNA-LNP therapeutic coding for an autogenic peptide with the goal of loading and presenting that peptide on the endogenous MHC that resides on, and is often limited to, the surface of the cell.[105] An mRNA therapeutic coding for pMHCI/EABR may result in increased presentation of the fully formed pMHCI complex on the cell surface in addition to the release of pMHCI-loaded APVs that could distribute throughout the body, mirroring the natural release of endogenous APVs seen during an immune response and potentially increasing their therapeutic effect.[33]

The increase in purified pMHCI product resulting from the single-chain construct may be due to the single-chain heterotrimer's increased stability.[91] The D9 variant in particular has previously been shown to have increased traffic to the cell surface and maintains a steady-state presence there by bypassing cellular quality control steps.[50] This increased cell surface expression and stability may be acting synergistically with the EABR sequence to increase APV budding and release in the comparatively lower-expressing HEK293T and NMuMG cell lines, which would make the pMHCI/EABR APV approach particularly powerful as an injectable mRNA therapeutic that would likely be translated in lower-expressing primary cells *in vivo*. Future studies will investigate whether pMHCI/EABR APVs, or lipid nanoparticles encapsulating mRNA encoding a pMHCI/EABR construct, are effective as an autoimmune therapy.

In summary, we present a new method for efficiently generating APVs from non-immune cells. We demonstrate that these APVs display complete pMHCI complexes and are capable of specific stimulation of cognate T cells, warranting further investigation as a potential cell-free therapeutic strategy for targeted immunoregulation.

2.5 Acknowledgements

We thank the NIH Tetramer Core Facility (contract number 75N93020D00005) for providing NYESO1:HLA-A*02:01 monomers and tetramers. We thank J. Vielmetter, A. Lam, and the Caltech Protein Expression Center for assistance with protein production; P. Gnanapragasam, A. Rorick, L. Segovia for cell culture reagents; W. Chour for MHC plasmid maps and helpful discussions. We thank D. Rees, R. Voorhees, N. Pierce, J. Keeffe, and M. Legendre for equipment access and training. We thank P. Bjorkman and O. Witte (UCLA) for helpful discussions. Immuno-electron microscopy was performed in the Caltech Cryo-EM Center with assistance from M. Ladinsky. Figures 1A, 1B, 1C, 1D, and 2C were created with Biorender.com. Research was sponsored by the U.S. Army Research Office and accomplished under cooperative agreement W911NF-19-2-0026 for the Institute for Collaborative Biotechnologies. The content of the information on this page does not necessarily reflect the position or policy of the Government, and no official endorsement should be inferred. This project has been made possible in part by grant 2023-332386 from the Chan Zuckerberg Initiative Donor Advised Fund (CZI DAF), an advised fund of the Silicon Valley Community Foundation.

2.6 Author Contributions

B.A.O., S.L.M., and R.M.M. conceived and designed the study and analyzed the data. M.A.G.H. participated in study design. B.A.O. constructed, expressed, and evaluated DNA constructs by western blot, ELISA, DLS, Immuno-EM, and ELISPOT. K.E.H.-T. performed SEC. Z.M. created and provided 1G4 transduced T cells. B.A.O wrote the first draft of the manuscript. All authors participated in editing the manuscript.

2.7 Methods

Key resources table

REAGENT or RESOURCE	SOURCE	IDENTIFIER
Antibodies		
HLA-A Polyclonal Antibody	Thermo Fisher Scientific	Cat# PA5-29911 RRID: AB_2547385
Recombinant Anti-HLA-A2-peptide (SLLMWITQV) Complex (3M4E5) Mouse Monoclonal Antibody	ProteoGenix	Reference: RHM03002-100

Purified anti-human CD81 (TAPA-1) Antibody	Biolegend	Cat# 349502 RRID: AB_10643417
Biotin anti-human CD81 (TAPA-1) Antibody	Biolegend	Cat# 349514 RRID: AB_2572038
Ultra-LEAF™ Purified anti-human CD63 Antibody	Biolegend	Cat# 353039 RRID: AB_2800940
Biotin anti-human CD63 Antibody	Biolegend	Cat# 353017 RRID: AB_2561675
Goat Anti-Human IgG Fc, Multi-Species SP ads-HRP	SouthernBiotech	Cat# 2014-05 RRID: AB_2795580
Goat Anti-Mouse IgG Fc, Human/Bovine/Horse SP ads-HRP	SouthernBiotech	Cat# 1013-05 RRID: AB_2794190
Goat Anti-Rabbit IgG Fab, Mouse/Human SP ads-HRP	SouthernBiotech	Cat# 4058-05 RRID: AB_2795982
Goat anti-Rabbit IgG (H+L) Highly Cross-Adsorbed Secondary Antibody, Alexa Fluor™ Plus 488	Thermo Fisher Scientific	Cat# A32731 RRID: AB_2633280
Goat anti-Mouse IgG (H+L), Superclonal™ Recombinant Secondary Antibody, Alexa Fluor™ Plus 488	Thermo Fisher Scientific	Cat# A55058 RRID: AB_2921066
MHC Class I (H-2Kd/H-2Dd) Monoclonal Antibody (34-1-2S)	Thermo Fisher Scientific	Cat# 14-5998-82 RRID: AB_467822
MHC Class I (H-2Kd/H-2Dd) Monoclonal Antibody (34-1-2S), Biotin	Thermo Fisher Scientific	Cat# 13-5998-82 RRID: AB_466872
beta-2 Microglobulin Monoclonal Antibody (34)	Thermo Fisher Scientific	Cat#: MA5-36022 RRID: AB_2866634
6 nm Colloidal Gold AffiniPure™ Goat Anti-Rabbit IgG (H+L) (EM Grade)	Jackson ImmunoResearch	Cat# 111-195-144 RRID: AB_2338015
Bacterial and virus strains		
E. coli DH5 Alpha	Zymo Research	Cat# T3009
Chemicals, peptides, and recombinant proteins		
Luria Broth Base (Miller's LB Broth Base), powder	Thermo Fisher Scientific	Cat# 12795084
Dulbecco's Modified Eagle Medium (DMEM)	Gibco	Cat# 11995-065
Fetal bovine serum (FBS)	R&D Systems	Cat# S12450H
Penicillin-Streptomycin	Gibco	Cat# 15-140-122
FuGENE® HD Transfection Reagent	Promega	Cat# E2311
OPTI-MEM I Reduced Serum Medium	Gibco	Cat# 31985-062
Expi293 Expression Medium	Gibco	Cat# A14351-01
Expi293 Transfection Kit	Gibco	Cat# A14524
mMESSAGE mMACHINE™ T7 Transcription Kit	Invitrogen	Cat# AM1344
MEGAclear™ Transcription Clean-Up Kit	Invitrogen	Cat# AM1908
RiboRuler High Range RNA Ladder	Thermo Fisher Scientific	Cat# SM1821
RNase AWAY™ Surface Decontaminant	Thermo Fisher Scientific	Cat# 21-402-178
SeeBlue Plus2 Prestained Standard	Thermo Fisher Scientific	Cat# LC5925
NuPAGE™ LDS Sample Buffer	Thermo Fisher Scientific	Cat# NP0007
20X Bolt™ MES SDS Running Buffer	Thermo Fisher Scientific	Cat# B0002
NucleoBond™ Xtra Maxi Plus	Macherey-Nagel	Cat# 12758412

Zyppy Plasmid Miniprep Kit	Zymo Research	Cat# D4019
Sucrose	Sigma-Aldrich	Cat# S5016-1KG
NaCl	Fisher Scientific	Cat# BP358-212
Sodium hydroxide	Macron Chemicals	Cat# 7708-10
Sodium bicarbonate	Macron Chemicals	Cat# 7412-12
Sodium phosphate dibasic	Sigma-Aldrich	Cat# 04272-1KG
Tris-HCl	Fisher Scientific	Cat# BP153-1
TWEEN® 20	Sigma-Aldrich	Cat# P1379-500ML
BSA	Sigma-Aldrich	Cat# B4287-5G
Trypsin	Gibco	Cat# 25200-056
L-glutamine	Gibco	Cat# 25030-149
Phytohemagglutinin, M form	Gibco	Cat# 10576015
Paraformaldehyde 16% Aqueous Solution EM Grade	Electron Microscopy Sciences	Cat# 15710
Uranyl Formate	Electron Microscopy Sciences	Cat# 22451
Biotinylated NYESO1-HLA-A*02:01 monomer	NIH Tetramer Core Facility at Emory	Task order# 73345
Unlabeled NYESO1-HLA-A*02:01 monomer	NIH Tetramer Core Facility at Emory	Task order# 74599
Unlabeled NYESO1-HLA-A*02:01 tetramer	NIH Tetramer Core Facility at Emory	Task order# 73346, 78618
1-Step™ Ultra TMB-ELISA Substrate Solution	Thermo Fisher Scientific	Cat# 34029
EZ-Link NHS-PEG4 Biotinylation Kit	Thermo Fisher Scientific	Cat# 21455
Streptavidin (HRP)	Abcam	Cat# AB7403
Critical commercial assays		
Human IFN-γ Single-Color ELISPOT- Rapid	ImmunoSpot	Cat# hIFNgp-1M/5-Rapid
Human IFN-γ / IL-10 / IL-2 Three-Color Fluorospot	ImmunoSpot	Cat# hT3025Fp
Bolt™ Bis-Tris Plus Mini Protein Gels, 4-12%, 1.0 mm, WedgeWell™ format	Thermo Fisher Scientific	Cat# NW04120BOX
iBlot2 NC Mini Stacks	Thermo Fisher Scientific	Cat# IB23002
iBind Cards	Thermo Fisher Scientific	Cat# SLF1010
iBind Flex Fluorescent Detection (FD) Solution Kit	Thermo Fisher Scientific	Cat# SLF2019
iBlot2 Gel Transfer Device	Thermo Fisher Scientific	Cat# IB21001
Experimental models: Cell lines		
HEK293T cells	[106]	RRID:CVCL_0063
Expi293F cells	Gibco	RRID:CVCL_D615
NMuMG cells	ATCC	CRL-1636
Recombinant DNA		
HLA-A2-peptide (SLLMWITQV) Complex (3M4E5) Human Monoclonal Antibody heavy chain	[94]	https://patentscope.wipo.int/search/en/detail.jsf?docId=EP32586798
HLA-A2-peptide (SLLMWITQV) Complex (3M4E5) Human Monoclonal Antibody light chain	[94]	https://patentscope.wipo.int/search/en/detail.jsf?docId=EP32586798

p3BNC-SARS-CoV-2 S-2P-DCT-EABR (a.k.a. SARSCoV2-S/EPM/EABR)	[47]	doi:10.1016/j.cell.2023.04.024
D1 SCT MART1/ HLA-A*02:01	This paper	N/A
D1 SCT MART1/ HLA-A*02:01/EABR	This paper	N/A
D9 SCT MART1/ HLA-A*02:01	This paper	N/A
D9 SCT MART1/ HLA-A*02:01/EABR	This paper	N/A
D1 SCT NYESO1/ HLA-A*02:01	This paper	N/A
D1 SCT NYESO1/HLA-A*02:01/EABR	This paper	N/A
D9 SCT NYESO1/ HLA-A*02:01/MHCI	This paper	N/A
D9 SCT NYESO1/ HLA-A*02:01/EABR	This paper	N/A
NYESO1/β2M	This paper	N/A
β2M	This paper	N/A
D9 SCD β2M/ HLA-A*02:01	This paper	N/A
D9 SCD β2M/ HLA-A*02:01/EABR	This paper	N/A
D9 HLA-A*02:01 HC	This paper	N/A
D9 HLA-A*02:01 HC/EABR	This paper	N/A
CD81	This paper	N/A
CD81/EABR	This paper	N/A
CD63	This paper	N/A
CD63/EABR	This paper	N/A
NRP-V7/H-2Kd	This paper	N/A
NRP-V7/D9_H-2Kd	This paper	N/A
IGRP/H-2Kd	This paper	N/A
IGRP/D9_H-2Kd	This paper	N/A
NYESO1/D9/H-2Db	This paper	N/A
NYESO1/D9/H-2Db/EABR	This paper	N/A
NYESO1/D9/H-2Kb	This paper	N/A
NYESO1/D9/H-2Kb/EABR	This paper	N/A
Software and algorithms		
Image J 1.54f	NIH	https://imagej.net/ RRID: SCR_003070
Prism 10.3.1	GraphPad	
Other		
Amicon Ultra-15 100 kDa MWCO Centrifugal Filter Unit	EMD Millipore	Cat# UFC910096
Amicon Ultra-4 10 kDa MWCO Centrifugal Filter Unit	EMD Millipore	Cat# UFC801024
Nanosep with 100K Omega	Pall Life Sciences	Cat# OD100C34
Erlenmeyer cell culture flasks - 500mL	Corning	Cat# 431145
6-well Clear Flat Bottom TC-treated Multiwell Cell Culture Plate, with Lid	Falcon	Cat# 353046
30 mL BD Luer-Lok™ Syringe	BD	Cat# 302832
3 mL BD Luer-Lok™ Syringe	BD	Cat# 309657
AirOtop enhanced seal for 125 ml ultra yield flask	VWR	Cat# 899421
Costar® Spin-X® Centrifuge Tube Filters, 0.22 µm Pore CA Membrane	Corning	Cat# 8160
Polycarbonate centrifuge tubes	Beckman Coulter	Cat# 349622

0.45um syringe filter	Corning	Cat# 431220
0.2um syringe Filter	VWR	Cat# 28143-300
Nalgene™ Rapid-Flow™ Sterile Disposable Filter Unit - 0.45um	Thermo Fisher Scientific	Cat# 156-4045
Costar high binding plates, 96-well	Corning	Cat# 9018
TempPlate Sealing Foil	USA Scientific	Cat# 2923-0100
HiTrap MabSelect	Cytiva	Cat# 28408253
Superose 6 Increase 10/300 column	Cytiva	Cat# 29-0915-96
HiLoad 16/600 Superdex 200 column	Cytiva	Cat# 28-9893-35
Formvar/Carbon 300 Mesh grids	Electron Microscopy Sciences	Cat# FCF300-Cu-50

Experimental Model and Subject Details

Bacteria

E. coli DH5 Alpha cells (Zymo Research) used for expression plasmid productions were cultured in LB broth (Sigma-Aldrich) with shaking at 225 rpm at 37 °C. Plasmids were purified for transfection using Zymogen miniprep kits (Zymo Research) or maxiprep kits (Macherey-Nagel).

Cell lines

HEK293T cells plated in 6-well plates (Falcon) were cultured in Dulbecco's modified Eagle's medium (DMEM, Gibco) supplemented with 10% heat-inactivated fetal bovine serum (FBS, R&D Systems) and 1 U/mL penicillin-streptomycin (Gibco) at 37 °C and 5% CO_2. Transfections were carried out with FuGENE transfection reagent (Promega) diluted in Opti-MEM (Gibco). Expi293F cells (Gibco) for APV expression and antibody expression were maintained at 37 °C and 8% CO_2 in Expi293 expression medium (Gibco). Transfections were carried out with an Expi293 Expression System Kit (Gibco). Falcon tubes sealed with AirOtops (VWR) or culture flasks (Corning) containing Expi293F cells were maintained under shaking at 470 rpm for 10-30 mL transfections and 130 rpm for transfections larger than 30 mL. Expi293F and HEK293T cell lines were derived from female donors and were not specially authenticated. NMuMG cells plated in 6-well plates (Falcon) were cultured in Dulbecco's modified Eagle's medium (DMEM, Gibco) supplemented with 10% heat-inactivated fetal bovine serum (FBS, R&D Systems) and 10 ug/mL insulin (Gibco) at 37 °C and 5% CO2. Transfections were carried out with Invitrogen Lipofectamine MessengerMAX

Transfection Reagent (Invitrogen) diluted in Opti-MEM (Gibco). Transfection mRNA was synthesized using the mMessage mMachine T7 Transcription Kit (Invitrogen) and purified with the MEGAclear™ Transcription Clean-Up Kit (Invitrogen) according to the manufacturer's instructions.

T cells

T cells were isolated from human donor whole blood samples by negative selection using the RosetteSep Human T Cell Enrichment Cocktail Kit (STEMCELL Technologies). Isolated T cells were seeded in a fresh complete ImmunoCult™-XF T cell expansion medium (STEMCELL Technologies) at 1 x 10^6 cells/mL with 2 µL/mL ImmunoCult™ human CD3/CD28 T cell activator. T cells were activated for 3 days and expanded for up to 12 days by changing into fresh expansion medium every 2-3 days. All cells were cultured in incubators at 37 °C and 5% CO_2.

Design of EABR constructs

The EABR sequence was identical to the sequence used by Hoffmann et al. to create SARS-CoV2-S eVLPs.[47] Briefly, the EABR domain (residues 160-217) of the human CEP55 protein was fused to the C-terminus of the SCT MART1/HLA-A*02:01 α chain separated by a $(Gly)_3Ser$ (GS) linker to generate "D1" and "D9" single-chain heterotrimer pMHCI constructs inserted in the p3BNC expression plasmid. To generate the "D1" SCT construct, the N-terminus of the HLA-A*02:01 α chain was extended with a 4x(G_4S) linker connecting to the C-terminus of β2M, which was itself extended at its N-terminus by a 3x(G_4S) linker connecting to either the 10-mer MART1 (ELAGIGILTV) or 9-mer NYESO1 (SLLMWITQV) cancer-related peptides to make a single-chain heterotrimer (SCT)[91] (Fig. 2.1B). To generate the SCT "D9" construct, the "D1" SCT construct was edited with Y84C and A139C substitutions.[50]

The "single-chain dimer" (SCD) construct removed both the peptide and the 3x(G_4S) linker between the peptide and β2M of the "D9" SCT construct. The "heavy chain" (HC) construct removed the peptide, the 3x(G_4S) linker between the peptide and β2M, β2M, and the 4x(G_4S)

linker between β2M and the MHCI heavy chain of the "D9" SCT construct (Fig. 2.2C). Both the SCD and HC constructs were inserted in p3BNC expression plasmids.

Murine SCT MHCI H-2Kd was constructed similar to the human D1 SCT HLA-A*02:01 design, with either an NRP-V7 or $IGRP_{206-214}$ presenting peptide fused to a 3x(Gly_4Ser) linker, murine β2M, a 4x(Gly_4Ser) linker, and the H-2Kd heavy chain, i.e., NRP-V7/H-2Kd and $IGRP_{206-214}$/H-2Kd, respectively. The chimeric human/mouse MHCI HLA-A2/H-2Db and HLA-A2/H-2Kb were designed according to the D9 SCT design, with an NYESO1 presenting peptide fused to a 3x(Gly_4Ser) linker, human β2M, a 4x(Gly_4Ser) linker, and a chimeric MHCI α chain composed of the extracellular α1 and α2 domains of human Y84A,A139C HLA-A*02:01 heavy chain and the α3, transmembrane, and cytoplasmic domains of murine H-2Kb or H-2Db heavy chain, i.e., NYESO1/A2_D9/H-2Db and NYESO1/A2_D9/H-2Kb, respectively. Murine and chimeric human/murine SCT pMHCI constructs were inserted into the p3BNC expression plasmid.

Production of EABR APVs

EABR APVs were generated by one of three means: 1) transfecting Expi293F cells (Gibco) cultured in Expi293F expression media (Gibco) on an orbital shaker at 37 °C and 8% CO2 with plasmid DNA pre-filtered through 0.22 μm Spin-X filters (Corning); 2) transfecting HEK293T cells cultured in Dulbecco's modified Eagle's medium (DMEM, Gibco) supplemented with 10% heat-inactivated fetal bovine serum (FBS, Sigma-Aldrich) and 1 U/ml penicillin-streptomycin (Gibco) at 37 °C and 5% CO_2. 3) transfecting NMuMG cells cultured in Dulbecco's modified Eagle's medium with 4.5 g/L glucose (DMEM, Gibco) supplemented with 10% heat-inactivated fetal bovine serum (FBS, Sigma-Aldrich) and 10ug/mL insulin at 37 °C and 5% CO2. 72 hours post-transfection, cells were centrifuged at 1000 x g for 10 min, supernatants were passed through a 0.45 um filter (Corning) with Luer-Lok syringes (BD) or a 0.45 um vacuum filter (Thermo Fisher Scientific), and concentrated using Amicon Ultra-15 centrifugal filters with 100 kDa molecular weight cut-off (Millipore). APVs were purified by ultracentrifugation at 50,000 rpm (135,000 x g) for 2 hours at 4 °C using a TLA100.3 rotor and an OptimaTM TLX ultracentrifuge (Beckman Coulter) on a

20% w/v sucrose cushion in polycarbonate centrifuge tubes (Beckman Coulter). Supernatants and the sucrose cushion were removed, and pellets were re-suspended in 200 uL sterile pH 7.4 PBS at 4 °C overnight. To remove residual cell debris, re-suspended samples were transferred to microcentrifuge tubes and centrifuged at 10,000 x g for 10 min; clarified supernatants were collected for subsequent ELISA, DLS, and western blot assays. For immuno-EM grid preparations, quantitative western blots, and ELISPOT assays, APVs were further purified by SEC using a Superose 6 Increase 10/300 column (Cytiva) equilibrated with pH 7.4 PBS. Peak fractions in the void volume corresponding to pMHCI APVs were combined and concentrated to 250-500 uL in Amicon Ultra-4 centrifugal filters with 100 kDa molecular weight cut-off (Millipore) or Nanosep with 100K Omega centrifugal filters (Pall). Samples were stored at 4 °C and imaged directly after purification.

Transduction of TCRs in PBMC

Peripheral blood mononuclear cells (PBMCs) were isolated and processed following a previously published protocol with some modifications.[107] The MSGV retroviral backbone was utilized to overexpress the target T cell receptors (TCRs) with a truncated human nerve growth factor receptor (tNGFR) serving as the transduction marker. TCR alpha and beta chains were expressed with a F2A linker to maintain approximately equal copy numbers. To reduce mispairing with endogenous human TCRs, the human TCR constant regions were replaced with murine constant regions. Commercially obtained, cryopreserved PBMCs from healthy donors (AllCells) were revived in T cell media (TCM) comprising AIM V media (Thermo Fisher, #12055-091), 5% Human AB serum (Omega Scientific), 50 U/mL human recombinant IL-2 (Peprotech, #200-02), 1 ng/mL human recombinant IL-15 (Peprotech, #200-15), 1X Glutamax (Thermo Fisher, 35050-061), and 50 μM β-mercaptoethanol. These cells were mixed with CD3/CD28 dynabeads (Thermo Fisher, #11132D) at a concentration of 25 μL beads per million PBMCs and incubated overnight at 37°C and 5% CO2 (day 0). On days 1 and 2, TCR-expressing retroviral supernatant was added at a ratio of 2 mL per two million PBMCs, followed by a 90-minute spin infection at 1,350 x g and 30°C. Excess retrovirus was removed on day 3 with a phosphate-buffered saline (PBS) wash, and cells were resuspended in TCM. CD3/CD28 dynabeads were removed using magnets on day 5,

and PBMCs were maintained in TCM at a concentration of one million cells per mL. Cell phenotypes (CD3, CD8), transduction efficiency (NGFR) and TCR membrane trafficking (murine TCRβ or mTCRb) were assessed using flow cytometry on day 7. For long-term storage, transduced PBMCs were preserved in CryoStor CS10 serum-free cryopreservation medium (STEMCELL Technologies #07930) at -80°C overnight before transferring to liquid nitrogen.

Antibody Expression

Anti-HLA-A2-peptide (SLLMWITQV) Complex (3M4E5) antibody was made in-house by expressing the heavy chain and light chain of the 3M4E5 antibody at a 1.5:1 plasmid ratio in Expi293F cells.[94] Supernatant from the transiently-transfected Expi293F cells (Gibco) was separated from the cells by pelleting at 3500g for 15 minutes and filtering the clarified supernatant through a 0.2 um syringe filter (VWR) or 0.45 um vacuum filter unit (Thermo Fisher Scientific). The filtered supernatant was further purified using Fc-affinity chromatography (HiTrap MabSelect, Cytiva) and SEC (HiLoad 16/600 Superdex 200 column, Cytiva). Peak fractions corresponding to purified antibody proteins were pooled, concentrated, and stored at 4 °C. Biotinylated antibodies for ELISAs were generated and purified using an EZ-Link biotinylation kit (Thermo Fisher Scientific). The in-house generated antibody was compared to a commercially available 3M4E5 antibody (RHM03002-100; ProteoGenix) with ELISA and showed identical performance (data available upon request).

Western blot analysis

The presence of HLA-A on purified APVs was detected by Western blot analysis. Samples were diluted in NuPage SDS-PAGE loading buffer (Thermo Fisher Scientific) under reducing conditions, separated on Bolt™ Bis-Tris Plus Mini Protein Gels, 4-12% (Thermo Fisher Scientific), and transferred to nitrocellulose membranes in the form of an iBlot2 NC Mini Stack (Thermo Fisher Scientific) using the iBlot2 Gel Transfer Device (Thermo Fisher Scientific). Nitrocellulose membranes from the stack were transferred to water for 1-5 minutes, then transferred to Flex FD solution (Thermo Fisher Scientific), before placing on

an iBind card (Thermo Fisher Scientific) for staining with antibodies per the iBlot2 protocol. The following antibodies were used for detecting pMHCI: rabbit anti-HLA-A protein (PA5-29911; Thermo Fisher Scientific) at 1:1,000, mouse anti-β2M protein (MA5-36022; Thermo Fisher Scientific) at 1:1,000, Alex488-conjugated goat anti-rabbit IgG (A32731; Thermo Fisher Scientific) at 1:1,000, and Alex488-conjugated goat anti-mouse IgG (A55058; Thermo Fisher Scientific) at 1:1,000. Protein was compared to a SeeBlue Plus2 Prestained protein ladder (Thermo Fisher Scientific). For T cell studies, the amount of MHCI on APVs was determined by quantitative Western blot analysis. Various dilutions of SEC-purified pMHCI APV samples and known amounts of soluble, biotinylated pMHCI protein (NIH Tetramer Core Facility at Emory) were separated by SDS-PAGE and transferred to nitrocellulose membranes as described above. Band intensities of the pMHCI standards and pMHCI APV sample dilutions were measured using ImageJ to determine MHCI concentrations.

Mass Spectrometry

Expi293F cells were DNA transfected with NYESO1/D9/EABR or NYESO1/D9 pMHCI constructs, and supernatant was concentrated using 100kDa MWCO (EMD Millipore; #UFC910096) to be ultracentrifuged on a 20% w/v sucrose cushion before SEC purification. Elution volumes corresponding with extracellular vesicles (Fig. 2.1D) were collected, digested with trypsin, and run on an Orbitrap Eclipse Tribrid Mass Spectrometer. Proteins were searched and identified against the human proteome using Proteome Discoverer 3.2.

Immuno-EM of pMHCI/EABR APVs

SEC-purified MART1/MHCI/EABR APVs were prepared on grids for negative stain transmission electron microscopy at room temperature. Formvar/Carbon 300 Mesh grids (Electron Microscopy Sciences) were first glow discharged. 20 uL of purified sample was pipetted onto paraffin, glow discharged formvar/carbon 300 mesh grids were placed on the droplet of sample for 5 minutes, then gently wicked away by dabbing the edge of the grid on filter paper. The grids were then placed on a 20uL droplet of 1% paraformaldehyde (Electron Microscopy Sciences) in pH 7.4 PBS for 10 minutes, and subsequently wicked away. Grids

were washed three times by placing the grids on droplets of pH 7.4 PBS for 5 minutes, and wicking away the PBS with filter paper after each wash. Grids were then blocked by placing the grids on droplets of 5% FBS diluted in pH 7.4 PBS for one hour. Blocking solution was wicked away from the grids, and the grids were then placed on droplets of rabbit anti-HLA-A antibody (PA5-29911; Thermo Fisher Scientific) diluted 1:100 dilution in 5% sucrose, 5% FBS pH 7.4 PBS for 2 hours; to prevent drying of the primary antibody solution, the grids were placed in a humidified chamber made from wet paper towels folded under a pyrex glass dish. Grids were again washed three times by placing the grids on droplets of pH 7.4 PBS for 10 minutes, and wicking away the PBS with filter paper after each wash. The grids were then placed on droplets of 6 nm colloidal gold goat anti-rabbit antibody (PA5-29911; Thermo Fisher Scientific) diluted 1:20 dilution in 5% sucrose, 5% FBS pH 7.4 PBS for 1 hour. Grids were then washed three times, ten minutes per wash with pH 7.4 PBS, wicking away the PBS after the ten minute wash each time. Finally, the grid was placed on a droplet of 1.5% uranyl formate (Electron Microscopy Sciences), prepared fresh within 1 week of use, for 1 minute. The excess uranyl formate was wicked away and the grid was left to air dry for 30 minutes before storing at room temperature away from light. Imaging of the grids was performed on a FEI Tecnai T12 Transmission Electron Microscope within two weeks after the grids were prepared.

Indirect ELISA

96-well plates (Corning) were coated with APV samples diluted 1:10 or 1:4 or 1:1, 4-fold serially diluted in sterile 0.1 M $NaHCO_3$ pH 9.6, and sealed with TempPlate sealing foil (USA Scientific) overnight at 4 °C. Plates were emptied and blocked with TBS-T/3% BSA (Sigma-Aldrich) for at least 30 minutes. Plates were again emptied, and 5 ug/mL of primary antibody diluted in TBS-T/3% BSA was added to the plates. The following were used as primary antibodies for detecting pMHCI: rabbit anti-HLA-A antibody (PA5-29911; Thermo Fisher Scientific), mouse anti-HLA-A2-peptide (SLLMWITQV) Complex (3M4E5) antibody (RHM03002-100; ProteoGenix), mouse anti-H-2Kd antibody (14-5998-82; Thermo Fisher Scientific).

After a 2-hour incubation at room temperature, plates were emptied, washed three times with TBS-T, and 5 ug/mL of HRP-conjugated secondary antibody diluted in TBS-T/3% BSA was added to the plates for 30 minutes at room temperature. The following were used as secondary antibodies: HRP-conjugated goat anti-rabbit IgG (4058-05; Southern Biotech) at 1:2,000, HRP-conjugated goat anti-mouse IgG (1013-05; Southern Biotech) at 1:2,000.

After washing three times with TBS-T, plates were developed using 1-Step™ Ultra TMB-ELISA Substrate Solution (Thermo Fisher Scientific) and absorbance was measured at 450 nm. Standard 4-parameter sigmoidal binding curves were calculated using GraphPad Prism 10.3.1 without any further editing.

Sandwich ELISA

96-well plates (Corning) were coated with 5 ug/mL of mouse anti-HLA-A2-peptide (SLLMWITQV) Complex (3M4E5) antibody (RHM03002-100; ProteoGenix) or in-house-made anti-HLA-A2-peptide (SLLMWITQV) Complex (3M4E5) antibody diluted in sterile 0.1 M $NaHCO_3$ pH 9.6, and sealed with TempPlate sealing foil (USA Scientific) overnight at 4 °C. Plates were emptied and blocked with TBS-T/3% BSA for at least 30 minutes. Plates were again emptied, and APV samples diluted 1:10 or 1:4, 4-fold serially diluted in TBS-T/3% BSA were added to the plates. After a 2-hour incubation at room temperature, plates were emptied, and 5 ug/mL of biotinylated detection antibody diluted in TBS-T/3% BSA was added to the plates. 5 ug/mL of biotinylated (Thermo Fisher Scientific) mouse anti-HLA-A2-peptide (SLLMWITQV) Complex (3M4E5) antibody (RHM03002-100; ProteoGenix) or in-house-generated human anti-HLA-A2-peptide (SLLMWITQV) Complex (3M4E5) antibody was used as a capture antibody. After another 2-hour incubation at room temperature, plates were washed three times with TBS-T. HRP-conjugated streptavidin (Abcam) was diluted to manufacturer's recommendations in TBS-T/3% BSA and added to plates for 30 minutes at room temperature. After washing three times with TBS-T, plates were developed using 1-Step™ Ultra TMB-ELISA Substrate Solution (Thermo Fisher Scientific) and absorbance was measured at 450 nm. Standard 4-parameter sigmoidal binding curves were calculated using GraphPad Prism 10.3.1 without any further editing.

ELISPOT

1G4 T cells were centrifuged at 300g for 10 min, and resuspended in CTL-Test^{TM} media (ImmunoSpot) containing 1% L-glutamine (Gibco) for ELISPOT analysis to evaluate T cell responses. APVs were added to human IFN-g single-color ELISPOT plates (ImmunoSpot) and 10-fold serially diluted. Phytohemagglutinin (Gibco) was added in a separate well at a final concentration of 1.5% as a positive control. 100,000 cells were added per well, and plates were incubated at 37 °C in 8% CO_2 for 24 hours. Biotinylated detection, streptavidin-alkaline phosphatase (AP), and substrate solutions were added according to the manufacturer's guidelines. Plates were gently rinsed with water three times to stop the reactions. Plates were air-dried for two hours in a running laminar flow hood. The number of spots and the mean spot sizes were quantified using a CTL ImmunoSpot S6 Universal-V Analyzer (Immunospot).

Quantification and Statistical Analysis

ELISA serial dilutions were plotted by fitting a standard sigmoidal four parameter logistic curve without weighting or special handling of outliers using Graphpad Prism 10.3.1. Statistical significance in IFN-γ ELISPOT data was calculated using multiple unpaired t-tests with Welch correction and Holm-Šídák's multiple comparison tests to obtain adjusted p-values in Graphpad Prism 10.3.1; adjusted p-values are reported for comparisons of the maximum concentrations. Statistical significance in IL-2 ELISPOT data was calculated using two-tailed unpaired t-tests with Welch's correction to obtain p-values in Graphpad Prism 10.3.1.

Chapter 3

FUNCTIONALIZING HYDROGELS WITH ESCRT-MEDIATED VESICLES IMPROVES T CELL CAPTURE & ACTIVATION FOR HIGH-THROUGHPUT SCREENING

Adapted from:

Olson, B. A., Mellody, M., Soemardy, C., Mao, Z., Mei, A., Lippert, K., Hoffmann, M. A. G., Carlo, D. D., & Mayo, S. L. (2025). Functionalizing hydrogel nanovials with vesicles mimicking antigen-presenting vesicles and cancer exosomes improves T cell capture and activation. *bioRxiv*, 2025.2006.2024.661128. https://doi.org/10.1101/2025.06.24.661128

3.1 Abstract

Recent advances have demonstrated the application of microcavity-containing hydrogel microparticles, known as nanovials, for the massively parallel and high-throughput screening of therapeutic T cell populations for adoptive cell therapies. Nanovial cavities coated with peptide-MHC (pMHC) or antigen tetramers selectively bind to their cognate T cell receptor (TCR) or chimeric antigen receptor (CAR) to activate T cells and capture secreted cytokines. However, binding of tetramers or recombinantly expressed antigen by T cells is not always correlated with T cell activation or cytotoxicity as the binding interface is not fully representative of the natural immunological synapse formed between T cells and professional antigen-presenting cells (APCs). Here, we leverage the recent discovery of an ESCRT- and ALIX-binding region (EABR) sequence to generate antigen-presenting vesicles and cancer-mimicking exosomes from standard HEK293T and Expi293F cell cultures. EABR-mediated vesicles present natural, full-length oncologically-relevant membrane proteins embedded in lipid bilayers to functionalize the nanovial cavity with cell-like membranes. These hydrogel nanovials functionalized with the EABR-mediated vesicles show improved T cell capture of 1G4 T cells and enhanced activation of HER2 CAR-T cells compared to hydrogel surfaces functionalized with recombinantly-expressed soluble proteins.

3.2 Introduction

Adoptive cell therapy has shown remarkable effectiveness in the treatment of advanced hematological malignancies, and chimeric antigen receptor (CAR) T cell therapy has achieved high rates of complete recovery in patients with treatment-resistant, relapsed or refractory B cell malignancies[108-113]. However, a major hurdle in developing effective immunotherapies is the identification of reactive TCRs or CARs that can recognize targets with sufficient affinity, selectivity, and potency[114]. Further, the T cells that are identified to harbor a reactive TCR of sufficient affinity are often limited by suboptimal *ex vivo* T cell expansion rates and final T cell products ultimately have dysfunctional or limited clinical functionality[115,116]. Current tools for enriching and screening promising T cell populations typically rely on TCR or CAR affinity by staining with peptide-MHC (pMHC) or antigen tetramers. However, binding of multimers to T cells is not always correlated with T cell activation or cytotoxicity[117] as the context in which these pMHC signals are presented is understandably not representative of how they are naturally presented by professional antigen-presenting cells (APCs) or cancer cells.[60]

To efficiently screen through a pool of T cells and identify those with therapeutic potential, Koo and Mao et al. recently reported a high-throughput approach to selectively capture single antigen-specific T cells in cavity-containing hydrogel microparticles[118], called nanovials.[119] Each nanovial acts as both an artificial APC that presents pMHC molecules to activate cells with cognate TCRs, and as a capture site for secreted effector molecules, such as IFN-γ and granzyme B, that enable high-throughput sorting of therapeutically relevant T cells by flow cytometry. While this capture and activation method was successful in isolating previously unidentified reactive T cells, we hypothesized that improved selection and activation would be possible by incorporating the immune-activating signaling molecules into lipid membranes with high fluidity. Signaling molecules in lipid membranes with high fluidity have been shown to activate T cells better than membranes with low fluidity[85] due to the improved ability to facilitate receptor clustering in the supramolecular activation complex, or “immunological synapse”, that forms between an APC and a T cell during antigen presentation and subsequent immune activation[60].

To recreate the potential benefits of these physiological lipid bilayers, researchers have previously imbued bioinert materials with bioactive cell-like membranes through extrusion, sonication, or centrifugation, which typically involve coating with non-specific cell lysates and may be difficult to achieve with heterogenous surfaces[120]. Recently, synthetic liposomes were coated on mesoporous silica micro-rods[121] to generate supported lipid bilayers harboring combinations of biotinylated T cell activation cues, such as pMHC and αCD28 antibodies, for the rapid expansion of highly functional T cells; while this method enabled biotinylated signaling molecules to have membrane fluidity for improved T cell activation, a known limitation of this approach is that many membrane proteins may be insoluble or display altered or absent activities if synthesized recombinantly outside of a lipid bilayer[122,123]; thus, an ideal functionalization strategy would allow for natural, full-length cell membrane proteins embedded in highly fluid lipid bilayers to coat the surface of the intended bioactive material without the need for recombinant expression of a soluble protein for surface conjugation. Accordingly, extracellular vesicles featuring natural, full-length membrane proteins have been increasingly pursued as a coating for biomaterials with successes seen in both tissue engineering[124-126] and immunomodulatory[127-130] settings. However, an ongoing struggle with natural extracellular vesicles is that their low expression yield[131] and the heterogeneity of their protein composition[132] precludes reliable experimentation and manufacturing. The surface density of certain immunoregulatory proteins, for example, is a critical parameter for immune activation[101], as previous studies have demonstrated that exosomes or cell sonicates must be derived from APCs that express a high density of pMHCI and CD80/CD54 complexes to induce T cell responses[133].

Here, we demonstrate the expression and purification of high concentrations of extracellular vesicles that are densely coated with desired compositions of immunoregulatory membrane proteins, which we then use to functionalize the surfaces of nanovial cavities for improved T cell capture and activation. As initially described by Hoffmann et al., vesicles are generated by transfecting standard HEK293T and Expi293F cell cultures with protein constructs containing an appended ESCRT- and ALIX-binding region (EABR) sequence[47] to the

cytoplasmic tail of the full-length membrane protein; this EABR sequence recruits ESCRT proteins to induce the budding of extracellular vesicles that can optionally mimic cancer-derived HER2-presenting extracellular vesicles or antigen-presenting vesicles (APVs)[134] co-presenting both pMHCI and the immunoregulatory proteins CD274, CD83, or CD80. As a demonstration of the biological relevance of these engineered extracellular vesicles for advancing adoptive cell therapies, we show the facile coating of heterogeneous surfaces of microparticle hydrogel nanovials with these engineered extracellular vesicles to improve the loading and activation of therapeutically-relevant T cells when compared to their soluble recombinantly expressed variants. T cells captured in these nanovials can be isolated for further downstream analysis, enabling both improved high-throughput single cell discovery of T cells with therapeutic potential as well as future single cell studies of extracellular vesicle membrane protein composition on T cell activation and differentiation.

3.3 Results

3.3.1. Hydrogen nanovials enable single-cell comparison of T cell activation by extracellular vesicles

Recent work by Hoffmann et al. demonstrated a generalizable method for inducing the release of transfected membrane proteins on densely coated, cell-derived extracellular vesicles[47]. Appending an endosomal sorting complex required for transport (ESCRT)- and ALG-2-interacting protein X (ALIX)- binding region (EABR) to the cytoplasmic tail of membrane proteins directly recruits the ESCRT machinery and induces the release of vesicles displaying the EABR-tagged protein (Fig. 3.1A). Transfecting common HEK293T or Expi293F cell cultures with DNA plasmids encoding EABR-tagged membrane proteins generates vesicles that can be purified from the cell culture supernatant by ultracentrifugation on a 20% sucrose gradient as is typical for the purification of viral particles and exosomes[92] (Fig. 3.1B). We hypothesized that these cell-derived extracellular vesicles would activate T cells more strongly than soluble protein by presenting cancer antigens and pMHCI complexes in a more physiologically-relevant format.

To evaluate the performance of these engineered extracellular vesicles for cell capture and activation, structured hydrogel microparticles, or "nanovials"[119], were manufactured to hold single cells in inner cavities functionalized with the EABR-mediated extracellular vesicles (Fig. 3.1C). Briefly, a microfluidic device generates uniform water-in-oil emulsions, where aqueous two-phase separation of polyethylene glycol (PEG) and gelatin occurs to create millions of monodisperse PEG-based nanovials with an inner cavity selectively coated with biotinylated gelatin. Multiple biotinylated antibodies or peptide-MHC (pMHC) monomers with epitopes of interest can be flexibly linked to the cavity's interior through streptavidin-biotin noncovalent interactions[118]. These antibodies can be used for non-specific T cell capture (e.g. CD45), for capture of T cell activation cytokines (e.g. IFN-γ), or for capture of EABR-mediated engineered extracellular vesicles by binding to transfected membrane proteins present on the surface of the vesicles (e.g. HER2, CD54, CD274, CD83, CD80, or pMHCI). CAR-T or T cells are captured in the cavity of nanovials by binding to the EABR-tagged membrane proteins of the extracellular vesicles functionalizing the nanovial surface. Subsequent T cell activation and IFN-γ release is measured by a sandwich antibody for IFN-γ captured in the nanovial cavity's interior (Fig. 3.1D). Extracellular vesicles, T cells, and their associated secretions are then analyzed and sorted using high-throughput commercial flow cytometers, which can conveniently isolate therapeutically-relevant, antigen-reactive T cells. This massively parallel and high-throughput system provides a single-cell resolution of T cell activation to compare the performance of T cell capture and activation by extracellular vesicles versus recombinantly expressed pMHCI and cancer antigen.

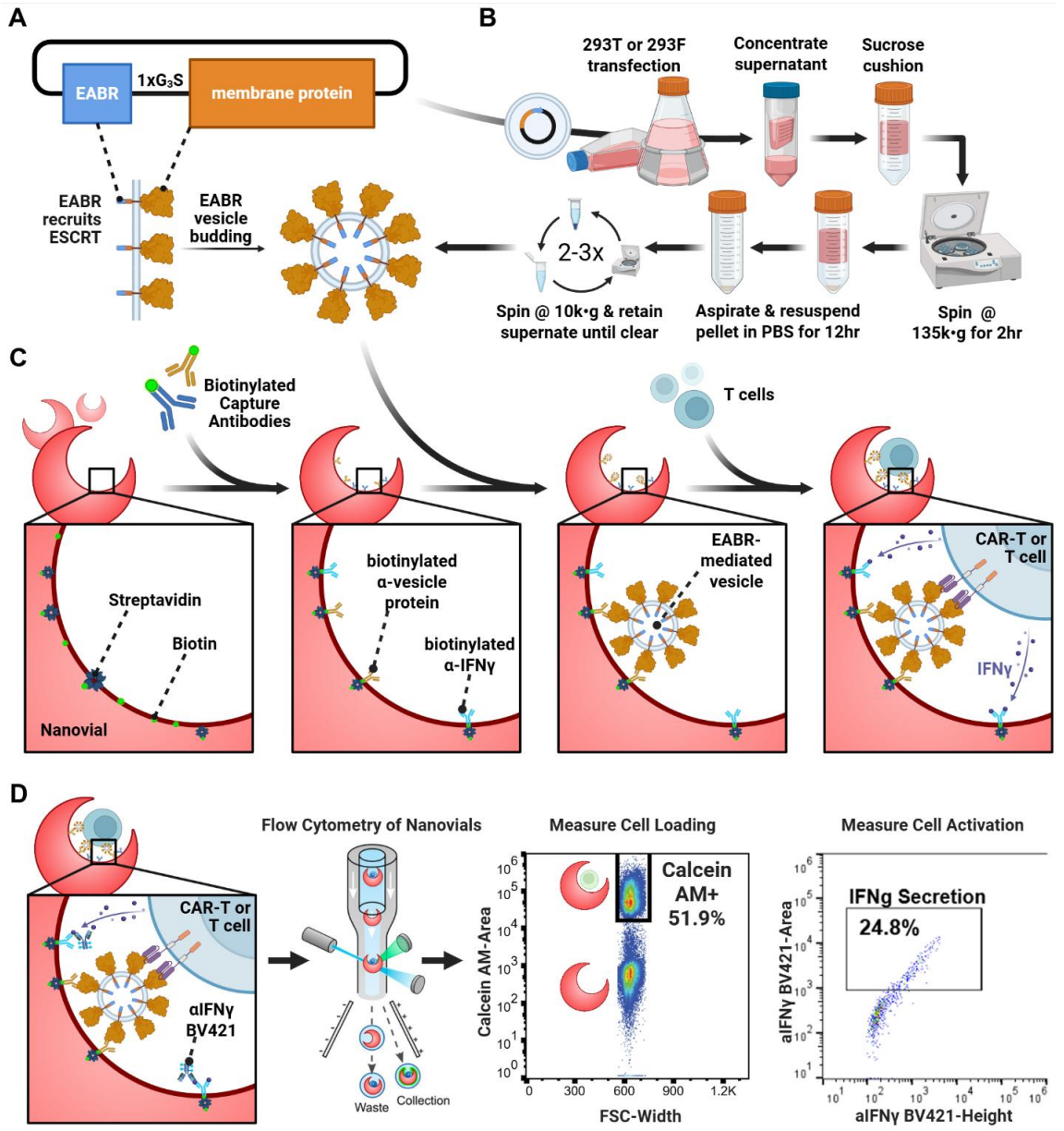

Figure 3.1. Engineered extracellular vesicles improve single cell capture and T cell activation of hydrogel nanovials

(A) Top: schematic of a plasmid construct containing a membrane protein fused to a Gly_3Ser spacer, and an EABR vesicle-forming sequence. Bottom: schematic of membrane-bound protein on a cell surface containing cytoplasmic tail EABR additions that induce budding of a vesicle comprising a lipid bilayer with embedded membrane proteins that contain the EABR sequence.

(B) Schematic showing production and purification of the engineered EABR-mediated extracellular vesicles.
(C) Post-fabrication biotinylation of hydrogel nanovials via gelatin are then functionalized with streptavidin, followed by biotinylated capture antibodies. Capture antibodies can be any protein present on the vesicle surface, including the EABR- tagged membrane protein that induces vesicle formation. Cells, such as CAR-T cells, bind to the captured extracellular vesicles within the nanovial cavity, and cell activation cytokines are captured using the biotinylated capture antbiodies covering the nanovial surface.
(D) Fluorescent sandwich antibodies detect cytokines released by activated cells that are captured within the nanovial to enable single-cell measurements of both cell capture and cell activation by flow cytometry.

3.2. Co-expression of SCT pMHCI/EABR and CD274, CD83, or CD80 generates immunoregulatory antigen-presenting vesicles

We previously demonstrated the engineered assembly and budding of pMHCI-displaying APVs from the cell surface of non-immune cells by DNA transfection of an engineered single-chain heterotrimer (SCT) pMHCI[134]. Expanding on this work, we simultaneously transfected cell cultures with two constructs encoding a single-chain heterotrimer peptide:MHCI (SCT pMHCI) complex and either programmed cell death ligand 1 (PD-L1) CD274, immunoregulatory CD83, or the costimulatory signal CD80, each of which has been found previously on immune cell surfaces[135], immunoregulatory APVs[136], and cancer-derived exosomes[137,138] (Fig. 3.2A). Continuing from our earlier work, we utilized the "D9" variant of SCT pMHCI[48-50], containing Y84C and A139C substitutions in the alpha heavy chain that were previously reported to improve both thermostability and TCR binding.

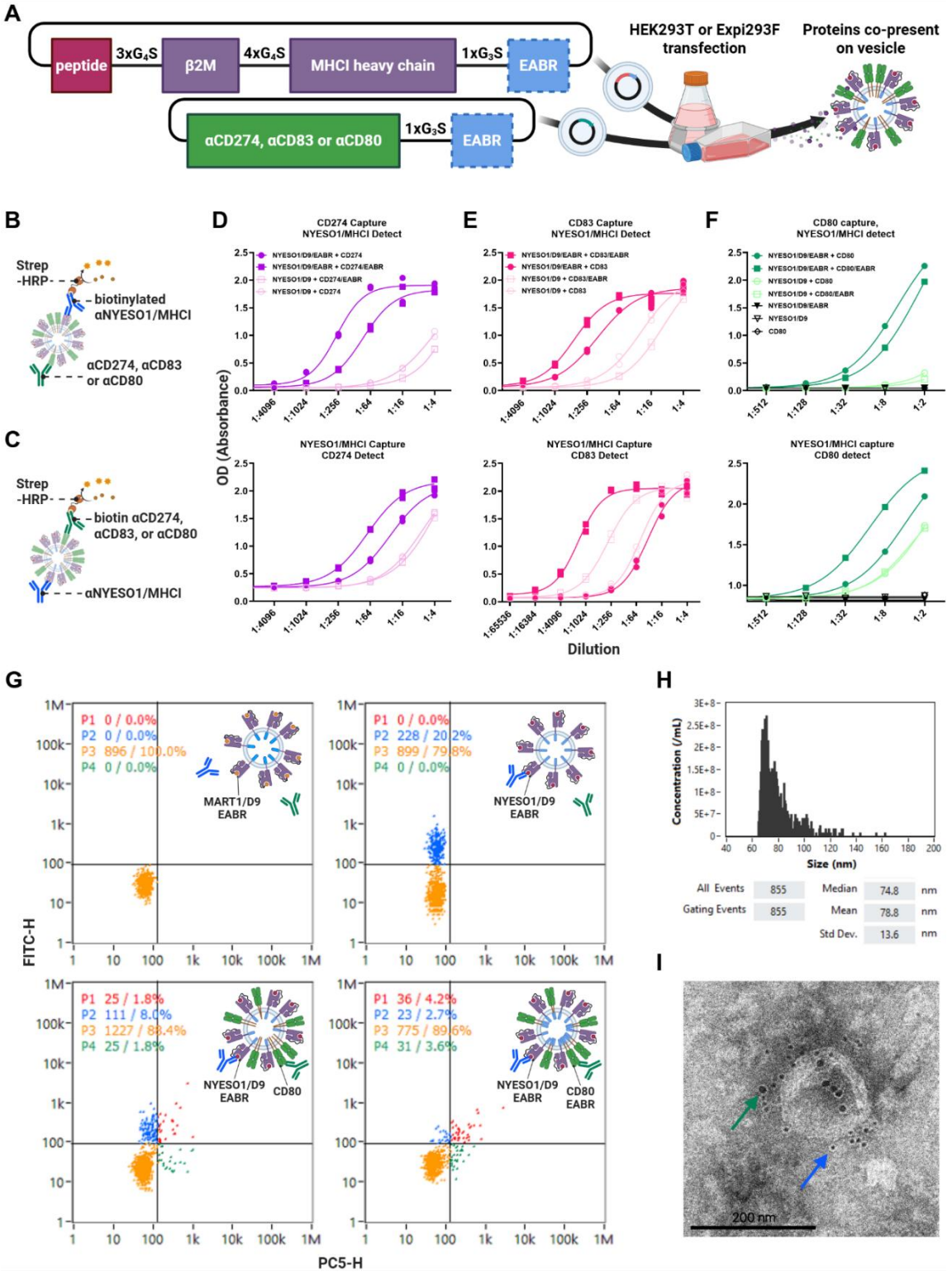

Figure 3.2. Co-expression of SCT pMHCI/EABR and CD274, CD83, or CD80 generates immunoregulatory antigen-presenting vesicles

(A) Schematic showing the plasmid constructs for vesicles co-presenting NYESO1/HLA-A*0201 and either CD274, CD83, or CD80 with an "EABR" vesicle-forming sequence optionally appended to the cytoplasmic tail. The plasmid is transfected into HEK293T or Expi293F cells and vesicles are harvested as shown previously in Figure 1B.

(B) Schematic of the assay performed for the top row of Fig. 3.2D-F). Expression of immunoregulatory membrane proteins CD274, CD83, or CD80 on engineered extracellular vesicles were captured with plated antibody, then co-presented NYESO1/HLA-A*02:01 were detected and quantified with biotinylated anti-NYESO:HLA-A*02:01 and HRP-conjugated streptavidin (strep-HRP).

(C) Schematic of the assay performed for the bottom row of Fig. 3.2D-F. Identical assay to (B), but the capture antibody and detection antibody have been swapped.

(D) Sandwich ELISA of APVs purified by ultracentrifugation from transfected Expi293F cells using anti-CD274 for capture, biotinylated anti-NYESO1:HLA-A*02:01 (3M4E5) for detection, and HRP-conjugated streptavidin secondary. Cells were co-transfected with SCT NYESO1/D9/EABR and CD274, SCT NYESO1/D9/EABR and CD274/EABR, SCT NYESO1/D9 and CD274/EABR, or SCT NYESO1/D9 and CD274 constructs (2 replicates per dilution).

(E) Sandwich ELISA of APVs purified by ultracentrifugation from transfected Expi293F cells using anti-CD83 for capture, biotinylated anti-NYESO1:HLA-A*02:01 (3M4E5) for detection, and HRP-conjugated streptavidin secondary. Cells were co-transfected with SCT NYESO1/D9/EABR and CD83, SCT NYESO1/D9/EABR and CD83/EABR, SCT NYESO1/D9 and CD83/EABR, or SCT NYESO1/D9 and CD83 constructs (2 replicates per dilution).

(F) Sandwich ELISA of APVs purified by ultracentrifugation from transfected HEK293T cells using anti-CD80 for capture, biotinylated anti-NYESO1:HLA-A*02:01 (3M4E5) for detection, and HRP-conjugated streptavidin secondary. Cells were co-transfected with SCT NYESO1/D9/EABR and CD80, SCT NYESO1/D9/EABR and CD80/EABR, SCT NYESO1/D9 and CD80/EABR, or SCT NYESO1/D9 and CD80 constructs (2 replicates per dilution).

(G) Nano flow cytometry (NanoFCM) of APVs purified by ultracentrifugation from transfected HEK293T cells, and co-stained with APC anti-CD80 and Alexa488 anti-NYESO1:HLA-A*02:01 (3M4E5). Top-Left: Vesicles purified from HEK293T transfected with the MART1/D9/EABR construct were used for gating non-specific signal from irrelevant extracellular vesicles. Top-Right: Vesicles from HEK293T cells transfected with the NYESO1/D9/EABR construct. Bottom-Left: Vesicles from HEK293T cells transfected with NYESO1/D9/EABR and CD80 constructs. Bottom-Right: Vesicles from HEK293T cells transfected with NYESO1/D9/EABR and CD80/EABR constructs.

(H) NanoFCM size analysis of vesicles purified by ultracentrifugation from HEK293T cells co-transfected with NYESO1/D9/EABR and CD80/EABR constructs.

(I) Immuno-EM image of vesicles purified by ultracentrifugation and size-exclusion chromatography from Expi293F cells co-transfected with NYESO1/D9/EABR and CD80/EABR constructs. Primary human anti-NYESO1:HLA-A*02:01 (3M4E5) antibody and mouse anti-CD80. Secondary 12 nm gold-conjugated anti-mouse antibody appears as black punctae in image and highlighted by green arrow. Secondary 6nm gold-conjugated anti-human antibody appears as smaller black punctae in image and highlighted by blue arrow. Scale bar, 200 nm.

To quantify the relative concentration of the transfected proteins on our engineered vesicles, we performed sandwich ELISAs of the purified APVs using capture antibodies for either the co-expressed immunoregulatory proteins (Fig. 3.2B) or the NYESO1:HLA-A*0201 complex (Fig. 3.2C) followed by biotinylated detection antibodies for the opposite co-presenting protein. For all conditions tested, the best vesicle production occurs when at least one of the transfected proteins contains an EABR sequence (Fig. 3.2D-F). Interestingly, our ELISA data revealed that the ratio of proteins on the surface of the vesicles is influenced not only by which of the two transfected proteins is appended by an EABR sequence, but also by the identity of the co-expressed immunoregulatory protein. To better understand the relative ratio of proteins on a per-vesicle basis, we performed nano flow cytometry (nanoFCM)[139] of the vesicles from Fig. 3.2F that co-present CD80 and NYESO/HLA-A*0201 (Fig. 3.2G). Using the same antibodies as those used for the ELISA from Fig. 3.2F,

the nanoFCM detected a more concentrated presence of CD80 on vesicles when CD80 was appended by an EABR sequence, which would be expected given that both CD80 and pMHCI would then be capable of inducing vesicle formation. The "unlabeled" P3 quadrant also shows that, while there may be cellular debris retained within the purified vesicle fraction that will appear in this unlabeled P3 quadrant, not all vesicles generated by cell cultures transfected with EABR-tagged proteins feature EABR-tagged proteins on their surface; in other words, it is possible that transfected CD80 and pMHCI proteins are competing with other vesicle-forming proteins for presentation on extracellular vesicles. Measurements of vesicle diameter provided by the nanoFCM demonstrate that most of the particles are between 60-80 nm in size, corroborating our previous APV size measurements[134] (Fig. 3.2H). Notably, some vesicles are over 100 nm in diameter, which we further confirmed with immuno-electron microscopy (Fig. 3.2I) by co-staining with the same anti-CD80 and anti-NYESO1:HLA-A*0201 antibodies used in Fig. 3.2F and Fig. 3.2G.

Altogether, these results demonstrate that the final protein composition of the vesicles generated using the EABR sequence can be finely tuned depending on the selective addition or removal of EABR from transfected proteins, and that inclusion of the EABR sequence allows for the high-yield synthesis of co-presenting immunoregulatory extracellular vesicles that mimic the endogenous immunoregulatory APVs studied extensively in literature[33,35].

3.3.3. Functionalizing nanovials with vesicles co-presenting pMHCI/EABR and CD80 improves T cell loading and activation

Koo and Mao et al. previously demonstrated that nanovials coated with peptide-major histocompatibility complex (pMHC) monomers could be used to isolate and selectively activate antigen-reactive T cells[118]. While this capture and activation method was successful in isolating previously unidentified reactive T cells, we hypothesized that functionalizing the nanovial surface with EABR-mediated APVs would provide a more physiologically representative interface for the "immunological synapse" that forms between an APC and a T cell during antigen presentation and subsequent immune activation[60]. As a known positive control for comparison, we recreated the original experimental conditions for pMHCI

nanovials by coating the interior cavity of nanovials with 20ug/mL biotinylated anti-human IFN-γ and 20ug/mL biotinylated NYESO1-MHCI monomer before incubating with human peripheral blood mononuclear cells (PBMCs) that had been transduced with the 1G4 TCR targeting the NYESO:MHCI complex[140,141]. Truncated nerve growth factor receptor (NGFR) was used as the cotransduction marker for the presence of the 1G4 TCR, and Calcein AM stain confirmed the cells captured in the nanovials were alive and capable of responding to pMHCI activation with IFN-γ secretion (Fig. 3.3A). The Calcein AM signal threshold was set using live 1G4 T cells not loaded into nanovials as a positive control. The IFN-γ signal threshold was set using 1G4 T cells loaded into nanovials via biotinylated anti-CD45, which is not associated with T cell activation.

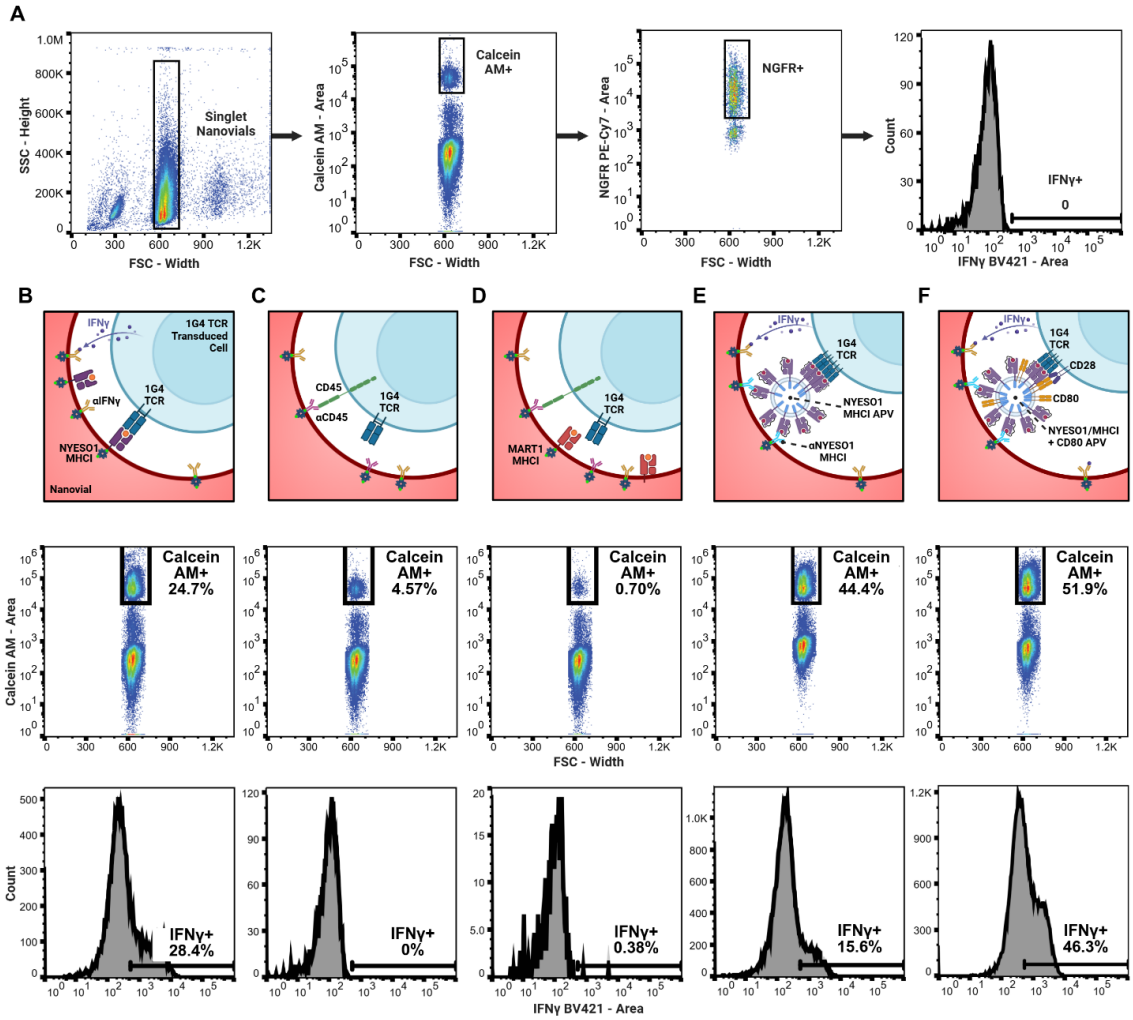

Figure 3.3. Functionalizing nanovials with vesicles co-presenting pMHCI/EABR and CD80 improves T cell loading and activation

(A) Flow cytometry gating strategy for T-cell loaded nanovials and secretion detection. Singlet nanovials are identified as separate from hydrogel debris and nanovial doublets. Positive Calcein AM signal represents living cells. Positive NGFR signal represents successful transduction of 1G4 TCR. IFN-γ release is measured by an αIFN-γ BV421 sandwich antibody.

(B-F) First row: Comparison of different pMHC vesicles conjugated to nanovial cavity surface. Second row: Relative cell loading rates into nanovials using different binding moieties. Third row: IFN-γ secretion levels from single T cells on nanovials. T cell loading is significantly improved by using a matched pMHC relative to standard anti-CD45 antibody-based binding or inappropriately matched MART1/HLA-A*0201 for 1G4 TCRs. EABR-mediated pMHC vesicles further improve T cell loading rates. NYESO1/HLA-A*0201 pMHCs in both protein monomer and vesicle format trigger 1G4 T cell activation.

(B) Top: Schematic showing nanovials incubated with 20 μg/mL biotinylated NYESO1:HLA-A*0201 monomer and 20 μg/mL biotinylated αIFN-γ for 1G4 T cell and IFN-γ capture respectively. Middle: 24.7% of nanovials captured live T cells. Bottom: 28.4% of the live cells captured in nanovials stained positively for IFN-γ release.

(C) Top: Schematic showing nanovials incubated with 20 μg/mL biotinylated αCD45 and 20 μg/mL biotinylated αIFN-γ for 1G4 T cell and IFN-γ capture respectively. Middle: 4.57% of nanovials captured live T cells. Bottom: 0% of the live cells captured in nanovials stained positively for IFN-γ release.

(D) Top: Schematic showing nanovials incubated with 20 μg/mL biotinylated MART1:HLA-A*0201 monomer and 20 μg/mL biotinylated αIFN-γ for 1G4 T cell and IFN-γ capture respectively. Middle: 0.70% of nanovials captured live T cells. Bottom: 0.38% of the live cells captured in nanovials stained positively for IFN-γ release.

(E) Top: Schematic showing nanovials incubated with 20 μg/mL biotinylated αNYESO1:HLA-A*0201 antibody and 20 μg/mL biotinylated αIFN-γ, followed by incubation with NYESO1/HLA-A*0201/EABR APVs for 1G4 T cell and IFN-γ capture.

Middle: 44.4% of nanovials captured live T cells. Bottom: 15.6% of the live cells captured in nanovials stained positively for IFN-γ release.
(F) Top: Schematic showing nanovials incubated with 20 μg/mL biotinylated αNYESO1:HLA-A*0201 antibody and 20 μg/mL biotinylated αIFN-γ, followed by incubation with NYESO1/HLA-A*0201/EABR+CD80/EABR APVs for 1G4 T cell and IFN-γ capture. Middle: 51.9% of nanovials captured live T cells. Bottom: 46.3% of the live cells captured in nanovials stained positively for IFN-γ release.

In accordance with the original flow cytometry experiment by Koo and Mao et al.[118], we achieved comparable cell capture with live 1G4 T cells occupying ~25% of the nanovials, of which 28.4% were activated when using a ratio of 300,000 cells to 300,000 nanovials (Fig. 3.3B). By comparison, nanovials coated with 20 μg/mL biotinylated anti-CD45 (Fig. 3.3C), which should capture T cells independent of TCR, or a combination of 20 μg/mL biotinylated anti-CD45 and 20 μg/mL biotinylated MART1-MHCI monomer (Fig. 3.3D), which is a non-cognate pMHCI for 1G4 T cells, showed poor cell capture (4.57% and 0.70% respectively) and activation (0% and 0.38% respectively).

We then captured our EABR-mediated APVs in nanovials by coating the surface with 20 μg/mL biotinylated anti-human NYESO1/HLA-A2 (3M4E5) before incubating with our engineered vesicles (Fig. 3.3E). We intentionally chose the TCR-like anti-human NYESO1/HLA-A2 (3M4E5) antibody, which binds to the TCR binding site on pMHCI[142,143], for vesicle capture to confirm that the activation of T cells would be due to intact APVs and not soluble pMHCI monomer from lysed vesicles. Nanovials functionalized with NYESO1/HLA-A2/EABR APVs improved T cell loading to ~45%, and 15.6% of these cells were activated to release IFN-γ. We used the same 20 μg/mL biotinylated anti-human NYESO1/HLA-A2 (3M4E5) antibody to capture APVs co-presenting NYESO1/HLA-A*0201/EABR and CD80 (Fig. 3.3F); T cell capture increased further to ~52%, of which an increased fraction of 46.3% were activated to release IFN-γ, a result that would be expected from costimulation by CD80.[144] This 100% improvement in cell loading is in spite of our use of the single-chain heterotrimer format of pMHCI[48-50], which should theoretically bind with

less affinity than the recombinant, refolded soluble pMHCI used by Koo and Mao et al.; the flexible glycine-serine linker connecting the presenting NYESO1 peptide to β2m travels outward from the closed groove of the MHCI peptide binding cleft toward the TCR, and is thus expected to interfere with optimal TCR binding[48,49].

As a result, we conclude that EABR-mediated APVs improve the interface of hydrogel surfaces for T cell capture and activation compared to recombinant protein alone. This improvement in cell binding and activation may enable greater sensitivity and improve the recovery rate of rare cancer-specific functional TCRs for adoptive T cell therapies. Further, we demonstrated that a single antibody can be used to capture a variety of co-presenting immunoregulatory vesicles, which will enable future high-throughput single cell studies of extracellular vesicle protein composition on T cell capture, activation, and differentiation.

3.3.4. Co-expression of HER2/EABR and CD54 generates vesicles mimicking cancer exosomes

Following the successful functionalization of nanovials with EABR-mediated APVs for the capture of T cells, we hypothesized that we could also capture CAR-T cells by functionalizing the nanovial surfaces with EABR vesicles presenting membrane-bound cancer antigens. Membrane proteins in general have long presented a challenge to biochemical and functional studies as membrane proteins may be insoluble or display altered or absent activities in the absence of a lipid bilayer[122,123]. For instance, while antibodies screened against recombinant HER2 have been demonstrated to similarly bind membrane-bound HER2, HER2 is known to homodimerize when the protein is overexpressed and densely populated in the lipid bilayer of the cancer cell membrane[145]; in this context, rare HER2 CAR-T cells that specifically bind the homodimer complex may activate more selectively against cancer cells, but these reactive CAR-T cells might otherwise be lost when screening with recombinant HER2. To generate vesicles presenting more natural, membrane-bound HER2, we appended the EABR vesicle-forming sequence to the cytoplasmic tail of the full-length HER2 protein and purified the vesicles from transfected Expi293F cell culture supernatant (Fig. 3.4A). Recent observations on the immunological synapse formed by CAR-

T cells has highlighted the significance of membrane-bound CD54 for organizing and maintaining the supramolecular activation complex that leads to T cell activation[146] or suppression[147], so we additionally generated vesicles co-presenting both HER2/EABR and CD54 by co-transfecting cell cultures with DNA plasmids encoding both constructs (Fig. 3.4B). An added benefit of co-expressing CD54 was that future cancer-relevant membrane proteins, such as mesothelin[148], carcinoembryonic antigen[149], or prostate-specific membrane antigen[150], could be presented similar to HER2 on the EABR-mediated vesicles and the vesicles could be captured within nanovials by using the same CD54 antibody without requiring a bespoke antibody for every tested cancer antigen.

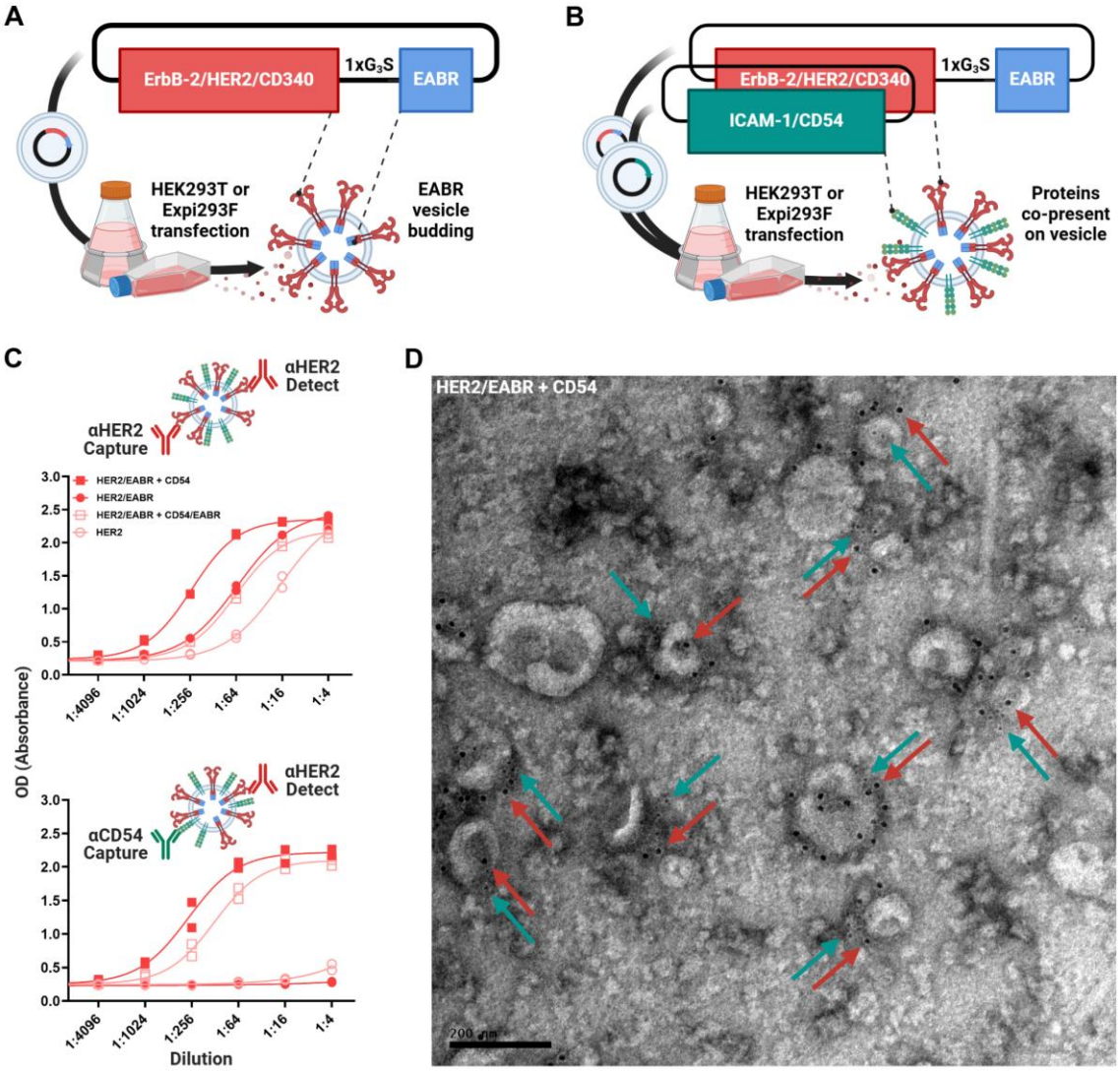

Figure 3.4. Co-expression of HER2/EABR and CD54 presents both proteins on purified extracellular vesicles

(A) Schematic showing the plasmid construct for HER2 vesicles featuring a G3S spacer and the "EABR" vesicle-forming sequence. The plasmid is transfected into HEK293T or Expi293F cells and vesicles are harvested as shown previously in Figure 1B.

(B) Schematic showing the plasmid construct for HER2 + CD54 vesicles. Only HER2 requires a vesicle-forming "EABR" sequence to be appended for both CD54 and HER2 to appear on the harvested vesicles.

(C) Sandwich ELISA of APVs purified by ultracentrifugation from transfected Expi293F cells. Cells were co-transfected with HER2/EABR and CD54, HER2/EABR alone, HER2/EABR and CD54/EABR, or HER2 constructs (2 replicates per dilution). Top: anti-HER2 for capture, biotinylated anti-HER2 for detection, and HRP-conjugated streptavidin secondary. Bottom: anti-CD54 for capture, biotinylated anti-HER2 for detection, and HRP-conjugated streptavidin secondary.

(D) Immuno-EM image of vesicles purified by ultracentrifugation and size-exclusion chromatography from Expi293F cells co-transfected with HER2/EABR and CD54 constructs. Primary mouse anti-HER2 antibody and rabbit anti-CD54. Secondary 12 nm gold-conjugated anti-mouse antibody appears as black punctae in image and highlighted by red arrows. Secondary 6nm gold-conjugated anti-rabbit antibody appears as smaller black punctae in image and highlighted by blue arrows. Scale bar, 200 nm.

To quantify the relative yield of HER2-presenting vesicles by addition of the EABR sequence, we performed sandwich ELISAs with either HER2 antibodies or a sandwich of CD54 capture antibody and HER2 detection antibody (Fig. 3.4C). In agreement with previous studies on HER2-presenting exosomes that originate from HER2 over-expressing cancer cells[151], over-expression of the full-length HER2 sequence in high-expressing Expi293F cells spontaneously generated vesicles without the addition of an appended EABR sequence. However, addition of the EABR sequence to HER2 further improved the yield of HER2+ vesicles. Interestingly, CD54 seems to act synergistically with HER2 to boost HER2 vesicle production, as co-transfection with separate DNA plasmids encoding HER2/EABR

(5ug) and CD54 (5ug) leads to better vesicle expression than transfection with 10ug of plasmid DNA encoding HER2/EABR alone. Appending EABR to both HER2 and CD54 leads to a reduction in total HER2 detected on the purified vesicles, which is likely due to an increase in CD54 presentation on the vesicles at the expense of HER2 presentation, a phenomenon that was observed previously when co-transfecting DNA constructs encoding equal amounts of NYESO1/HLA-A*0201I/EABR and CD80/EABR (Fig. 3.2G). We further confirmed that the detected co-presentation of HER2 and CD54 is localized on vesicle membranes by performing immuno-EM of the supernatant from transfected cells (Fig. 3.4D). Simultaneous co-staining of αCD54 and αHER2 showed halos of black punctae surrounding exosome-like vesicles mimicking cancer exosomes. Because our goal was to maximize HER2 presentation on vesicles while co-presenting a generalizable "capture" protein on the vesicle membrane, we moved forward with subsequent nanovial characterization experiments using the co-presenting HER2/EABR+CD54 vesicles as well as the HER2/EABR vesicles for comparison.

3.3.5. Functionalizing nanovials with vesicles co-presenting HER2/EABR and CD54 improves CAR-T cell loading and activation

To optimize the capture of HER2/EABR vesicles inside the nanovial cavity, we incubated the nanovials with different concentrations of αHER2 capture antibody to determine the minimal concentration necessary for maximal HER2 signal as detected by a fluorophore-conjugated αHER2 sandwich antibody. HER2 signal from captured HER2/EABR vesicles was saturated at 20 ug/mL αHER2 capture antibody (Fig. 3.5A), a concentration similar to that of the pMHCI nanovials. Surprisingly, this maximum fluorescent signal from HER2/EABR vesicles was orders of magnitude lower than the nanovials functionalized with biotinylated recombinant HER2. In comparison, coating the nanovials with biotinylated αCD54 capture antibodies and subsequent incubation with co-presenting HER2/EABR+CD54 vesicles produced an αHER2 fluorescent signal that was equivalent to biotinylated recombinant HER2 (Fig. 3.5B). As was demonstrated by previous nanoFCM analysis, immuno-EM micrographs, and ELISA results of EABR vesicles, we believe this dramatic increase in signal between the HER2/EABR and co-presenting

HER2/EABR+CD54 vesicles is likely due to differences in the binding affinities of the αHER2 and αCD54 capture antibodies for their target proteins, and not due to differences in vesicle stability or the relative density of HER2 or CD54 protein on the vesicle surface. Nonetheless, the comparable level of HER2 signal that was detected between the recombinant HER2 and HER2/EABR+CD54 vesicles captured within the nanovials provided a convenient comparison for our ensuing studies on the relative importance of a lipid bilayer and CD54 co-presentation for T cell capture and activation.


A
HER2 eVLP Signal on Nanovials
MFI Relative to Maximum
1.0
0.5
0.0
0
20
40
60
80
Concentration of aHER2 (ug/mL)
35um NV
50um NV
B
MFI Fold Change
10000
1000
100
10
1
(+) Control
HER2 eVLP
CD54/HER2 eVLP
aHER2 NV
aCD54 NV
rHER2 NV
C
HER2 eVLP
HER2 + CD54 eVLP
UTX cells
0.09%
CAR cells
0.20%
UTX cells
4.09%
CAR cells
2.67%
UTX cells
0.14%
CAR cells
0.12%
UTX cells
0.58%
CAR cells
4.71%
αHER2 nanovial
αCD54 nanovial
(FL2-A) Calcein AM – Cell Loading
D
rHER2
αCD54
HER2 eVLP
αCD54
HER2 + CD54 eVLP
IFNg Secretion
0%
IFNg Secretion
0.41%
IFNg Secretion
0%
IFNg Secretion
9.16%
IFNg Secretion
3.25%
IFNg Secretion
24.8%
(FL1-A) aIFNg-BV421 – Area
(FL1-H) aIFNg-BV421 – Height
UTX cells
αHER2
CAR-T cells

Figure 3.5. Functionalizing nanovials with vesicles co-presenting HER2/EABR and CD54 improves CAR-T cell loading and activation

(A) Immobilization of HER2 vesicles on 35um and 50um nanovials based on concentration of αHER2 capture antibodies on the nanovials. Maximum capture signal is detected at 20 ug/mL αHER2 for both 35um and 50um nanovials.

(B) HER2/EABR+CD54 vesicles show significantly higher capture rate on nanovials compared to the HER2-only vesicles. This signal is comparable to the positive control of nanovials conjugated with 20 ug/mL recombinant HER2 (rHER2).

(C) αHER2 CAR T cell and control untransfected (UTX) T cell loading in nanovials using both HER2/EABR vesicles and HER2/EABR+CD54 vesicles. Nanovials conjugated with αHER2 antibodies, then incubated with either HER2/EABR or HER2/EABR+CD54 vesicles, cannot bind control UTX cells nor αHER2 CAR T cells. Nanovials conjugated with αCD54 antibodies show non-specific cell loading which may be due to endogenous CD54 expression on T cells. This non-specific binding is significantly reduced when HER2/EABR+CD54 vesicles are immobilized on nanovials. Nanovials conjugated with αCD54 antibodies, then incubated with HER2/EABR+CD54 vesicles, bind αHER2 CAR T cells selectively.

(D) Flow data showing improvement in nanovial assay from using EABR-mediated vesicles. Nanovials functionalized with rHER2 show 9.16% of captured, living CAR T cells are activated to release IFN-γ. Nanovials functionalized with αCD54 antibodies, then incubated with HER2/EABR+CD54 vesicles, show 24.8% of captured, living CAR T cells are activated to release IFN-γ.

To investigate the significance of a lipid bilayer and co-presentation of CD54 on T cell capture and activation by cancer antigens, we compared the efficiency of nanovial loading between untransfected (UTX) T cells and T cells transfected with an αHER2 CAR (Fig. 3.5C). Nanovials that were conjugated with biotinylated αHER2 antibodies and incubated with either HER2/EABR or HER2/EABR+CD54 vesicles did not appreciably bind UTX cells nor αHER2 CAR T cells, which aligned with our previous tests of HER2 signal intensity in nanovials (Fig. 3.5B) and would support our conjecture that our chosen αHER2 antibody

has low affinity for HER2. Alternatively, nanovials that were conjugated with biotinylated αCD54 antibodies and incubated with HER2/EABR+CD54 vesicles bound αHER2 CAR T cells selectively; these functionalized nanovials also showed a dramatic increase in CAR T cell activation compared to recombinant HER2 as measured by the levels of IFN-γ release and fraction of cells releasing IFN-γ (Fig. 3.5D). Nanovials conjugated with biotinylated αCD54 antibodies and incubated with HER2/EABR vesicles bound both αHER2 CAR T cells and UTX T cells indiscriminately; this non-specific binding of UTX cells is significantly reduced when HER2/EABR+CD54 vesicles are instead immobilized on the αCD54 nanovials, suggesting that the HER2/EABR+CD54 vesicles are saturating the αCD54 antibodies present on the nanovial surface and preventing binding to possible endogenous CD54 expression on T cells.

Our results demonstrate that EABR-mediated cancer-mimicking vesicles that co-present CD54 and HER2 improve CAR T cell capture and activation on hydrogel surfaces. Antibody affinity is a limiting factor for vesicle functionalization on hydrogel surfaces, but, as we demonstrated, CD54 co-expression enables convenient and generalizable functionalization of hydrogel surfaces with EABR-mediated vesicles that present the natural structure of cancer antigens for high-throughput capture, activation, and downstream analysis of therapeutically-relevant CAR T cells.

3.4 Discussion

Here, we present a method for improving the T cell activation potential and T cell capture rates of the artificial antigen-presenting cavities in nanovials by functionalizing their hydrogel surface with engineered EABR-mediated vesicles mimicking APVs and cancer exosomes. EABR-mediated vesicles are densely coated in transfected immunoregulatory proteins embedded in a natural, cell-derived lipid bilayer, which provides a more physiologically representative interface for the “immunological synapse” that forms between an APC and a T cell during antigen presentation and subsequent immune activation. This approach can increase the sensitivity and control of nanovial-based enrichment of T cell and CAR-T cell libraries to identity and isolate reactive antigen-specific T cells on a single-cell

basis. Microparticle hydrogel nanovials functionalized with the EABR-mediated vesicles show a two-fold improvement in T cell capture of 1G4 T cells and an over two-fold improvement in activation of HER2 CAR-T cells compared to nanovials functionalized with recombinantly-expressed soluble protein. Further, we demonstrated the ability to fine-tune the composition of multiple co-presenting immunoregulatory proteins on single particles to more accurately reflect, or systematically modulate, the components of the cell surface of an APC. Future studies can either repurpose our methods for capturing endogenous EVs on nanovials or synthesize EABR-mediated immunoregulatory extracellular vesicles to study the influence of EV protein composition on T cell activation and differentiation.

As observed by the synergistic increase in vesicle release when both HER2/EABR and CD54 constructs were co-transfected, a future point of optimization for EV synthesis is seeing what parameters can be further engineered to maximize vesicle production. The vast majority of vesicles we detected by nanoFCM did not feature an EABR-tagged protein, implying that transfected EABR-proteins compete with endogenous vesicle-forming proteins or existing, unexploited vesicle-forming pathways for presentation on extracellular vesicles. Similarly, the range of vesicles detected by nano-FCM suggests that it may be possible to control the size distribution of the vesicles. Previous studies have demonstrated an improvement in T cell activation when synthetic antigen-presenting nanoparticles are larger in diameter[152], but it is unclear how vesicle size will influence T cell activation when the vesicles are immobilized as a collection on the surface of a hydrogel. The improvement in T cell capture and activation we observed with our EABR-mediated vesicles compared to recombinant protein may be due to the density of stimulatory cues on the EABR-mediated vesicles[133], the fluid lipid bilayer[60,85], the co-presentation of cell-membrane derived proteins like CD54[146,147], or the presence of the natural full-length membrane proteins[123]. Future studies that isolate the critical elements of T cell activation by these EABR-mediated vesicles will lead to more optimal hydrogel functionalization strategies for T cell activation. Nanovial-based approaches may also be useful to select cells that secrete more extracellular vesicles, as was previously done for natural extracellular vesicles released by mesenchymal stem cells.

In summary, our current work here expands upon the growing collection of characterization studies and workflows already pioneered by nanovials[118,119,153-156], which allow standard flow sorters and single-cell sequencing instrumentation to accelerate the development of personalized cell therapies. Additionally, with respect to the growing interest in cell-free, cell-like therapies[42,56,157,158], we demonstrate here a system for optimizing the engineering and characterization of extracellular vesicles that can be used either cooperatively[159] or in place of adoptive cell therapies[160,161] for targeted immunoregulation.

3.5 Acknowledgements

We would like to thank other members of Di Carlo lab and Witte lab for helpful comments and discussion in preparation of this manuscript. We thank UCLA Jonsson Comprehensive Cancer Center (JCCC) and Center for AIDS Research Flow Cytometry Core Facility. We thank J. Vielmetter, A. Lam, and the Caltech Protein Expression Center for assistance with protein production; P. Gnanapragasam, A. Rorick, L. Segovia for cell culture reagents; W. Chour for MHC plasmid maps and helpful discussions. We thank R. Voorhees and J. Keeffe for equipment access and training. Immuno-electron microscopy was performed in the Caltech Cryo-EM Center with assistance from Songye Chen. Figures 1A-D, 2A-C, 2G, 3B-F, 4A-C, and 5B-D were created with Biorender.com. Research was sponsored by the U.S. Army Research Office and accomplished under cooperative agreement W911NF-19-2-0026 for the Institute for Collaborative Biotechnologies. The content of the information on this page does not necessarily reflect the position or policy of the Government, and no official endorsement should be inferred. This project has been made possible in part by grant 2023-332386 from the Chan Zuckerberg Initiative Donor Advised Fund (CZI DAF), an advised fund of the Silicon Valley Community Foundation.

3.6 Author Contributions

B.A.O., M.M., C.S., Z.M., D.D.C., and S.L.M. designed research; B.A.O., M.M., C.S., and K.L. performed research; A.M. and Z.M. contributed new reagents/analytic tools; B.A.O., M.M., C.S., Z.M., K.L., M.A.G.H., D.D.C., and S.L.M. analyzed data; B.A.O. wrote the manuscript; all authors edited the manuscript.

3.7 Methods

Key resources table

REAGENT or RESOURCE	SOURCE	IDENTIFIER
Antibodies		
Recombinant Anti-HLA-A2-peptide (SLLMWITQV) Complex (3M4E5) Mouse Monoclonal Antibody	ProteoGenix	Reference: RHM03002-100
Purified anti-human CD340 (erbB2/HER-2) Antibody	Biolegend	Cat# 324402 RRID: AB_756118
ICAM-1 Recombinant Rabbit Monoclonal Antibody (ST0487)	Thermo Fisher Scientific	Cat# MA5-41137 RRID: AB_2898891
CD54 (ICAM-1) Monoclonal Antibody (HA58)	Thermo Fisher Scientific	Cat# 14-0549-82 RRID: AB_467304
ErbB2 (HER-2) Monoclonal Antibody (3B5), Biotin	Thermo Fisher Scientific	Cat# MA5-13672 RRID: AB_10982527
CD54 (ICAM-1) Monoclonal Antibody (HA58), Biotin	Thermo Fisher Scientific	Cat# 13-0549-82 RRID: AB_466483
CD80 (B7-1) Monoclonal Antibody (2D10.4)	Thermo Fisher Scientific	Cat# 14-0809-82 RRID: AB_467350
CD80 (B7-1) Monoclonal Antibody (2D10.4), Biotin	Thermo Fisher Scientific	Cat# 13-0809-82 RRID: AB_466513
Purified anti-human CD83 Antibody	Biolegend	Cat# 305302 RRID: AB_314509
Biotin anti-human CD83 Antibody	Biolegend	Cat# 305304 RRID: AB_314511
CD274 (PD-L1, B7-H1) Monoclonal Antibody (MIH1)	Thermo Fisher Scientific	Cat# 14-5983-82 RRID: AB_467784
CD274 (PD-L1, B7-H1) Monoclonal Antibody (MIH1), Biotin	Thermo Fisher Scientific	Cat# 13-5983-82 RRID: AB_466840
6 nm Colloidal Gold AffiniPure® Goat Anti-Human IgG (H+L) (EM Grade)	Jackson ImmunoResearch	Cat# 109-195-088 RRID: AB_2337747
6 nm Colloidal Gold AffiniPure® Goat Anti-Rabbit IgG (H+L) (EM Grade)	Jackson ImmunoResearch	Cat# 111-195-144 RRID: AB_2338015
12 nm Colloidal Gold AffiniPure® Goat Anti-Mouse IgG (H+L) (EM Grade)	Jackson ImmunoResearch	Cat# 115-205-146 RRID: AB_2338733
anti-IFN-γ ms mAb – BV421	BioLegend	Cat# 502532
anti-HER2/ErbB2 Antibody – biotin	Sino Biological	Cat# 10004-MM01-B
Biotin anti-human CD45 Ab, 2D1	BioLegend	Cat# 368534
Human IFN-γ Biotinylated Antibody	Biotechne/R&D Systems	Cat# BAF285
Anti-CD340 (erbB2/HER2) ms mAb – PE/Cy7	BioLegend	Cat# 324413
Bacterial and virus strains		
E. coli DH5 Alpha	Zymo Research	Cat# T3009
Chemicals, peptides, and recombinant proteins		

Luria Broth Base (Miller's LB Broth Base), powder	Thermo Fisher Scientific	Cat# 12795084
Dulbecco's Modified Eagle Medium (DMEM)	Gibco	Cat# 11995-065
Fetal bovine serum (FBS)	R&D Systems	Cat# S12450H
Penicillin-Streptomycin	Gibco	Cat# 15-140-122
FuGENE® HD Transfection Reagent	Promega	Cat# E2311
OPTI-MEM I Reduced Serum Medium	Gibco	Cat# 31985-062
Expi293 Expression Medium	Gibco	Cat# A14351-01
Expi293 Transfection Kit	Gibco	Cat# A14524
NucleoBond™ Xtra Maxi Plus	Macherey-Nagel	Cat# 12758412
Zyppy Plasmid Miniprep Kit	Zymo Research	Cat# D4019
Sucrose	Sigma-Aldrich	Cat# S5016-1KG
NaCl	Fisher Scientific	Cat# BP358-212
Sodium hydroxide	Macron Chemicals	Cat# 7708-10
Sodium bicarbonate	Macron Chemicals	Cat# 7412-12
Sodium phosphate dibasic	Sigma-Aldrich	Cat# 04272-1KG
Tris-HCl	Fisher Scientific	Cat# BP153-1
TWEEN® 20	Sigma-Aldrich	Cat# P1379-500ML
BSA	Sigma-Aldrich	Cat# B4287-5G
Trypsin	Gibco	Cat# 25200-056
L-glutamine	Gibco	Cat# 25030-149
Phytohemagglutinin, M form	Gibco	Cat# 10576015
Paraformaldehyde 16% Aqueous Solution EM Grade	Electron Microscopy Sciences	Cat# 15710
Uranyl Formate	Electron Microscopy Sciences	Cat# 22451
1-Step™ Ultra TMB-ELISA Substrate Solution	Thermo Fisher Scientific	Cat# 34029
EZ-Link NHS-PEG4 Biotinylation Kit	Thermo Fisher Scientific	Cat# 21455
Streptavidin (HRP)	Abcam	Cat# AB7403
Sulfo-NHS-Biotin	ApexBio	Cat# A8001
Streptavidin	Thermo Fisher Scientific	Cat# 434302
Human HER2/ErbB2 Protein (ECD), Biotinylated	Sino Biological	Cat# 10004-HCCH-B
X-VIVO15 Serum-free Media	Lonza	Cat# 04-418Q
Invitrogen Molecular Probes Calcein, AM	Thermo Fisher Scientific	Cat# C3099
Critical commercial assays		
Experimental models: Cell lines		

HEK293T cells	[106]	RRID:CVCL_0063
Expi293F cells	Gibco	RRID:CVCL_D615
Recombinant DNA		
HLA-A2-peptide (SLLMWITQV) Complex (3M4E5) Human Monoclonal Antibody heavy chain	[94]	https://patentscope.wipo.int/search/en/detail.jsf?docId=EP325866798
HLA-A2-peptide (SLLMWITQV) Complex (3M4E5) Human Monoclonal Antibody light chain	[94]	https://patentscope.wipo.int/search/en/detail.jsf?docId=EP325866798
D9 SCT MART1/ HLA-A*0201/EABR	This paper	N/A
D9 SCT NYESO1/ HLA-A*0201	This paper	N/A
D9 SCT NYESO1/ HLA-A*0201/EABR	This paper	N/A
CD80	This paper	N/A
CD80/EABR	This paper	N/A
CD83	This paper	N/A
CD83/EABR	This paper	N/A
CD274	This paper	N/A
CD274/EABR	This paper	N/A
HER2	This paper	N/A
HER2/EABR	This paper	N/A
CD54	This paper	N/A
CD54/EABR	This paper	N/A
Software and algorithms		
Image J 1.54f	NIH	https://imagej.net/ RRID: SCR_003070
Prism 10.3.1	GraphPad	
Other		
Amicon Ultra-15 100 kDa MWCO Centrifugal Filter Unit	EMD Millipore	Cat# UFC910096
Amicon Ultra-4 10 kDa MWCO Centrifugal Filter Unit	EMD Millipore	Cat# UFC801024
Nanosep with 100K Omega	Pall Life Sciences	Cat# OD100C34
Erlenmeyer cell culture flasks - 500mL	Corning	Cat# 431145
6-well Clear Flat Bottom TC-treated Multiwell Cell Culture Plate, with Lid	Falcon	Cat# 353046
30 mL BD Luer-Lok™ Syringe	BD	Cat# 302832
3 mL BD Luer-Lok™ Syringe	BD	Cat# 309657
AirOtop enhanced seal for 125 ml ultra yield flask	VWR	Cat# 899421
Costar® Spin-X® Centrifuge Tube Filters, 0.22 µm Pore CA Membrane	Corning	Cat# 8160
Polycarbonate centrifuge tubes	Beckman Coulter	Cat# 349622
0.45um syringe filter	Corning	Cat# 431220
0.2um syringe Filter	VWR	Cat# 28143-300
Nalgene™ Rapid-Flow™ Sterile Disposable Filter Unit - 0.45um	Thermo Fisher Scientific	Cat# 156-4045

Costar high binding plates, 96-well	Corning	Cat# 9018
TempPlate Sealing Foil	USA Scientific	Cat# 2923-0100
HiTrap MabSelect	Cytiva	Cat# 28408253
Superose 6 Increase 10/300 column	Cytiva	Cat# 29-0915-96
HiLoad 16/600 Superdex 200 column	Cytiva	Cat# 28-9893-35
Formvar/Carbon 300 Mesh grids	Electron Microscopy Sciences	Cat# FCF300-Cu-50

Experimental Model and Subject Details

Bacteria

E. coli DH5 Alpha cells (Zymo Research) used for expression plasmid productions were cultured in LB broth (Sigma-Aldrich) with shaking at 225 rpm at 37 °C. Plasmids were purified for transfection using Zymogen miniprep kits (Zymo Research) or maxiprep kits (Macherey-Nagel).

Cell lines

HEK293T cells plated in 6-well plates (Falcon) were cultured in Dulbecco's modified Eagle's medium (DMEM, Gibco) supplemented with 10% heat-inactivated fetal bovine serum (FBS, R&D Systems) and 1 U/mL penicillin-streptomycin (Gibco) at 37 °C and 5% CO_2. Transfections were carried out with FuGENE transfection reagent (Promega) diluted in Opti-MEM (Gibco).

Expi293F cells (Gibco) for APV expression and antibody expression were maintained at 37 °C and 8% CO_2 in Expi293 expression medium (Gibco). Transfections were carried out with an Expi293 Expression System Kit (Gibco). Falcon tubes sealed with AirOtops (VWR) or culture flasks (Corning) containing Expi293F cells were maintained under shaking at 470 rpm for 10-30 mL transfections and 130 rpm for transfections larger than 30 mL. All cell lines were derived from female donors and were not specially authenticated.

T cells

T cells were isolated from human donor whole blood samples by negative selection using the RosetteSep Human T Cell Enrichment Cocktail Kit (STEMCELL Technologies).

Isolated T cells were seeded in a fresh complete ImmunoCult™-XF T cell expansion medium (STEMCELL Technologies) at 1 x 10^6 cells/mL with 2 µL/mL ImmunoCult™ human CD3/CD28 T cell activator. T cells were activated for 3 days and expanded for up to 12 days by changing into fresh expansion medium every 2-3 days. All cells were cultured in incubators at 37 °C and 5% CO_2.

Design of EABR constructs

The EABR sequence was identical to the sequence used by Hoffmann et al. to create SARS-CoV2-S eVLPs[47]. Briefly, the EABR domain (residues 160-217) of the human CEP55 protein was fused to the C-terminus of full length membrane proteins separated by a $(Gly)_3Ser$ (GS) linker to generate constructs inserted in a p3BNC expression plasmid. To generate the SCT pMHCI construct, the N-terminus of the HLA-A*0201 alpha chain was extended with a 4x(G_4S) linker connecting to the C-terminus of B2M, which was itself extended at its N-terminus by a 3x(G_4S) linker connecting to either the 10-mer MART1 (ELAGIGILTV) or 9-mer NYESO1 (SLLMWITQV) cancer-related peptides to make a single-chain heterotrimer (SCT)[91]. To generate the "D9" version of SCT pMHCI, the alpha heavy chain was further edited with Y84C and A139C substitutions[48-50]. Constructs encoding CD80/EABR, CD83/EABR, CD274/EABR, HER2/EABR, and CD54/EABR all similarly appended an EABR domain onto the full-length native CD80, CD83, CD274, HER2, or CD54 proteins respectively.

Production of EABR APVs

EABR APVs were generated by one of two means: 1) transfecting Expi293F cells (Gibco) cultured in Expi293F expression media (Gibco) on an orbital shaker at 37 °C and 8% CO2 with plasmid DNA pre-filtered through 0.22 µm Spin-X filters (Corning); 2) transfecting HEK293T cells cultured in Dulbecco's modified Eagle's medium (DMEM, Gibco) supplemented with 10% heat-inactivated fetal bovine serum (FBS, Sigma-Aldrich) and 1 U/ml penicillin-streptomycin (Gibco) at 37 °C and 5% CO_2. 72 hours post-transfection, cells were centrifuged at 1000 x g for 10 min, supernatants were passed through a 0.45 um filter (Corning) with Luer-Lok syringes (BD) or a 0.45 um vacuum filter (Thermo Fisher

Scientific), and concentrated using Amicon Ultra-15 centrifugal filters with 100 kDa molecular weight cut-off (Millipore). APVs were purified by ultracentrifugation at 50,000 rpm (135,000 x g) for 2 hours at 4 °C using a TLA100.3 rotor and an OptimaTM TLX ultracentrifuge (Beckman Coulter) on a 20% w/v sucrose cushion in polycarbonate centrifuge tubes (Beckman Coulter). Supernatants and the sucrose cushion were removed, and pellets were re-suspended in 200 uL sterile pH 7.4 PBS at 4 °C overnight. To remove residual cell debris, re-suspended samples were transferred to microcentrifuge tubes and centrifuged at 10,000 x g for 10 min; clarified supernatants were collected for subsequent ELISA and nanoFCM assays. For immuno-EM grid preparations, APVs were further purified by SEC using a Superose 6 Increase 10/300 column (Cytiva) equilibrated with pH 7.4 PBS. Peak fractions in the void volume corresponding to pMHCI APVs were combined and concentrated to 250-500 uL in Amicon Ultra-4 centrifugal filters with 100 kDa molecular weight cut-off (Millipore) or Nanosep with 100K Omega centrifugal filters (Pall). Samples were stored at 4 °C and imaged directly after purification.

Transduction of TCRs in PBMC

Peripheral blood mononuclear cells (PBMCs) were isolated and processed following a previously published protocol with some modifications. The MSGV retroviral backbone was utilized to overexpress the target T cell receptors (TCRs) with a truncated human nerve growth factor receptor (tNGFR) serving as the transduction marker. TCR alpha and beta chains were expressed with a F2A linker to maintain approximately equal copy numbers. To reduce mispairing with endogenous human TCRs, the human TCR constant regions were replaced with murine constant regions. Commercially obtained, cryopreserved PBMCs from healthy donors (AllCells) were revived in T cell media (TCM) comprising AIM V media (Thermo Fisher, #12055-091), 5% Human AB serum (Omega Scientific), 50 U/mL human recombinant IL-2 (Peprotech, #200-02), 1 ng/mL human recombinant IL-15 (Peprotech, #200-15), 1X Glutamax (Thermo Fisher, 35050-061), and 50 μM β-mercaptoethanol. These cells were mixed with CD3/CD28 dynabeads (Thermo Fisher, #11132D) at a concentration of 25 μL beads per million PBMCs and incubated overnight at 37°C and 5% CO2 (day 0). On days 1 and 2, TCR-expressing retroviral supernatant was

added at a ratio of 2 mL per two million PBMCs, followed by a 90-minute spin infection at 1,350 x g and 30°C. Excess retrovirus was removed on day 3 with a phosphate-buffered saline (PBS) wash, and cells were resuspended in TCM. CD3/CD28 dynabeads were removed using magnets on day 5, and PBMCs were maintained in TCM at a concentration of one million cells per mL. Cell phenotypes (CD3, CD8), transduction efficiency (NGFR), and TCR membrane trafficking (murine TCRβ or mTCRb) were assessed using flow cytometry on day 7. For long-term storage, transduced PBMCs were preserved in CryoStor CS10 serum-free cryopreservation medium (STEMCELL Technologies #07930) at -80°C overnight before transferring to liquid nitrogen.

Antibody Expression

Anti-HLA-A2-peptide (SLLMWITQV) Complex (3M4E5) antibody was made in-house by expressing the heavy chain and light chain of the 3M4E5 antibody at a 1.5:1 plasmid ratio in Expi293F cells.[94] Supernatant from the transiently-transfected Expi293F cells (Gibco) was separated from the cells by pelleting at 3500g for 15 minutes and filtering the clarified supernatant through a 0.2 um syringe filter (VWR) or 0.45 um vacuum filter unit (Thermo Fisher Scientific). The filtered supernatant was further purified using Fc-affinity chromatography (HiTrap MabSelect, Cytiva) and SEC (HiLoad 16/600 Superdex 200 column, Cytiva). Peak fractions corresponding to purified antibody proteins were pooled, concentrated, and stored at 4 °C. Biotinylated antibodies for ELISAs were generated and purified using an EZ-Link biotinylation kit (Thermo Fisher Scientific). The in-house generated antibody was compared to a commercially available 3M4E5 antibody (RHM03002-100; ProteoGenix) with ELISA and showed identical performance (data available upon request).

Immuno-EM of EABR-mediated vesicles

SEC-purified EABR-mediated vesicles were prepared on grids for negative stain transmission electron microscopy at room temperature. Formvar/Carbon 300 Mesh grids (Electron Microscopy Sciences) were first glow discharged. 20 uL of purified sample was pipetted onto paraffin, glow discharged formvar/carbon 300 mesh grids were placed on the

droplet of sample for 5 minutes, then gently wicked away by dabbing the edge of the grid on filter paper. The grids were then placed on a 20uL droplet of 1% paraformaldehyde (Electron Microscopy Sciences) in pH 7.4 PBS for 10 minutes, and subsequently wicked away. Grids were washed three times by placing the grids on droplets of pH 7.4 PBS for 5 minutes, and wicking away the PBS with filter paper after each wash. Grids were then blocked by placing the grids on droplets of 5% FBS diluted in pH 7.4 PBS for one hour. Blocking solution was wicked away from the grids, and the grids were then placed on droplets of primary antibody (pMHCI vesicles: αNYESO1:HLA-A*02:01 (3M4E5) diluted to 150ug/mL and mouse αCD80 (#14-0809-82; Thermo Fisher Scientific) diluted 1:10; HER2 vesicles: aCD54 (#MA5-41137; Thermo Fisher Scientific) diluted 1:10 and aHER2 (#324402; BioLegend) diluted 1:20) in 5% sucrose, 5% FBS pH 7.4 PBS for 2 hours. To prevent drying of the primary antibody solution, the grids were placed in a humidified chamber made from wet paper towels folded under a pyrex glass dish. Grids were again washed three times by placing the grids on droplets of pH 7.4 PBS for 10 minutes, and wicking away the PBS with filter paper after each wash. The grids were then placed on droplets of colloidal gold-conjugated secondary antibody (pMHCI vesicles: 6 nm colloidal gold goat anti-human antibody (#109-195-088; Jackson ImmunoResearch) diluted 1:20 and 12 nm colloidal gold goat anti-mouse antibody (#115-205-146; Jackson ImmunoResearch) diluted 1:20; HER2 vesicles: 6 nm colloidal gold goat anti-rabbit antibody (#111-195-144; Jackson ImmunoResearch) diluted 1:20 and 12 nm colloidal gold goat anti-mouse antibody (#115-205-146; Jackson ImmunoResearch) diluted 1:20) in 5% sucrose, 5% FBS pH 7.4 PBS for 1 hour. Grids were subsequently washed three times, ten minutes per wash with pH 7.4 PBS, wicking away the PBS after the ten minute wash each time. Finally, the grid was placed on a droplet of 1.5% uranyl formate (Electron Microscopy Sciences), prepared fresh within 1 week of use, for 1 minute. The excess uranyl formate was wicked away and the grid was left to air dry for 30 minutes before storing at room temperature away from light. Imaging of HER2 grids were performed on a FEI Tecnai T12 Transmission Electron Microscope within two days after the grids were prepared. The NYESO1/HLA-A*0201/EABR+CD80 formvar grids were unexpectedly sensitive to the T12 beam and

frequently ruptured before we could acquire an image, so these negative-stain grids were imaged using an FEI Talos Arctica.

Sandwich ELISA

96-well plates (Corning) were coated with 5 ug/mL of capture antibody diluted in sterile 0.1 M $NaHCO_3$ pH 9.6, and sealed with TempPlate sealing foil (USA Scientific) overnight at 4 °C. Capture antibodies included: CD340 (erbB2/HER-2) (#324402; Biolegend), CD54 (ICAM-1) (#14-0549-82; Thermo Fisher Scientific), CD80 (B7-1) (#14-0809-82; Thermo Fisher Scientific), CD83 (#305302; Biolegend), CD274 (PD-L1, B7-H1) (#14-5983-82; Thermo Fisher Scientific). Plates were emptied and blocked with TBS-T/3% BSA for at least 30 minutes. Plates were again emptied, and vesicle samples 4-fold serially diluted in TBS-T/3% BSA were added to the plates. After a 2-hour incubation at room temperature, plates were emptied, and 5 ug/mL of biotinylated detection antibody diluted in TBS-T/3% BSA was added to the plates. Detection antibodies included: biotinylated αErbB2 (HER-2) (#MA5-13672; Thermo Fisher Scientific), biotinylated αCD54 (ICAM-1) (#13-0549-82; Thermo Fisher Scientific), biotinylated αCD80 (B7-1) (#13-0809-82; Thermo Fisher Scientific) biotinylated αCD83 (#305304; Biolegend), biotinylated αCD274 (PD-L1, B7-H1) (#13-5983-82; Thermo Fisher Scientific). After another 2-hour incubation at room temperature, plates were washed three times with TBS-T. HRP-conjugated streptavidin (Abcam) was diluted to manufacturer's recommendations in TBS-T/3% BSA and added to plates for 30 minutes at room temperature. After washing three times with TBS-T, plates were developed using 1-Step™ Ultra TMB-ELISA Substrate Solution (Thermo Fisher Scientific) and absorbance was measured at 450 nm. Standard 4-parameter sigmoidal binding curves were calculated using GraphPad Prism 10.3.1 without any further editing.

Nanovial Fabrication

Polyethylene glycol biotinylated nanovials with 35 μm diameters were fabricated using a three-inlet flow-focusing microfluidic droplet generator, sterilized and stored at 4 °C in Washing Buffer consisting of Dulbecco's Phosphate Buffered Saline (Thermo Fisher) with

0.05% Pluronic F-127 (Sigma), 1% 1X antibiotic-antimycotic (Thermo Fisher), and 0.5% bovine serum albumin (Sigma) as previously reported.[119]

Nanovial Functionalization

Streptavidin conjugation to the biotinylated cavity of nanovials. Sterile nanovials were diluted in Washing Buffer five times the volume of the nanovials (i.e., 100 μL of nanovial volume was resuspended in 400 μL of Washing Buffer). A diluted nanovial suspension was incubated with equal volume of 200 μg/mL of streptavidin (Thermo Fisher) for 30 min at room temperature on a tube rotator. Excess streptavidin was washed out three times by pelleting nanovials at 2,000 × g for 30 s on a Galaxy MiniStar centrifuge (VWR), removing supernatant and adding 1 mL of fresh Washing Buffer.

Anti-CD45 and cytokine capture antibody labeled nanovials. Streptavidin-coated nanovials were reconstituted at a five times dilution in Washing Buffer containing 140 nM (20 μg/mL) of each biotinylated antibody or cocktail of antibodies: anti-CD45 (Biolegend, 368534) and anti-IFN-γ (R&D Systems, BAF285), anti-human NYESO1/HLA-A2 (3M4E5). Nanovials were incubated with antibodies for 30 min at room temperature on a rotator and washed three times as described above. Nanovials were resuspended at a five times dilution in Washing Buffer or culture medium prior to each experiment.

pMHC labeled nanovials. MHC monomers with peptides of interest were synthesized and prepared according to a published protocol.[162] Streptavidin-coated nanovials were reconstituted at a five times dilution in Washing Buffer containing 20 μg/mL biotinylated pMHC and 20 μg/mL biotinylated anti-human IFN-γ antibody.

Chapter 4

HUMAN TONSIL ORGANOIDS AS A TESTBED FOR ENGINEERING ANTIGEN-PRESENTING VESICLES & ADENO-ASSOCIATED VIRUS IMMUNOGENICITY

4.1 Abstract

Recent advances have demonstrated the application of human tonsil organoids for studying the adaptive immune response during vaccination.[163] Under the guidance of Dr. Lisa Wagar's lab at UC Irvine, we recreated this nascent platform and subsequently performed initial experiments with EABR-mediated synthetic antigen-presenting vesicles to explore their immunomodulatory potential in a more physiologically-relevant environment than the monoclonal TCR-transduced T cells assayed in Chapter 2. The latter half of this chapter then explores the potential for human tonsil organoids to recapitulate anti-AAV antibodies seen in clinical gene therapy trials.[68,69] The translatability of AAVs into clinical settings is still limited by the prevalence of pre-existing anti-AAV antibodies and the adaptive immune-responses that neutralize the therapeutic efficacy of the virus, as well as immune-mediated toxicity that leads to adverse-events post-AAV administration. Optimization of AAV capsids to evade the host immune response is needed to create the ideal vehicle for *in vivo* gene delivery, and human tonsil organoids provide a high-throughput platform for directed evolution of AAV capsids with reduced immunogenicity.

4.2 Introduction

Recent studies have demonstrated the importance of physiologically relevant model systems for studying immune cell activation by extracellular vesicles (EVs), particularly in the context of cancer and autoimmune diseases.[3,84,136,147] However, these curated cell assays and animal models, while valuable, do not fully recapitulate the inherent complexity of human immune organs, potentially limiting their physiological relevance. More than two decades ago, foundational work by Owen and Jenkinson illustrated the capacity of dissociated murine thymic cells to reassociate *in vitro*, successfully recapitulating critical aspects of T cell

development, including T cell selection and precursor differentiation.[164,165] More recently, Wagar et al. characterized a method for generating human tonsil organoids from routine tonsillectomies.[163] These tonsil organoids provide a facile, physiologically-relevant context for examining immune cell dynamics, including B cell and T cell maturation upon antigen exposure. Under the guidance of the Wagar lab, we replicated the human tonsil organoid platform and subsequently investigated the immunomodulatory properties of EABR-mediated pMHCI synthetic antigen-presenting vesicles. Early results with HLA-A*0201 donors show that purified antigen-presenting vesicles displaying for $M1_{58-66}$(GILGFVFTL)/HLA-A*0201/EABR antigen-presenting vesicles stimulate changes in the relative surface expression of CD25 and CD69 in T cells after enriching for $M1_{58-66}$(GILGFVFTL):HLA-A*0201 binding. Importantly, human tonsil organoids support future studies of pMHCII antigen-presenting vesicles, enabling detailed investigations of their immunomodulatory roles in B cell activation, differentiation, and antibody production.

We then build upon Dr. Wagar's tonsil organoid studies of immunogenicity by stimulating the production of anti-AAV (Adeno-associated virus) antibodies to model the adaptive immune response of patients that respond negatively to gene therapy. Adeno-associated viruses are small, non-pathogenic viruses that have become the leading candidate vector for *in vivo* gene therapy due to their ability to achieve stable long-term transgene expression without integration into the host genome. AAV-based gene therapies have already shown preliminary success in the clinic, with 7 FDA and EMA approved on market and many more in trials. However, the translatability of AAVs into clinical settings is still limited by the prevalence of pre-existing anti-AAV antibodies and the adaptive immune-responses that neutralize the therapeutic efficacy of the virus, as well as immune-mediated toxicity that leads to adverse-events post-AAV administration.[69,71] Previous methods for AAV immunogenicity reduction have relied on computational models that have not been experimentally validated, simplified *in vitro* models that do not measure the critical endpoint of antibody production, or non-human animal models which cannot accurately recapitulate the human immune response.[81-83] Leveraging Wagar's tonsil organoid system, we demonstrate the expansion of B cell plasmablasts in cultures stimulated with AAV9, and subsequently quantify their de novo antibody production that is specific to AAV. Not all

tonsil donors respond to AAV challenge, and future work will look to identify what features are critical for inducing antibody production in reactive donors, as well as scaling this platform to support directed evolution of non-immunogenic AAV capsid variants.

4.3 Results

4.3.1. Human tonsil organoids provide a testbed for engineering immunomodulatory antigen-presenting vesicles

Mirroring the original tonsil organoid protocol in Wagar et al.,[163] healthy human tonsils collected from routine patient tonsillectomies are dissociated into single-cell suspensions within 36 hours of removal and assayed for HLA-A*0201 positivity during cryopreservation (Fig. S4.1). Subsequent thaw and plating of these HLA-A*0201+ donor single-cell suspensions are co-cultured with synthetic antigen-presenting vesicles generated as described in Chapter 2. After 7 days of culture, aggregates of tonsillar immune cell organoids are resuspended by aspiration, washed, and stained with APC-conjugated M1:A2 tetramer that binds T cells with TCRs specific for the $M1_{58\text{-}66}$ (GILGFVFTL):HLA-A*0201 epitope. Tetramer staining was followed by FITC anti-CD8, PE-Cy7 anti-CD25, PE-Dazzle 594 anti-CD127, Brilliant Violet 785 anti-CD69, and Zombie Violet Live/Dead stain. Subsequent washes are followed by incubation with anti-APC magnetic beads that allow for enrichment of M1:A2-specific T cells (Fig. 4.1). As described in prior work, this magnetic bead enrichment is often necessary for significant isolation and identification of M1:A2-specific T cells, even when monitoring $M1_{58\text{-}66}$ (GILGFVFTL)-specific T cell proliferation after influenza vaccination.[166] The CD8+ T cell population of the cells retained by the magnetic beads was significantly increased compared to unfiltered tonsil organoid cells, and the APC fluorescence of this enriched population was increased compared to the filtrate (Fig S4.2). Human tonsil organoid cells that were stimulated with 10ug of M1/D9/EABR antigen-presenting vesicles immediately after plating showed a noticeable increase in CD69+ cells, an early activation marker on T cells (Fig. 4.2). More specifically, the CD25+ CD69+ population increased and the CD25+ CD69- population decreased compared to unstimulated control, demonstrating a change in T cell activation. Though only one donor is shown here, and only simple markers of activation were assayed, these results provide a first

demonstration of the utility of human tonsil organoids for assaying and engineering the immunomodulatory potential of antigen-presenting vesicles for targeted T cell and B cell therapies.

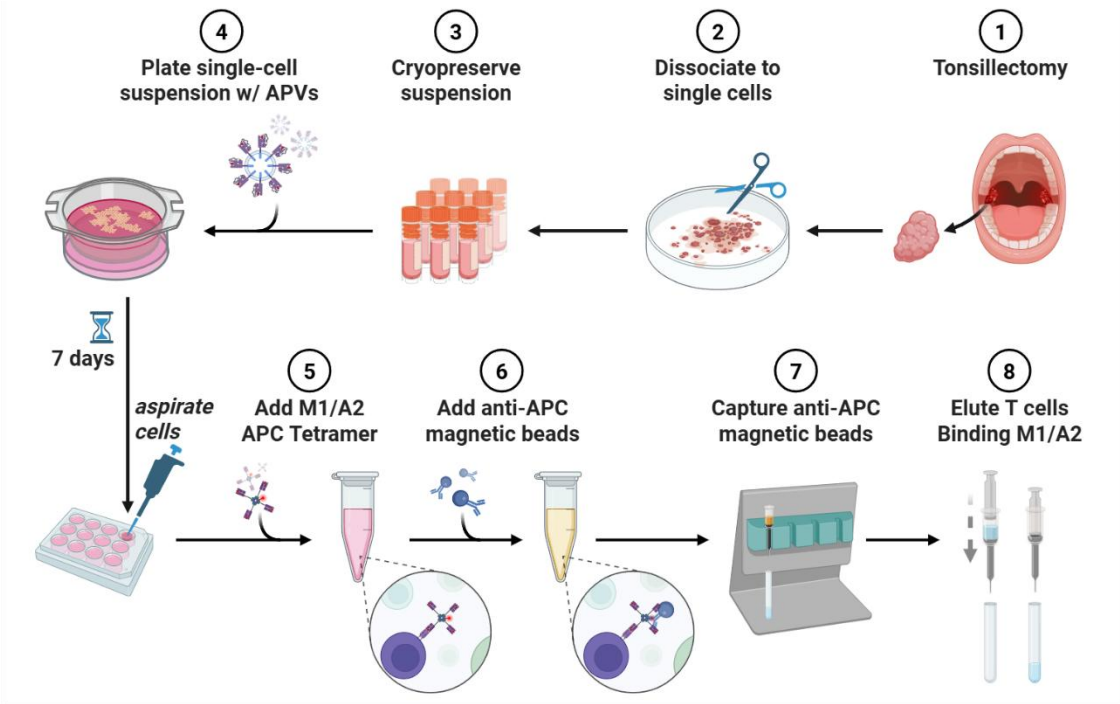

Figure 4.1. Human tonsil organoids provide a testbed for engineering immunomodulatory antigen-presenting vesicles

Schematic demonstrating the pipeline for testing and analyzing the immunomodulatory potential of synthetic antigen-presenting vesicles.

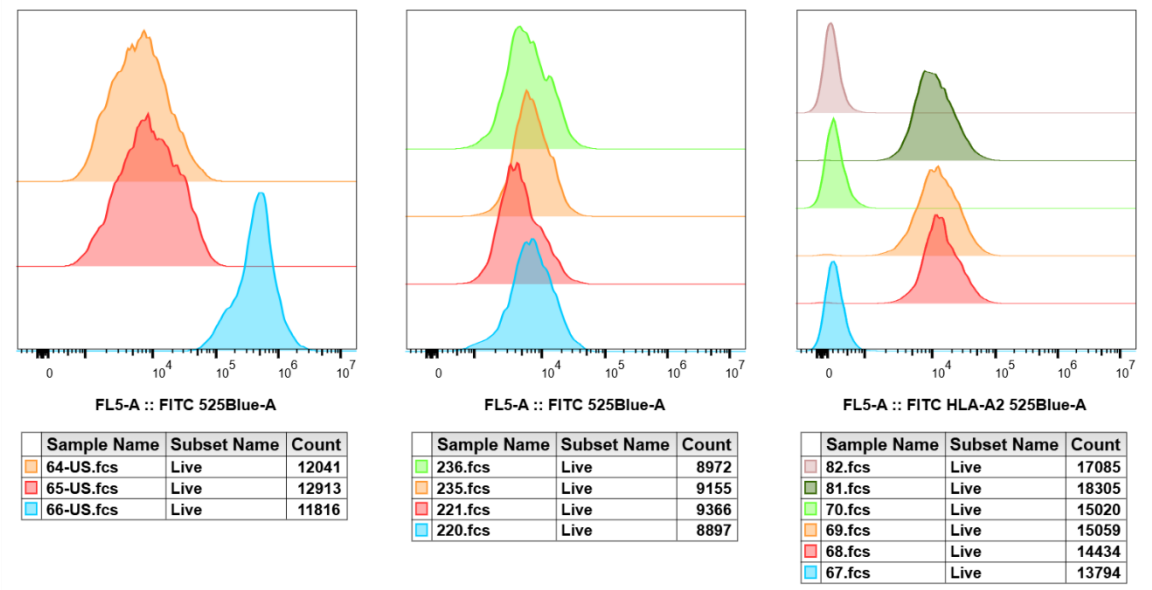

Sample Name	Subset Name	Count
64-US.fcs	Live	12041
65-US.fcs	Live	12913
66-US.fcs	Live	11816

Sample Name	Subset Name	Count
236.fcs	Live	8972
235.fcs	Live	9155
221.fcs	Live	9366
220.fcs	Live	8897

Sample Name	Subset Name	Count
82.fcs	Live	17085
81.fcs	Live	18305
70.fcs	Live	15020
69.fcs	Live	15059
68.fcs	Live	14434
67.fcs	Live	13794

Figure S4.1. Flow cytometry of human tonsil donors showing HLA-A*0201 positivity

Tonsils from patient donors arrived in three separate deliveries and were assayed for HLA-A*0201 presence by flow cytometry on three separate days (left, middle, and right). Donor 68 (right) was found to be both HLA-A*0201+ and had a pronounced population of CD8+ T cells (8-10% of the tonsil cells were CD8+ after processing), so initial testing of EABR-mediated pMHCI APVs was performed with this donor.

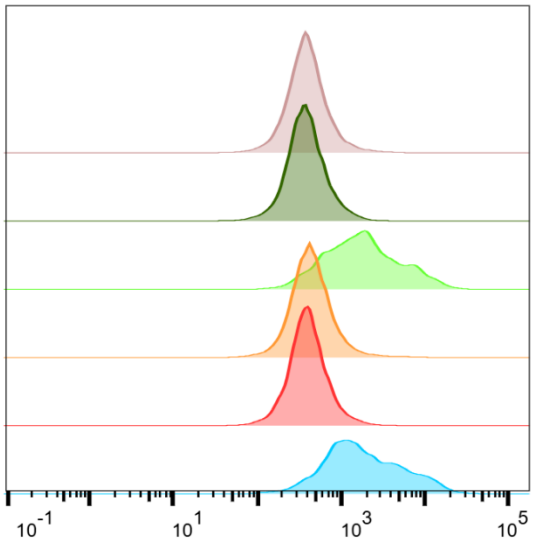

	Subset Name	Count
	LAIV, unfiltered	16660
	LAIV, filtrate	7945
	LAIV, M1:A2 enriched	603
	Unstimulated, unfiltered	23838
	Unstimulated, filtrate	3848
	Unstimulated, M1:A2 enriched	787

Figure S4.7.2. Comparison of flow cytometry signals from unfiltered, filtrate, and retained M1:A2-binding tonsil organoid cells

Flow cytometry of cells stained with APC-conjugated M1:A2 tetramer and gated as in Fig. 4.7.2.A after magnetic bead separation with anti-APC magnetic MicroBeads. “Unfiltered” cells were not passed through a magnetic bead column. “Filtered” cells were tonsil organoid cells that were not retained on the magnetic bead column and passed through to collection during multiple washes. “M1:A2 enriched” cells were retained on the magnetic bead column after multiple washes with FACS buffer and were subsequently eluted after removal from the magnetic field. Cells bound to M1:A2 tetramer are noticeably difficult to identify in the “unfiltered” fraction, but are much more pronounced after magnetic bead enrichment.

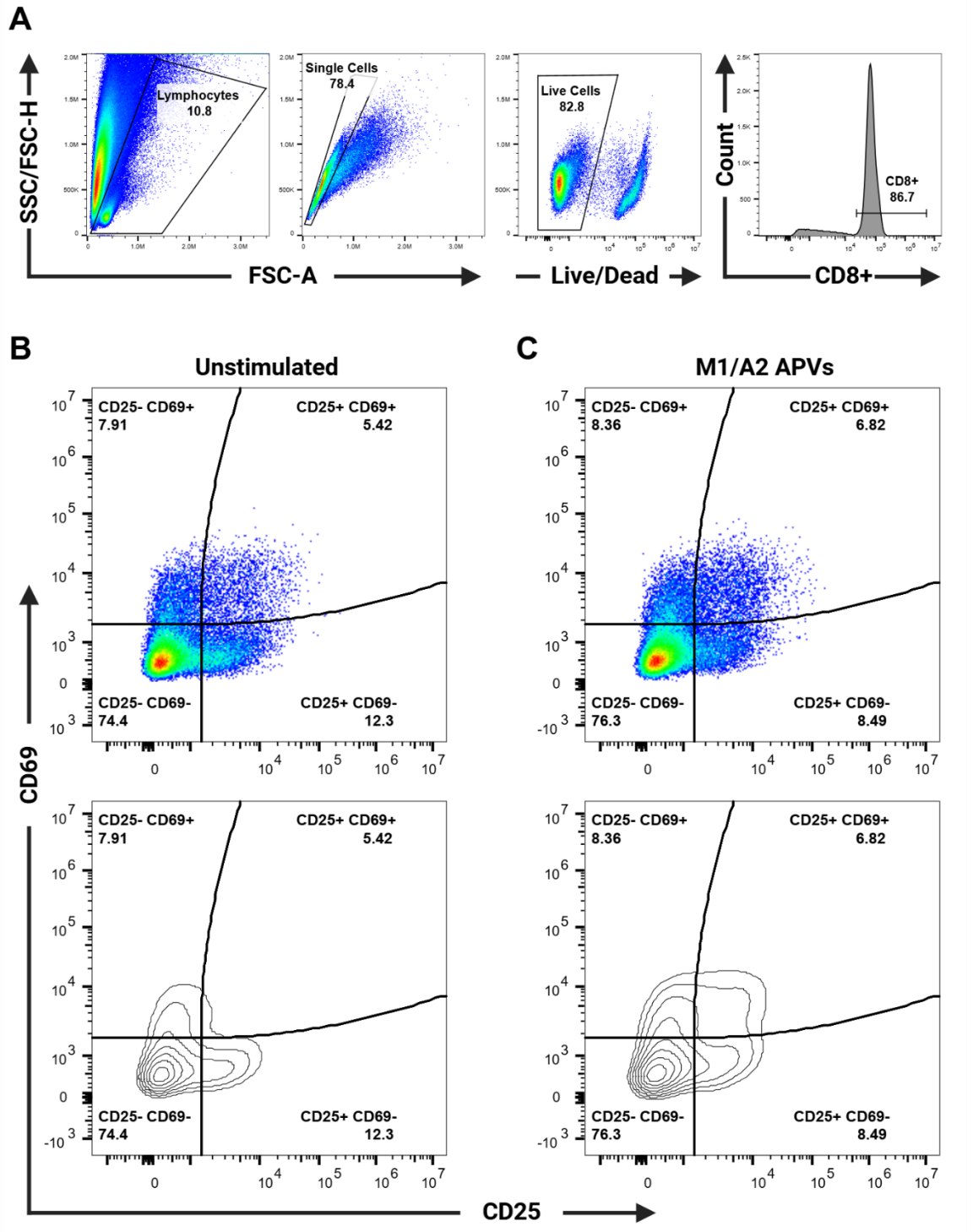

Figure 4.2. Flow cytometry of human tonsil organoids after stimulation by EABR-mediated antigen-presenting vesicles & magnetic-bead enrichment by M1:A2 tetramer

(A) Representative gating pipeline for identifying CD8+ T cells isolated from human tonsil organoids after magnetic bead sorting in Fig. 4.6.1. From left to right: lymphocytes are identified by comparing SSC to FSC-A, single cells are identified when comparing FSC-H to FSC-A, zombie violet separates live cells from dead, and FITC CD8+ cells should subsequently be enriched.

(B-C) Flow cytometry of human tonsil organoids that were enriched by magnetic bead sorting of M1:A2-binding cells as described in Fig. 4.6.1. Cells were co-stained with FITC anti-CD8, PE-Cy7 anti-CD25, PE-Dazzle 594 anti-CD127, and Brilliant Violet 785 anti-CD69, and then gated as in Fig. 4.6.2.A.

(B) Flow cytometry results of unstimulated cells from a single donor after a 7-day culture in a single transwell. The top subplot is a pseudocolor display of individual data points that is represented in the bottom subplot by a log contour plot of the same data.

(C) Flow cytometry results of cells from the same donor as Fig. 4.6.2.B after a 7-day culture in a single transwell; cells were stimulated with 10ug of M1/D9/EABR antigen-presenting vesicles immediately after plating. The top subplot is a pseudocolor display of individual data points that is represented in the bottom subplot by a log contour plot of the same data. The CD25+ CD69- population has decreased and the other quadrants, most notably the CD25+ CD69+ population, have increased compared to Fig. 4.6.2.B.

4.3.2. Human tonsil organoids provide a testbed for engineering the immunogenicity of Adeno-Associated Viruses

We next explored the utility of human tonsil organoids for characterizing the immunogenicity of the AAV9 capsid that is used for current clinical trials of gene therapy.[63,81] Human tonsil organoids from four donors were dosed with a series titration of AAV9 capsid after confirming that all four donors were responsive to FluMist live attenuated influenza A virus (Fig. S4.3). One of the donors was completely unresponsive to AAV9, one of the donors generated non-specific antibodies against AAV9 that were similar to unstimulated control, and two of the donors generated AAV9-specific antibody. “Donor 2” seemed capable of generating anti-AAV9 IgG in a narrow AAV9 dosing window, and “Donor 3” generated high concentrations of anti-AAV9 IgM. This same “Donor 3” generated

anti-AAVx1.1 antibodies that were broadly cross-reactive with AAV9 and AAV-DJ (data not shown). Though anti-AAV9 antibody production and plasmablast differentiation was not as pronounced as the response to FluMist LAIV, flow cytometry of these donors' tonsil organoids demonstrated an increase in the CD27+ CD38+ plasmablast population when dosed with AAV9 capsid, indicating B cell differentiation and de novo antibody production (Fig. 4.3). Further engineering and assays of AAV9 immunogenicity using human tonsil organoids are ongoing.

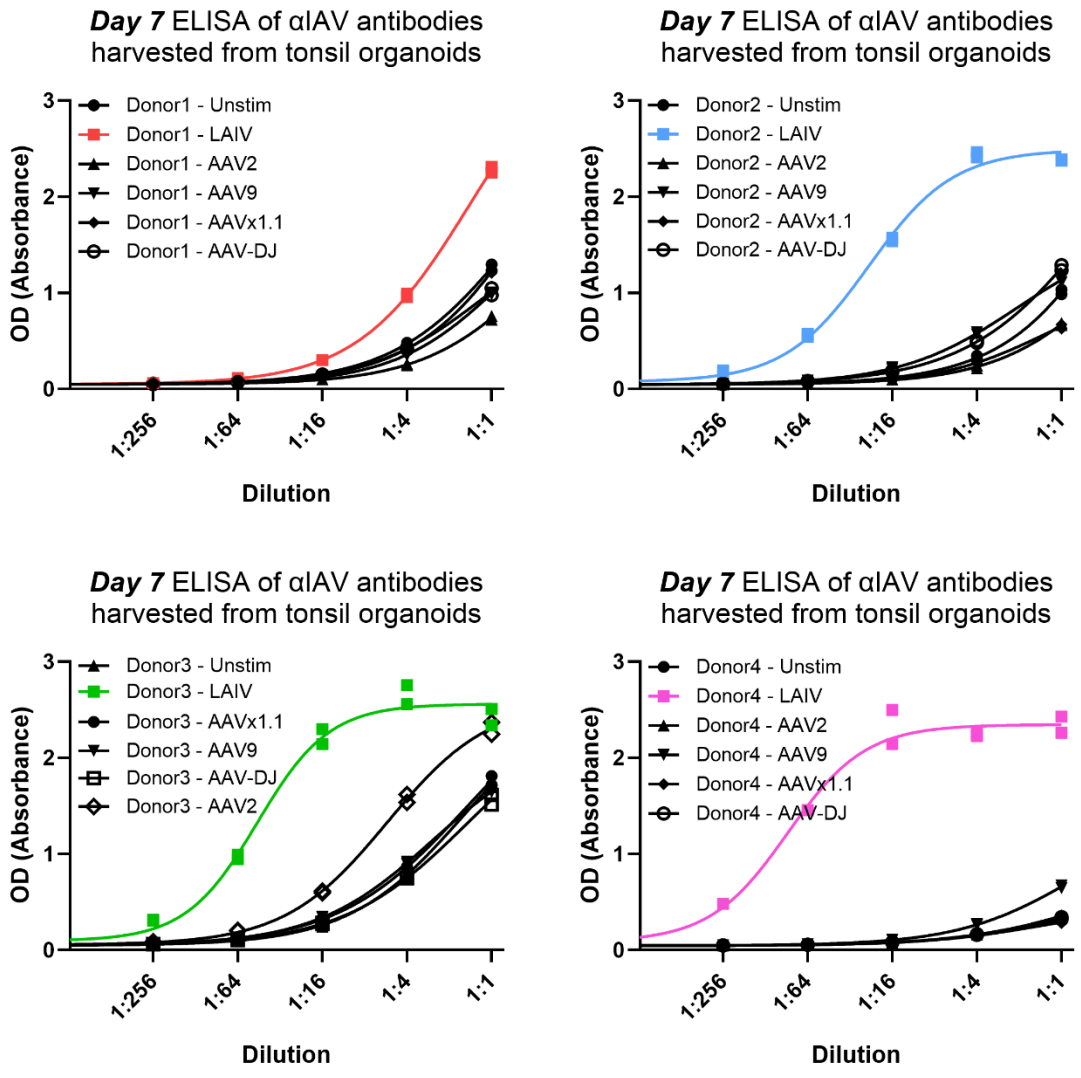

Figure S4.3. Indirect ELISA of human tonsil donors demonstrating influenza-specific antibody responses after stimulation by multiple antigens

Indirect ELISA of inactivate influenza A virus (Fluzone) using primary antibody from human tonsil organoid cultures. Human tonsil organoids from each donor were challenged with LAIV, AAVx1.1, AAV9, AAV-DJ, AAV2, or left unstimulated. Primary antibody from organoid cultures that bound inactivated influenza A virus (Fluzone) were detected using secondary HRP-conjugated IgG and IgM anti-human antibody.

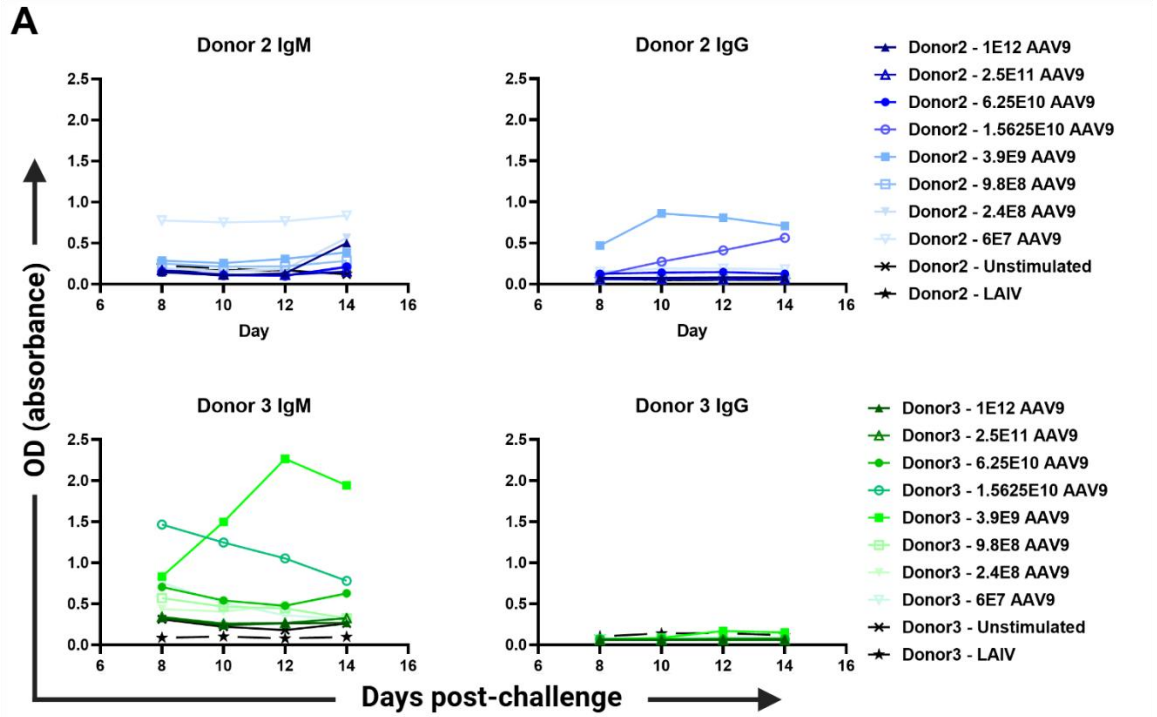
A
Donor 2 IgM
Donor 2 IgG
Donor 3 IgM
Donor 3 IgG
OD (absorbance)
Day
Days post-challenge
Donor2 - 1E12 AAV9
Donor2 - 2.5E11 AAV9
Donor2 - 6.25E10 AAV9
Donor2 - 1.5625E10 AAV9
Donor2 - 3.9E9 AAV9
Donor2 - 9.8E8 AAV9
Donor2 - 2.4E8 AAV9
Donor2 - 6E7 AAV9
Donor2 - Unstimulated
Donor2 - LAIV
Donor3 - 1E12 AAV9
Donor3 - 2.5E11 AAV9
Donor3 - 6.25E10 AAV9
Donor3 - 1.5625E10 AAV9
Donor3 - 3.9E9 AAV9
Donor3 - 9.8E8 AAV9
Donor3 - 2.4E8 AAV9
Donor3 - 6E7 AAV9
Donor3 - Unstimulated
Donor3 - LAIV

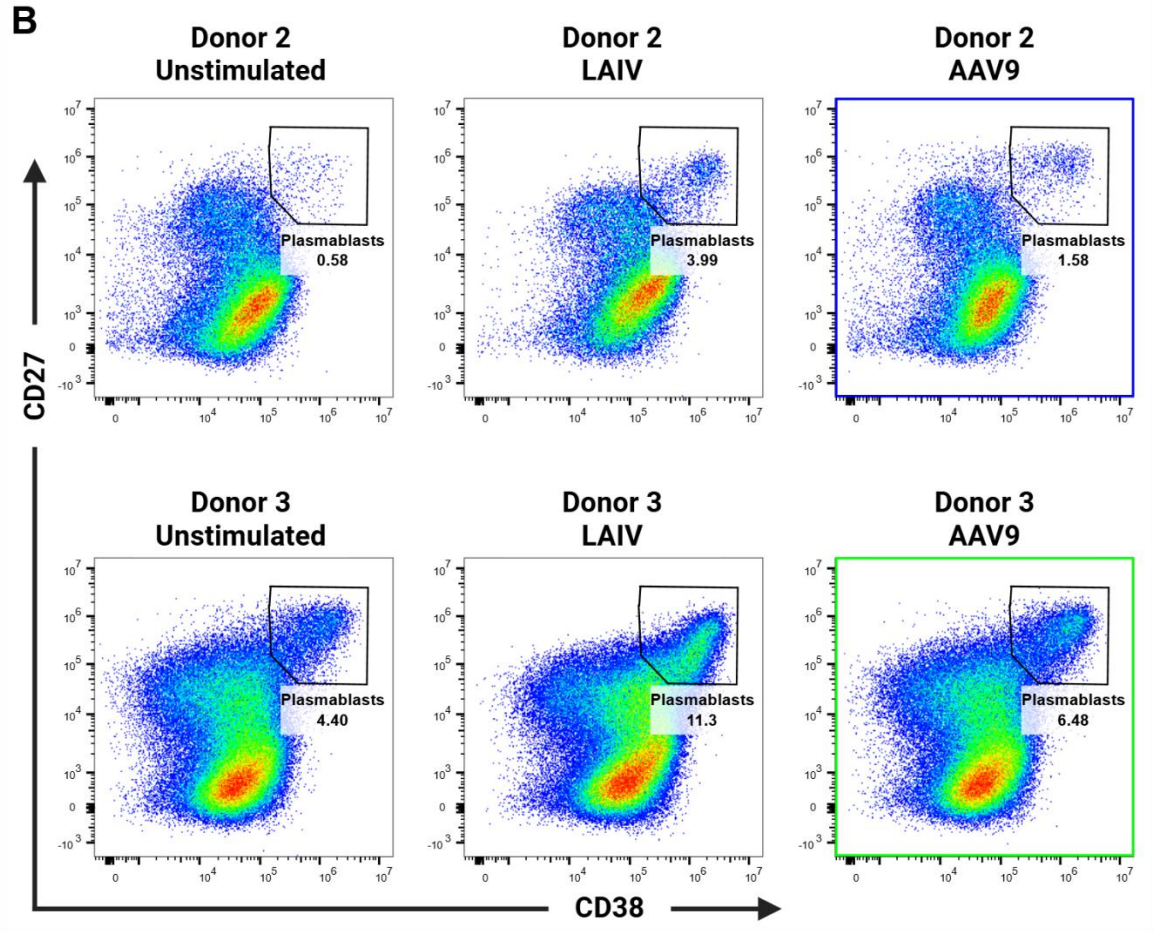
B
Donor 2 Unstimulated
Donor 2 LAIV
Donor 2 AAV9
Donor 3 Unstimulated
Donor 3 LAIV
Donor 3 AAV9
Plasmablasts 0.58
Plasmablasts 3.99
Plasmablasts 1.58
Plasmablasts 4.40
Plasmablasts 11.3
Plasmablasts 6.48
CD27
CD38

Figure 4.3. ELISA and flow cytometry data of two tonsil donors that generated anti-AAV9 antibodies during a titration study in human tonsil organoids

(A) ELISA of IgM and IgG antibody responses from human tonsil organoids that were challenged with a series titration of AAV9 capsid carrying DNA encoding GFP.

(B) Flow cytometry results of Donors 2 and 3 from (A) that were gated on live, CD19+ single cells. The antibody-forming plasmablast populations are increased when the organoids are dosed with 2E10 AAV9 capsid or 1uL of FluMist LAIV.

4.4 Discussion

Here, we demonstrate the use of human tonsil organoids for characterizing the T cell activation potential of pMHCI EABR-mediated synthetic antigen-presenting vesicles. This initial feasibility study acts as a proof of concept for further characterization studies of the immunomodulatory potential of extracellular vesicles, including EABR-mediated vesicles generated by mRNA transfection. Further, we show here initial experimental results demonstrating that human tonsil organoids can be used to advance our understanding of AAV immunogenicity.

After processing the tissue for cryopreservation, a typical tonsil from a human donor contains ~1 billion viable cells that can be used for tonsil organoid cultures. Considering 1.5E6 of these cryopreserved cells are used per well for a 96-well organoid culture, and each donor yields two tonsils, over 1,000 wells of a 96-well plate can be plated per donor, enabling high-throughput assays of immunogenicity. With over 250,000 tonsillectomies performed annually in children less than 15 years of age,[167] tonsils are a readily available resource with which we can build a platform for pre-clinical optimization and analysis of AAV immunogenicity in preparation for AAV clinical studies.

Together, these findings demonstrate the utility of human tonsil organoids for engineering antigen-presenting vesicles and the feasibility of using human tonsil organoids as a quantitative assay for adenoviral vector immunogenicity, enabling directed evolution approaches for immunogenicity reduction as well as generation of an immunogenicity dataset to tailor modern computational protein design algorithms for human applications (Fig. 4.4).

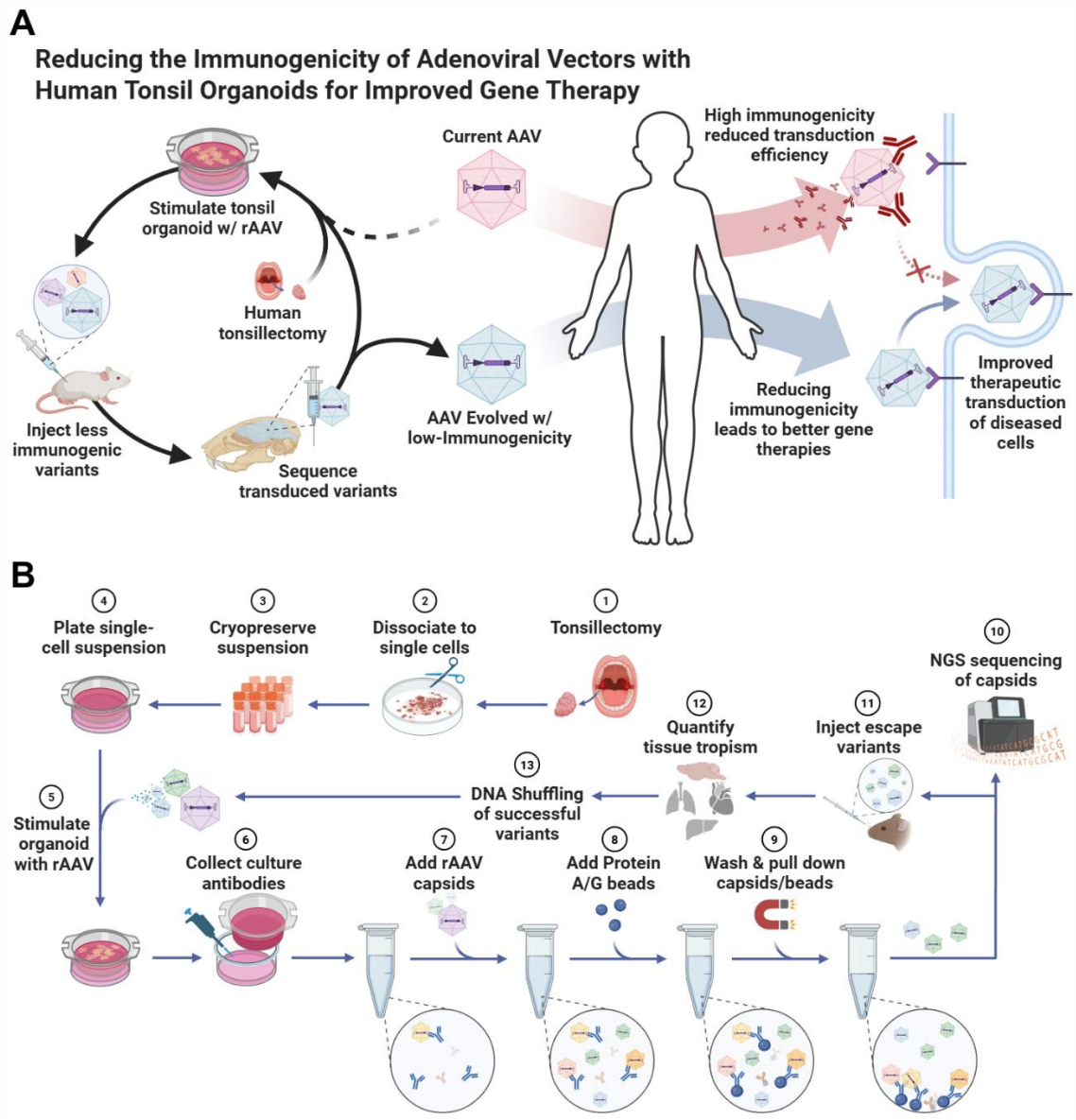

Figure 4.4. Human tonsil organoids provide a testbed for engineering the immunogenicity of Adeno-Associated Viruses

(A) A schematic describing the high-level clinical need for reduced AAV immunogenicity and an experimental approach to reducing immunogenicity through directed evolution and human tonsil organoids.

(B) A schematic providing further details for how AAV capsids with reduced immunogenicity could be engineered and selected in a high-throughput fashion.

4.5 Acknowledgments

B.A.O. thanks the NIH Tetramer Core Facility (contract number 75N93020D00005) for providing M1:HLA-A*02:01 tetramers. B.A.O. thanks Changfan Lin, Rana Eser, and Viviana Gradinaru of the Gradinaru Lab for helpful discussions. B.A.O. thanks Rana Eser for her work generating AAV capsids and for providing commercial antibody for AAV9 detection. B.A.O. thanks Zach Wagoner and Lisa Wagar of the Wagar Lab at UCI for providing human tonsils for an initial pilot study of AAV9 immunogenicity in human tonsil organoids. B.A.O. thanks Sam Kim of the Wagar Lab at UCI for helpful discussions and training the Mayo Lab for human tonsil organoid processing and culture. B.A.O. thanks Olive Cheng for tonsil processing, tonsil antigen challenge with AAV9, performing ELISA of tonsil organoid supernatant, and for performing flow cytometry of tonsil organoid cultures.

4.6 Methods

Informed consent and sample collection

Whole palatine tonsils from 12 consented individuals with no prior chemotherapy or radiation therapy undergoing routine tonsillectomy for obstructive sleep apnea (OSA) or benign tonsillar hypertrophy were collected by the Cooperative Human Tissue Network (CHTN) with ethics approval granted by the California Institute of Technology IRB (protocols IR24-1440). After surgery, whole tonsils were collected in RPMI supplemented with 10% FBS and 100 ug/mL Penicillin, 100 ug/mL Streptomycin, and 2.5ug/mL Amphotericin B. Tonsils were delivered within 24 hours of surgery and subsequently immersed in an antimicrobial bath of Ham's F12 medium (Gibco) containing Normocin (InvivoGen), penicillin, and streptomycin for at least 1 h at 4 °C for decontamination of the tissue. Tonsils were then briefly rinsed with Ham's F12 medium supplemented with 1% Anti-Anti (Gibco) and processed as needed for culturing (see below). Only de-identified demographic information was obtained.

Tonsil organoid preparation

For cryopreservation of tonsil cells, tissue was dissected into roughly 5 mm × 5 mm × 5 mm pieces and manually disrupted into a suspension by processing through a 100-μm strainer with a glass pestle. Tissue debris was reduced by Ficoll density gradient separation and the buffy coat was collected using plastic sterile Pasteur pipettes. After washing with complete medium (RPMI with glutamax, 10% FBS, 1× nonessential amino acids, 1× sodium pyruvate, 1× penicillin–streptomycin, 1× Normocin (InvivoGen) and 1× insulin/selenium/transferrin cocktail (Gibco)), cells were enumerated and frozen into aliquots in FBS + 10% DMSO. Frozen cells were stored at −150 °C until use.

For culture of cryopreserved cells, aliquots were thawed into complete medium, enumerated and resuspended to 6E7 cells per ml. Cells were plated, 100 μl per well, into permeable (0.4-μm pore size) membranes (24-well size PTFE or polycarbonate membranes in standard 12-well plates; Millipore), with the lower chamber consisting of complete medium (1 ml for 12-well plates) supplemented with 1 μg/ml of recombinant human B cell-activating factor (BAFF; BioLegend).

LAIV (1 μl per well, equivalent of 1.6E4 to 1.6E5 fluorescent focus units per strain; 2024-2025 FluMist Trivalent, Medimmune) or AAV9 (dosed as indicated in provided Figures) were then added directly to the cell-containing portion of the culture setup. Cultures were incubated at 37 °C, 5% CO2 with humidity and supplemented with additional complete culture medium to the lower wells every 3-4 days.

Tetramer staining & flow cytometry

Organoids were harvested from the upper portion of the permeable membranes by rinsing the membranes with complete medium from the respective lower wells. Cells were washed with FACS buffer (DPBS + 0.2% FBS) and were then incubated at 37°C in 100uL of 50nM Dasatinib protein kinase inhibitor (PKI; STEMCELL Technologies) for 30 minutes. 1.5ug of APC-conjugated M1:A2 tetramer (NIH Tetramer Core) and 5uL of Fc block (Biolegend) were added to the cells at 4°C for 60 minutes. Cells were washed again with FACS buffer before staining at 4°C for 30 minutes with FITC CD8 (Biolegend, #300906), Brilliant Violet 785 CD69 (Biolegend, #310932), PE/Cyanine7 CD25 (Biolegend, #302612), PE/Dazzle 594

CD127 (Biolegend, #351336), anti-APC MicroBeads (Miltenyi Biotec; #130-090-855). Cells were then washed in DPBS before staining at 4°C for 15 minutes with live/dead Zombie Violet (Biolegend, #423113), and subsequently washing with FACS buffer. Stained cells were passed through a Miltenyi Biotec MS column to separate and enrich for tetramer-stained cells before running the cells through a Cytoflex S Analyzer. All flow data was analyzed using FlowJo (TreeStar).

Antibody detection by ELISA

For detection of influenza-specific, ELISA plates (Costar) were coated with 0.1 µg per well of season-matched 2024-2025 Fluzone inactivated influenza vaccine (Sanofi) overnight at 4C to act as the capture antigen. For detection of AAV9-specific antibodies, ELISA plates (Costar) were coated with 25ng per well of AAV9 capsid overnight at 4C to act as the capture antigen. Tonsil organoid culture supernatants were series diluted in 3% BSA, 0.1% Tween TBS and added to influenza or AAV9-coated plates for 2hr at room temperature after blocking with 3% BSA, 0.1% Tween TBS for 30 minutes at room temperature. Plates were washed with 0.1% Tween TBS before adding horseradish peroxidase-conjugated anti-human secondary antibodies to either IgM (Southern Biotech; #2020-05) or IgG (Southern Biotech; 2014-05) for 2hr at room temperature to detect captured antibodies. Plates were again washed with 0.1% Tween TBS and then developed with TMB substrate solution (Thermo Scientific). Before 7 minutes had passed, color development was quenched with 1N hydrochloric acid and read at 450 nm.

Chapter 5

CONCLUDING REMARKS

Altogether, this thesis work describes a vesicle-mediated approach for selective T cell immunomodulation that may ultimately be useful as a form of cell-like, cell-free therapy for autoimmune diseases. Synthetic antigen-presenting vesicles were demonstrated to be useful for high-throughput T cell isolation assays investigating the relevance of co-receptor presentation, and these vesicles can be coupled with recent human organoid systems to probe their immunological significance within the greater cellular diversity and complexity of the human immune system. Although the work herein is focused on T cell-mediated immunomodulation by antigen-presenting vesicles, these initial results provide an experimental pathway for subsequent advances in extracellular vesicle engineering and protein immunogenicity reduction that can serve to advance the therapies available to patients in the near-term and, coupled with ongoing discoveries in synthetic biology and de novo protein design, enable humans to adapt faster than natural evolution to thrive within our rapidly changing environment.

Though small molecule drugs have historically been the pillars of traditional medicine, biologics are now among the best-selling drugs globally.[168] In parallel with continued innovation in the small molecule and biologics space, researchers have heralded the successes of stem cell and adoptive T cell therapies that have shown remarkable success in the clinic.[53] Sitting between the relative safety of protein biologics and tremendous potency of cell therapies is a nascent therapeutic platform gaining considerable attention in both the scientific community and biotech industry: extracellular vesicles.[34,42,44,157,169] EVs are naturally multivalent, feature adhesion proteins[147] for improved cell-binding and formation of immunological synapses,[60,85] and can be administered repeatedly without causing inflammation.[56] While this thesis expands upon Dr. Hoffmann's earlier work by demonstrating an immunocompatible, non-inflammatory application of EABR-mediated vesicles, additional near-term advances will serve to improve the safety, potency, and

translational potential of nanoparticles generated *in vivo*. The appendices following this chapter describe three example applications of therapeutic EABR-mediated vesicles and the advances required to enable their development: protein logic gates, chemically-induced dimerization, and mRNA longevity/packaging.

First, in Appendix A, an example project describes the delivery of therapeutics across the blood-brain barrier by extracellular vesicles generated *in vivo*. EABR-mediated vesicles could be used to improve drug delivery to specific cell types in the brain, which has previously been demonstrated by *ex vivo* engineered exosomes.[170] Dr. Hoffmann's group is already working on the packaging of therapeutic mRNA into EABR-mediated vesicles that could be delivered to diseased cells. Incorporating protein logic gates in these vesicles, either as simple OR gates, or potentially more recent AND gates and XOR gates,[171-175] could improve cell-targeting while maintaining the immunocompatibility of these vesicle-based therapeutic vectors.

Second, in Appendix B, an example project describes a method for increasing the safety and sensitivity of existing cancer therapies by using vesicle protein co-display and chemically induced dimerization (CID). EABR-mediated vesicles inherently feature increased avidity for cancer antigen due to protein co-display on the vesicles' membrane surface, and the activation of T cells would be limited by the presence of a titratable small molecule inducer that could be carefully monitored by the patient or physician.

Third, in Appendix C, an example project describes a "prophylaxis for trauma" that would provide intravascular hemostasis in the event of noncompressible hemorrhage. This project would require CID to be implemented to prevent unintended thrombosis, and advances in the longevity of exogenous mRNA after administration *in vivo* would subsequently enable long-acting protection from internal bleeds that are not readily apparent by visual inspection.

These three example projects provide use-cases to drive the engineering of extracellular vesicles toward key breakthroughs that can improve human health in our lifetime. Looking

farther into the future, when we have fully characterized the behavior of cells and the interactions of cell networks in tissues at a molecular level, an ideal outcome for synthetic biology may be to reprogram whole cells *in vivo* to achieve a desired function instead of transplanting whole cells and tissues or administering mRNA-LNP formulations for the expression of single proteins and nanovesicles. In this regard, the initial work described in Chapter 4 regarding human tonsil organoid assays of immunogenicity describe very early efforts to develop nonimmunogenic gene therapy vectors such as AAVs and, as Amgen is already planning,[176] develop immunogenicity datasets with which we can train modern protein design algorithms to develop immunocompatible de novo biologics that improve human health.[177] Hopefully, far in the future, when computational protein design algorithms can accurately design with immunogenicity in mind, we'll be able to imbue humans with ostentatious, immunocompatible metabolic pathways, like photosynthesis,[178] and the performance-enhancing "drug glands"[179] from Iain Banks' *Culture* series so that patients can diagnose and treat themselves from home with the aid of artificial intelligence while we invent new, currently unforeseeable ways to maintain the unsustainable healthcare costs and physician burnout rates of today.[180]

Appendix A

DELIVERY OF THERAPEUTICS ACROSS THE BLOOD-BRAIN BARRIER BY EXTRACELLULAR VESICLES GENERATED IN VIVO BY MRNA-LNP VACCINATION

Included here is another example therapeutic application of EABR-mediated vesicles. This brief research proposal was prepared for internal funding at Caltech and could be applied to a wide range of neurogenic diseases.

A.1 Abstract

The blood-brain barrier (BBB) presents a fundamental bottleneck for the delivery of effective research tools and therapeutics to the central nervous system (CNS),[181-183] as it can prevent the passage of therapeutically useful large molecules, biologics, and gene delivery vectors such as adeno-associated viruses (AAVs). Only a handful of receptors have been validated for crossing the BBB for research and therapy,[184-187] and these existing, non-specific receptors have shown off-target therapeutic delivery.[188] Further, while AAV-based gene therapies have seen preliminary success in the clinic,[68] the translatability of AAVs is still limited by the cost of production, the toxicity of the virus, and the host immune response which can neutralize the therapeutic efficacy of the virus.[189] However, recent advances from Caltech researchers have now 1) enabled the facile engineering of endogenous, biocompatible therapeutic delivery vesicles from a patient's own cells via mRNA-LNP vaccination[47,134] and 2) revealed a conserved carbonic anhydrase IV (CA-IV) receptor present with high specificity on the surface of BBB endothelial cells that is sufficient to shuttle biologic cargo across the BBB.[190] We intend to leverage these two advances to generate biocompatible, cell-secreted extracellular vesicles that will specifically target the CA-IV receptor and cross the BBB to deliver therapeutic cargo to the brain. We expect this combined approach will generate a superior gene delivery vehicle with reduced cost, reduced immunogenicity, improved avidity, and improved cell-targeting, addressing previous shortcomings[191] to establish a new therapeutic platform for brain diseases.

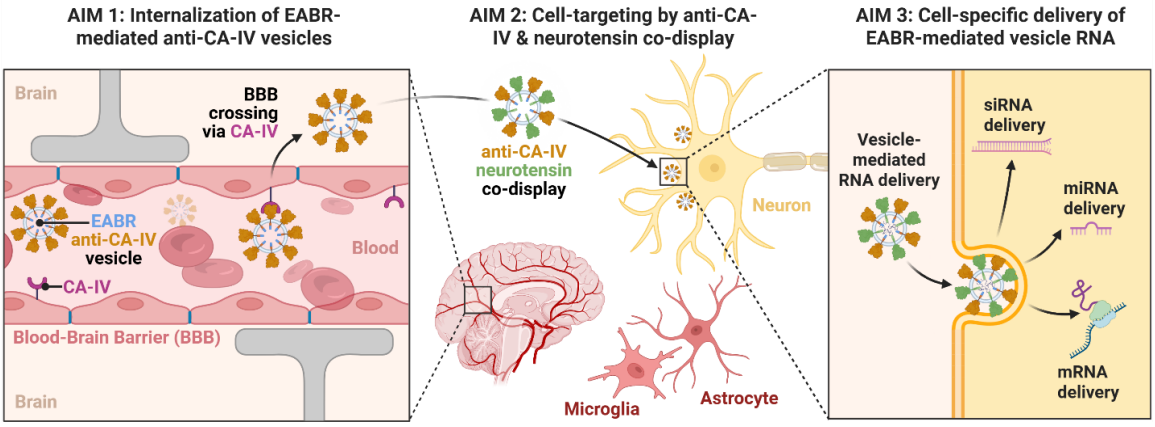

Figure A.1: (Left) EABR-mediated vesicles display anti-CA-IV, which will bind CA-IV present on cell surfaces and allow for cell-specific internalization and crossing of the BBB. (Middle) EABR-mediated vesicles co-displaying anti-CA-IV and neurotensin will bind CA-IV as well as the neurotensin receptor on neurons to support both BBB crossing and neuron-specific targeting. (Right) EABR-mediated vesicles will encapsulate therapeutically-relevant RNA by appending a RNA-binding motif to the EABR-tagged membrane proteins. *EABR: ESCRT and ALIX binding region, CA-IV: carbonic anhydrase IV, siRNA: silencing RNA, miRNA: micro RNA, mRNA: messenger RNA.*

A.2 Internalization of EABR-mediated anti-CA-IV vesicles in cells over-expressing CA-IV

Cell-secreted extracellular vesicles (EVs), such as exosomes, have emerged as promising therapeutic vehicles[42,43] because of their biocompatibility,[36,37] prolonged blood circulation,[38] and protective encapsulation of their contents.[40,41] Despite their many advantages, the application of exosomes in gene delivery has been limited because the impurities and foreign material from exogenously-produced exosomes can trigger immune responses,[192] and cell-targeting is typically defined by the exosome's cell source,[46] which is typically low in number and show low yield.[40] However, recent work by Hoffmann et al.[47] has demonstrated a generalizable method for inducing the release of membrane proteins on densely-coated, cell-derived extracellular vesicles from a patient's own cells *in vivo* by mRNA vaccination, abrogating the need for isolation and purification of the EVs and allowing for simple

intramuscular injection for therapeutic delivery. Appending an endosomal sorting complex required for transport (ESCRT)- and ALG-2-interacting protein X (ALIX)- binding region (EABR) to the cytoplasmic tail of membrane proteins directly recruits the ESCRT machinery and induces the release of vesicles displaying the EABR-tagged protein. We will append this EABR sequence to membrane-bound anti-CA-IV scFv or to recently-identified mini-protein binders specific for the CA-IV receptor identified by the Gradinaru Lab (developed with support from a Merkin Translational Research grant). The Gradinaru lab has established that the receptor-dependent BBB crossing *in vivo* by AAVs and other CA-IV binders correlates with receptor-dependent enhancement in cell internalization of these molecules in cell culture.[190] Therefore, for this initial proof of concept, we will harvest and purify the EABR-mediated anti-CA-IV vesicles from transfected Expi293F cells and co-incubate the vesicles with HEK293T cells over-expressing CA-IV. Successful targeting and internalization of the vesicles will be confirmed by immunocytochemistry.

A.3 Cell-specific targeting of EABR-mediated vesicles co-displaying anti-CA-IV and a neuron targeting protein

Cellular uptake of EVs is highly dependent on their protein corona,[193,194] which is critical for targeting particular brain cell populations with sufficient therapeutic concentrations while avoiding off-target effects.[195] The specificity of CA-IV expression in brain vasculature presents an opportunity for engineering cell type-specific targeting of therapeutic vesicles after BBB crossing through the incorporation of a second vesicle receptor-targeting moiety. The Mayo lab has recently demonstrated the co-display of defined proteins on EABR-mediated vesicles by simultaneous co-transfection of DNA constructs encoding two proteins (manuscript in preparation). We will extend this work by co-displaying an anti-CA-IV protein with a neuron-targeting protein, such as neurotensin,[196] on EABR-mediated vesicles. Successful targeting and internalization of these co-presenting EABR-mediated vesicles will be confirmed by engineering the co-presenting EABR-mediated vesicles to carry GFP and co-culturing with HEK293T cells over-expressing either the neurotensin receptor[197] or the CA-IV receptor. We expect co-displaying EABR vesicles to selectively enter cells expressing either receptor,

demonstrating the capability of both BBB endothelium targeting as well as neuron-specific targeting after successfully crossing the BBB.

A.4 Delivery of RNA via EABR-mediated vesicles

Because the lipid bilayer of extracellular vesicles naturally encapsulates and protects RNA from degradation, EVs have garnered attention as delivery vehicles for a diverse range of therapeutic RNA species, and studies have repeatedly demonstrated that exosomal RNA mediates the therapeutic effects of endogenous exosomes. Several RNA-binding proteins, their RNA recognition motifs, and their selective RNA cargo have already been identified and linked to EVs,[198] including SYNCRIP,[199] hnRNPU,[200,201] and YBX1.[202-205] We will append sequences from these known RNA-binding proteins to the EABR-tagged membrane proteins to support selective loading of over-expressed, therapeutically-relevant RNA[189] into EABR-mediated vesicles. To confirm successful packaging of RNA into vesicles and cell-specific delivery, the encapsulated vesicle RNA in this initial proof-of-concept study will encode a fluorescent NanoLuc[206] reporter that will fluoresce brightly in cells that have internalized the engineered EABR vesicles.

A.5 Acknowledgments

Thank you to Tim Shay, Viviana Gradinaru, and Steve Mayo for helpful discussions.

Appendix B

INCREASING THE SAFETY AND SENSITIVITY OF CANCER THERAPY WITH VESICLE PROTEIN CO-DISPLAY AND CHEMICALLY INDUCED DIMERIZATION

The following research proposal illustrates some of the possible cancer-focused uses of the EABR technology. While pursuing this opportunity is not planned by the author, it is presented here for use by others who may wish to explore it.

B.1 Abstract

Despite major advances in cancer treatment, protein biologics and cell therapies still struggle with tumor escape variants, tumor cells that express low levels of targeted cancer antigen, and maintaining efficacy within the immunosuppressive tumor microenvironment. Further, cell therapies are both expensive to manufacture and difficult to control, leading to a growing list of complicated receptors that bioengineers have designed to shepherd cell therapies away from healthy cells and to include “kill-switches” to shut down lethal, unpredictable adverse events that are still occurring in clinical trial and therapeutic settings. Extracellular vesicles (EVs) represent a therapeutic sweet spot between protein biologics and cell therapies that can address some of these shortcomings. EVs are cell-specific, have increased avidity compared to traditional protein-based biologics, and can harness the activation potential of cellular therapies without the drawback of uncontrolled mitotic proliferation and complex, expensive manufacturing. To advance EVs into the clinic, we will extend recent breakthroughs in vesicle-forming technology from the Bjorkman and Mayo Labs by co-displaying multiple therapeutic antigen-binding domains on extracellular vesicles generated by patients *in vivo* using an mRNA-LNP formulation. These multivalent EVs will have improved sensitivity for cancer antigens on low-expressing tumor cells as compared to their commercially available monoclonal antibody equivalents. Second, to improve the safety of our vesicles and enable titratable dosing, we will gate vesicle anti-CD3 T cell activation by administration of the small molecule cancer drug Venetoclax.

Together, these advances will increase the safety and sensitivity of EV therapies and establish a translational pathway for our EV-based therapeutic platform.

B.2 Introduction

Cell-secreted extracellular vesicles (EVs), such as exosomes[34], have emerged as promising therapeutic vehicles[42,43] because of their biocompatibility[36,37], prolonged blood circulation[38], multivalency[39], and protective encapsulation of their contents[40,41]. Despite their many advantages, the application of EVs in cancer therapy has been limited because of difficulties scaling manufacturing[44], the heterogeneity of the harvested exosomal population[45], and cell-targeting by EVs is often defined by the vesicle's original cell source[46], which is typically low in number and low yield[40]. However, recent work by Hoffmann et al.[47] in the Bjorkman lab has demonstrated a generalizable method for inducing the release of transfected membrane proteins on densely-coated EVs from a patient's own cells *in vivo*, abrogating the need for scale-up of manufacturing and subsequent purification. Appending an endosomal sorting complex required for transport (ESCRT)- and ALG-2-interacting protein X (ALIX)-binding region (EABR) to the cytoplasmic tail of membrane proteins directly recruits the ESCRT machinery and induces the release of vesicles displaying the EABR-tagged protein. We will append this EABR sequence to membrane-bound single-chain variable fragments (scFv) specific for cancer-relevant membrane proteins, such as human epidermal receptor 2 (HER2) and programmed cell death protein 1 (PD-1), to generate EVs that home to tumor sites and amplify the number of binding sites for T cell activation through vesicle protein co-display (Fig. 1). This amplification of T cell activation by EABR-mediated vesicles will outperform commercial biologics at inducing T cell-mediated tumor killing, and, because the vesicles can be generated endogenously by patients *in vivo* by administration of an mRNA lipid nanoparticle (mRNA-LNP) formulation, our therapy is cheaper, safer, and more convenient than adoptive cell therapies. If our RI2 proposal is successful, our ultimate product will be EABR-mediated anti-cancer EVs administered either as an mRNA-LNP vaccine encoding the vesicles or as a solution containing the vesicles themselves.

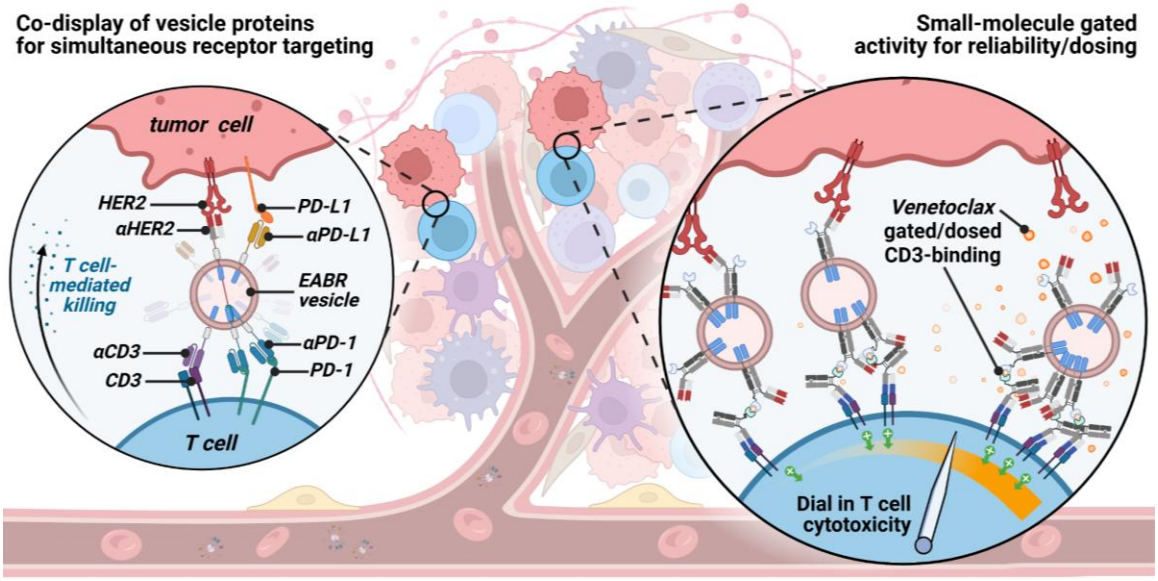

Figure B.1: Schematic of a solid tumor being treated with EABR-mediated anti-cancer vesicles. (Left circle inlet) Existing biologic designs have limited avidity for multiple therapeutic targets, and typically require multiple biologics to be administered for a combination therapy to be realized. EABR-mediated vesicles can target multiple receptors or cytokines simultaneously, improving antigen sensitivity, reducing off-target toxicity, improving T cell activation, and reducing the likelihood of tumor escape variants. (Right circle inlet) Chemically-induced dimerization of nanobodies by the small molecule Venetoclax allows for fine-tuned titration or gating of anti-CD3-mediated T cell cytotoxicity initiated by EABR-mediated vesicles.

B.3 Technical Approach

Mammalian Expi293F cells will be transfected with a DNA construct encoding anti-HER2 and anti-CD3 scFvs that are appended with a vesicle-forming EABR sequence; the resulting EABR-mediated extracellular vesicles released from the Expi293F cells will be harvested from the cell culture supernatant by ultracentrifugation and size-exclusion chromatography. Protein co-display and vesicle avidity will be characterized by immuno-electron microscopy, ELISA, and cryo-ET. Successful tumor cell targeting by the EABR EVs will be evaluated using well-established human breast cancer cell lines (SK-BR-3, HCC 1954) or gastric carcinoma lines (N87, SNU-216) compared to negative control cell lines (MDA-MB-468,

HEK293T), and the initiation of T cell-mediated killing by the EVs will be performed with human PBMCs from healthy volunteers. T cell-mediated killing will be evaluated using LDH cytotoxicity assays and ELISAs for markers of T cell activation (Granzyme B, IFN-γ). The performance of EABR-mediated vesicles that are simultaneously co-displaying anti-CD3, anti-HER2 and anti-PD-1 will be compared to commercially available anti-PD-1 antibody (pembrolizumab), anti-HER2 antibody (trastuzumab), and recent bispecific anti-HER2/anti-CD3 antibodies. If we see initial success with our co-displayed scFv vesicles, we will next co-display small-molecule gated anti-CD3 scFv (Figure 1) and evaluate our ability to titrate T cell-mediate tumor cell killing with the addition of the small molecule Venetoclax[207].

B.4 Rationale

Over the last few decades, targeted biological medications, such as anti-HER2 treatment against breast cancer and, more recently, immunotherapy with immune checkpoint inhibition, have achieved tremendous advances in managing cancer[56-58]. Despite the overexpression of cancer neoantigens and PD-L1 in various malignancies, only a subset of patients exhibit a durable response from these biologics[208] and off-target toxicity remains an especially critical issue for solid tumors[55]. Strategies to improve the response rate to biologic therapy include combinational approaches with biologics and chemotherapies, multiple checkpoint inhibition, and the development of increasingly sophisticated bispecific, trispecific, or combinatorial antibody designs[59]. These strategies remain limited in their coordinated delivery to the target of interest and activation of a full, targeted immune response at their intended site[209]. On the opposite end of the therapeutic spectrum, adoptive cell therapies, including chimeric antigen receptor (CAR) T cells, have demonstrated remarkable progress for hematological malignancies[53]. However, these cells struggle with trafficking to solid tumors, preferential targeting and elimination of antigenically heterogeneous tumors, and the loss of T cell effectiveness within the immunosuppressive tumor microenvironment[57]. Further, adoptive cell therapies are both harmful to the patient and difficult to scale; patients often require lymphodepletion before treatment, leading to an increased risk of infection, and the therapy is expensive to

manufacture and requires months of preparation before expanded autologous T cells can be administered to a patient that may have already passed from what can often be a rapidly progressive chemorefractory disease[53]. Clinical translation is further complicated by T cells remaining a biological blackbox with unpredictable adverse events such as cytokine release syndrome (CRS) and immune effector cell-associated neurotoxicity syndrome from overactive T cells[54], which have inspired a myriad of bioengineered receptors to provide cell-specificity and "kill-switches" to help manage the dangerous unpredictability of autonomous adoptive cell therapies[55]. However, these engineered receptors further complicate the manufacturing, validation, and clinical reliability of an already complex form of cancer therapy. Sitting between protein biologics and cell therapies is a nascent therapeutic platform gaining considerable attention in both the scientific community and biotech industry: extracellular vesicles[34,42,44,157,169]. EVs are naturally multivalent, feature adhesion proteins[147] for improved cell-binding and formation of immunological synapses[60,85], and can be administered repeatedly without causing inflammation[56]. Researchers have previously capitalized on these desirable properties by designing tumor-homing, cancer-killing exosomes that have demonstrated remarkable efficacy in models of cancer both *in vitro* and *in vivo*[38,39,43,210]. However, major limitations preventing clinical deployment of these therapies include difficulty with scaling-up manufacturing of the vesicles and the heterogeneity of the vesicles that are ultimately purified for therapy[45], which can vary considerably depending on the cell source and culturing conditions[211]. A major benefit of the EABR sequence pioneered at Caltech[47] is the ability to turn any cell into a high-secreting source of therapeutic EVs, and doing so without requiring immunogenic viral proteins that have been used previously to induce vesicle budding. These vesicles are more uniform compared to the heterogeneous nature of naturally-sourced extracellular vesicles, and encoding the EABR-tagged proteins in an mRNA-LNP formulation precludes the need for difficult scale-up and purification.

B.5 Acknowledgments

Thank you to Steve Mayo for helpful discussions.

Appendix C

INTRAVASCULAR HEMOSTATIC PROPHYLAXIS FOR NONCOMPRESSIBLE HEMORRHAGE

If performance athletes "carbo-load" or take various supplements before a sporting event to improve their performance or recovery, why don't we have similar supplementation for soldiers or surgical patients that are about to undergo significant physical trauma? I drafted the following research proposal for a "trauma prophylaxis" that could both reduce blood loss during combat trauma and potentially save lives in planned surgical scenarios. In addition to using EABR-mediated vesicles, this proposal describes the use of platelets as a chassis for therapeutic protein production, an idea that has been championed by Dr. Christian Kastrup at the Medical College of Wisconsin. Because they lack a nucleus and have no mitotic potential, platelets could be a compelling new cell-based therapy to rival existing T cell and stem cell therapies.

C.1 Basic Research Executive Summary

Noncompressible hemorrhage consistently emerges as the leading cause of potentially preventable trauma mortality on the battlefield,[212,213] and the recent conflict in Ukraine has demonstrated that future warfighters may not reach a medical care facility for days after injury as the long range fire capabilities of near-pear adversaries precludes timely medical evacuation.[214] Point-of-injury battlefield trauma care has previously focused on the use of synthetic intravascular hemostatic agents[215-220] and lyophilized platelets.[221] However, synthetic hemostatic agents suffer from immunogenic foreign body adverse events,[222] and platelet products demand a cold chain[223] or require additional time to resuspend the agent before injection,[221] limitations which have inspired a recent proposal for a trauma prophylaxis.[224]

This project aims to leverage recent breakthroughs in mRNA transfection of platelets,[225,226] mRNA stability,[227] *in vivo* nanoparticle synthesis,[47,134] and chemically induced dimerization

(CID)[207,228-231] to develop a "trauma prophylactic". The prophylactic is administered up to a week in advance of combat, and will activate either directly before or within seconds of injury by the convenient administration of an FDA-approved small molecule drug to chemically induce dimerization of platelets specifically at sites of hemorrhage. Unlike previous hemostatic agents, gating activation of a procoagulant therapeutic by a small molecule allows for long-term, prophylactic protection from noncompressible hemorrhage while minimizing the risk of thromboembolism, creating a paradigm shift in our approach to preventable trauma mortality on the frontline.

We propose creating three types of injectable hemostatic prophylaxis, at increasing levels of potency and implementation complexity, and subsequently exploring their potential for accelerated hemostasis while minimizing off-target clotting. The objectives for this two-year project are to (1) create an antibody-based chemically-induced hemostatic (CIH) agent; (2) utilize the ESCRT pathway to create a microplatelet-like nanoparticle-based CIH agent; (3) utilize recent advances in platelet transfection to create a platelet-based CIH agent as outlined in Figure 1; (4) study the potency of these hemostatic agents using an *in vitro* model of hemorrhage.

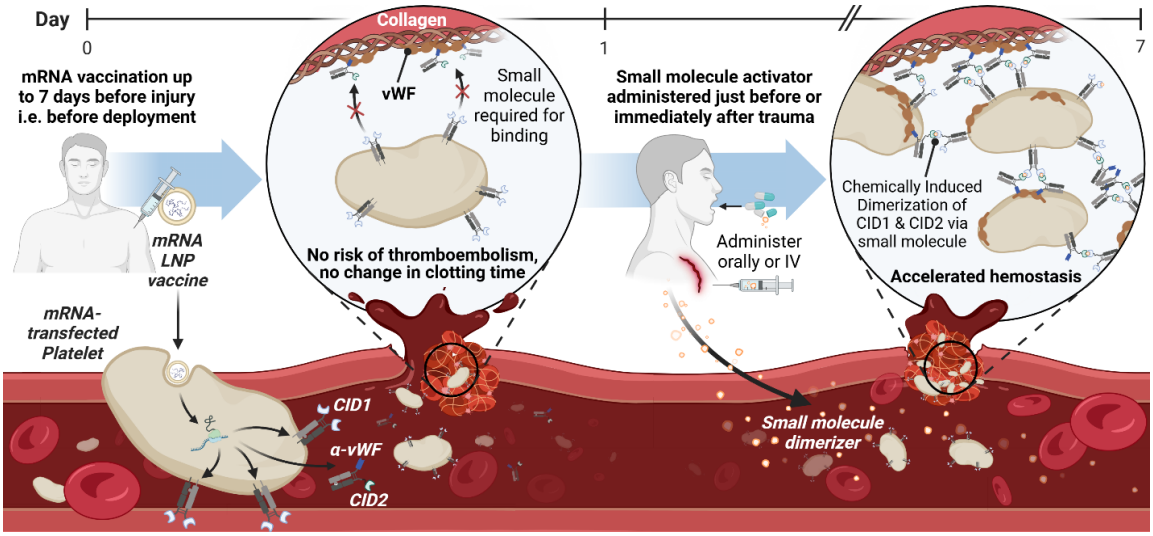

Figure C.1: mRNA-LNP vaccine of platelets for on-demand, small-molecule activated intravascular hemostasis and life-saving care. *vWF: von Willebrand Factor, CID1:*

chemically induced dimerization protein #1, CID2: chemically induced dimerization protein #2, LNP: lipid nanoparticle, IV: intravascular.

C.2 Scientific Objectives

The goals of this project are to create three novel approaches for prophylactic chemically-induced hemostatic (CIH) agents, and to study their relative hemostatic potency. The specific objectives for this two-year project are to (1) create an antibody-based CIH agent, (2) create a microplatelet-like nanoparticle-based CIH agent, (3) create an mRNA-transfected platelet-based CIH agent, and (4) study the potency of these hemostatic agents in an *in vitro* model of hemorrhage.

C.3 Rationale

A turning point in military prehospital trauma care came in 1996 when a review of battlefield deaths led to the recommendation for immediate application of limb tourniquets as the first-line treatment for extremity hemorrhage.[232] Over the next decade, the US military gradually adopted widespread implementation of extremity tourniquets for all deployed forces, ultimately resulting in an 85% decrease in deaths attributed to limb hemorrhage.[213] While efforts to control isolated extremity hemorrhage after injury have been remarkably successful, junctional and torso hemorrhage continues to be the leading cause of potentially preventable trauma mortality on the battlefield.[212] In a large contemporary autopsy study of combat deaths from 2001 to 2011, 87% of the 4574 battlefield deaths occurred prior to arrival at a medical treatment facility, and 24% of those prehospital deaths were considered potentially survivable. Hemorrhage was associated with 91% of these potentially survivable injuries, and bleeding overwhelmingly occurred in noncompressible areas: torso 67%, junctional 19%.[213] A rapid response is critical for counteracting fatal hemorrhage. Casualties with penetrating battlefield trauma often only have a “platinum 5 minutes” for life saving interventions as the mortality rate for high grade torso injury with hemorrhage can be >40% in as little as 15 minutes after injury.[233,234]

Point-of-injury battlefield trauma care has previously focused on reducing death from noncompressible hemorrhage through the use of synthetic intravascular hemostatic agents,[215-220] resuscitative endovascular balloons,[235] lyophilized platelets,[221] or antifibrinolytic tranexamic acid.[236,237] However, synthetic intravascular hemostatic agents suffer from immunogenic foreign body adverse events[222] and short half-life, and surgical intervention with endovascular balloons requires expert skill that may not be readily available on the frontline. Further, lyophilized platelet products and many proposed intravascular hemostatic agents either demand a cold chain,[223] require additional time to resuspend the agent before injection,[221] or expect precise intravenous administration which may not be possible within the "platinum 5 minutes" of a life-threatening injury. These limitations have inspired a new proposal to use tranexamic acid as a prophylactic measure for trauma,[224] but a large, multicenter randomized controlled trial demonstrated that prehospital administration of tranexamic acid does not result in a greater number of patients surviving with a favorable functional outcome at 6 months compared to placebo; rather, tranexamic acid intervention provided a mild benefit in converting patients from death toward severe disability.[237] A potent, convenient well-tolerated, safe, long-lasting molecular prophylactic for traumatic hemorrhage is needed to address the problems of intervention response time, the inaccessibility of internal bleeds, and the intractability of noncompressible bleeds during battlefield triage and frontline wound care.

We want to radically transform outcomes from noncompressible junctional and torso hemorrhage in the same way that the tourniquet radically decreased deaths from extremity hemorrhage. To that end, recent advances in mRNA transfection of platelets,[225,226] mRNA stability,[227] *in vivo* nanoparticle synthesis,[47,134] and chemically induced dimerization (CID)[207,228-231] have now enabled new approaches for the design of a safe, long-lasting intravascular hemostatic "trauma prophylaxis" that aims to significantly improve outcomes from noncompressible hemorrhage on the battlefield.

C.4 Technical Approach & Project Plans

We propose creating three types of hemostatic agents and characterizing their potential to accelerate hemostasis without increasing the risk of unwanted thromboembolism and off-target clotting. These three proposed hemostatic agents are related in that they all use chemically-induced dimerization to improve their safety profile to the extent that they could be administered prophylactically, but the agents differ in their level of avidity and thus differ in their expected hemostatic potential.[238-240] Designing and testing all three prototypes will reveal the relative significance of avidity for hemostasis as well as the hemostatic protein expression potential from platelet transfection.

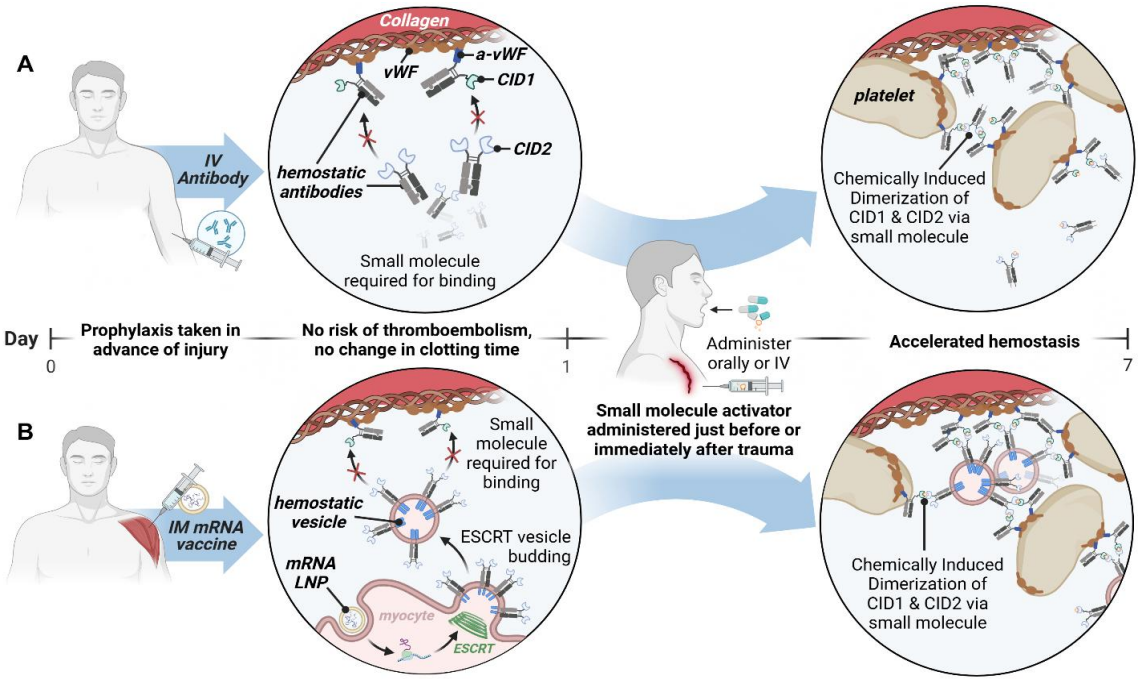

Figure C.2. (A) Antibody-mediated hemostatic agent is pharmacologically stable for up to a month *in vivo* and accelerates hemostasis only upon administration of a small molecule dimerizer. (**B)** mRNA-LNP vaccine that generates synthetic nanovesicular micro-platelets to supplement and accelerate hemostasis only upon administration of a small molecule dimerizer. *vWF: von Willebrand Factor, CID1: chemically induced dimerization protein #1, CID2: chemically induced dimerization protein #2, LNP: lipid nanoparticle, IV: intravascular, IM: intramuscular, ESCRT: endosomal sorting complex required for transport.*

(Objective 1) Antibody-mediated chemically induced hemostasis: Chemically induced dimerization (CID) is an approach for gating the binding of two proteins to be dependent on the presence of a conveniently administered small molecule.[207,228-231] Thus, CID gives pharmaceutical designers precise control over the therapeutic activity of a biologic drug after it is administered to a patient. CID has previously been explored as a safety mechanism for gating and tuning T cell activation during immunotherapy by preventing adverse events such as epitope spreading and cytokine storm[229]; titrating low doses of a dimerizing small molecule in mice enabled rapid, reversible, and tunable assembly of functional antibody complexes to control the tumor localization of a radioligand and the antitumor activity of bispecific t-cell engaging antibodies.[207] When immunotherapeutic antibody complexes were dosed into mice without the administration of a dimerizing small molecule, Martinko et al. found no T cell activation, no evidence of cytokine production, and a complete lack of T cell-mediated killing.[207] As an initial proof of concept to demonstrate the use of CID for switchable hemostasis, our plan is to extend this engineered CID system from an immunotherapy setting toward a hemostatic context (Figure 2A). The immune-activating anti-CD3 antibody arm used by Martinko et al.[207,228] will be replaced with a vWF-binding moiety[241] that has been shown to not interfere with normal clotting[242]; as a result, prophylactic administration of this antibody system should neither accelerate nor interrupt physiologically normal hemostasis. However, upon administration of a dimerizing small molecule, we expect therapeutic protein binding to specifically occur at sites of hemorrhage and accelerated hemostasis to occur within seconds.

(Objective 2) Nanoparticle-mediated chemically-induced hemostasis: Hoffmann et al. recently described a method for *in vivo* production of nanoparticles displaying desired proteins on their surface by utilizing the endogenous endosomal sorting complex required for transport (ESCRT) pathway.[47] Cells transfected with membrane proteins engineered to feature an ESCRT and ALIX-binding region (EABR) peptide appended to their cytoplasmic tail are preferentially assembled and released on nanoparticles originating from the transfected cells. Hoffmann et al. demonstrated that these nanoparticles are densely

decorated with engineered EABR-tagged proteins, and the nanoparticles are capable of stimulating immune responses in both *in vitro* and *in vivo* contexts.[47,134] Mimicking the existing physiological microplatelets[243] that are generated endogenously by natural platelets, we aim to induce the creation and release of synthetic microplatelet-like nanoparticles from human cells by mRNA transfection. Insertion of the EABR peptide into the cytoplasmic tail of a membrane-bound version of the CID antibodies from objective (1) will lead to EABR-mediated microplatelet-like nanoparticles displaying a human antibody-based CID system[207]; the antibody-decorated nanoparticles will dimerize with known epitopes of endothelial damage[242] at sites of hemorrhage only upon administration of a small molecule to safeguard against thromboembolism (Figure 2B). Because nanoparticles generated by ESCRT have been shown to be densely coated in EABR-tagged protein,[47,134] we expect the avidity of these microplatelet-like nanoparticles to contribute significantly to their clotting potential in comparison to an antibody-exclusive CID system.[238-240] Further, because of advances in mRNA stability, we expect the nanoparticles to be present in the blood to participate in CID hemostasis for up to a week.[227]

(Objective 3) Platelet-mediated chemically-induced hemostasis: Leung et al. recently described the successful transfection of platelets using an optimized mRNA-LNP formulation that increases protein expression in platelets 10-100 fold.[225] Leung et al. demonstrated that the coagulability or clotting potential of these transfected platelets is not statistically different from untransfected platelets either at baseline or post-trauma, and the transfected platelets were well-tolerated in mice.[225] Notably, platelets lack both a nucleus and DNA, and platelets do not perform mitosis, so the safety profile of genetically modified platelets is greatly improved over other cell-based engineering strategies. Further, previous work has shown that supramolecularly-conjugated platelets perform better than endogenous platelets at hemostasis when transfused at equal amounts into a mouse model of hemorrhage.[223] We intend to build upon this "platelet modification" approach by engineering a membrane-bound version of the CID antibodies from objective (1) to be encoded by an mRNA-LNP formulation that will preferentially transfect platelets (Figure 1). We expect no change in bleed times or blood loss between mRNA-transfected platelets and physiologically

normal platelets until a small molecule is administered, at which point we expect to see significantly accelerated hemostasis that leads to reduced blood loss and reduced bleeding times.

(Objective 4) In vitro characterization of chemically-induced hemostasis agents: Characterization of our antibody-mediated CID system and microplatelet-like nanoparticles will be performed by SDS-Page, Western Blot, and ELISA-based assays. Platelet protein expression after mRNA-LNP transfection will be evaluated using Western Blot with radioactive labels to increase the sensitivity of potentially low-expressing proteins in platelets. Microfluidic systems mimicking blood flow will be fabricated to better understand the performance of these systems under physiological conditions, and the hemostatic functionality of our prophylactic agents will be assessed using ROTEM (Tem International GmbH), including clotting time, clot-forming time, maximum clot formation, and clot firmness.

Success with our *in vitro* studies will provide motivation to perform *in vivo* testing using standard animal models of hemorrhage covered under a subsequent grant.

C.5 Expected Benefits and Military Relevance

For more than 20 years during the Global War on Terror (GWOT) in Iraq and Afghanistan, US military forces engaged enemies whose capability to mount offensive and defensive strategies against US forces was limited, and the air, ground, and sea dominance of the US assured relative freedom of movement for medical evacuation.[214] In the current conflict in Ukraine, however, which is representative of a war with a near-peer adversary, Russia has equivalent or superior combat forces to Ukraine, which limits Ukrainian mobility and evacuation.[244] There is minimal ability for the Ukrainian Air Force to perform airborne medical evacuation (MEDEVAC) from frontline positions or areas adjacent within the envelope of Russian antiaircraft fire.[245] MEDEVAC by ground forces also routinely comes under attack by Russian forces. The US should assume that advanced, accurate, and very long-range weapon systems will be readily available to future near-peer adversaries and,

consequently, future US service members may not reach definitive care for days after a combat injury.[214]

A shelf-stable, life-saving hemostatic agent that is activated by convenient administration of a small molecule pill or injection would provide a paradigm-changing solution to the greatest cause of preventable pre-hospital mortality in warfighters.[212] In addition to the obvious benefit of preventing lethal hemorrhage, warfighters will perform more confidently on the frontline knowing they can better survive being shot, stabbed, or hit by an explosive blast compared to their adversary. Further, for non-combatant personnel who are on anticoagulants, this CID hemostatic system could be repurposed as a form of reversible anticoagulant agent when these active-duty personnel need to undergo emergency surgery.

C.6 Acknowledgments

Thank you to Christian Kastrup and Steve Mayo for helpful discussions.

B i b l i o g r a p h y

1. Murphy, K., Weaver, C., Berg, L., Barton, G., and Janeway, C.A. (2022). Janeway's immunobiology, Tenth edition. / Kenneth Murphy, Casey Weaver, Leslie J. Berg. Edition (W.W. Norton and Company).
2. Punt, J., Owen, J.A., Stranford, S.A., Jones, P.P., and Kuby, J. (2019). Kuby immunology, Eighth edition. Edition (W.H. Freeman/Macmillan Learning).
3. Chen, X., Ghanizada, M., Mallajosyula, V., Sola, E., Capasso, R., Kathuria, K.R., and Davis, M.M. (2025). Differential roles of human CD4(+) and CD8(+) regulatory T cells in controlling self-reactive immune responses. Nat Immunol *26*, 230-239. 10.1038/s41590-024-02062-x.
4. Li, J., Zaslavsky, M., Su, Y., Guo, J., Sikora, M.J., van Unen, V., Christophersen, A., Chiou, S.H., Chen, L., Li, J., et al. (2022). KIR(+)CD8(+) T cells suppress pathogenic T cells and are active in autoimmune diseases and COVID-19. Science *376*, eabi9591. 10.1126/science.abi9591.
5. Laureano, R.S., Sprooten, J., Vanmeerbeerk, I., Borras, D.M., Govaerts, J., Naulaerts, S., Berneman, Z.N., Beuselinck, B., Bol, K.F., Borst, J., et al. (2022). Trial watch: Dendritic cell (DC)-based immunotherapy for cancer. Oncoimmunology *11*, 2096363. 10.1080/2162402x.2022.2096363.
6. Amon, L., Hatscher, L., Heger, L., Dudziak, D., and Lehmann, C.H.K. (2020). Harnessing the Complete Repertoire of Conventional Dendritic Cell Functions for Cancer Immunotherapy. Pharmaceutics *12*. 10.3390/pharmaceutics12070663.
7. Pastor, Y., Ghazzaui, N., Hammoudi, A., Centlivre, M., Cardinaud, S., and Levy, Y. (2022). Refining the DC-targeting vaccination for preventing emerging infectious diseases. Front Immunol *13*, 949779. 10.3389/fimmu.2022.949779.
8. Morisaki, T., Morisaki, T., Kubo, M., Morisaki, S., Nakamura, Y., and Onishi, H. (2022). Lymph Nodes as Anti-Tumor Immunotherapeutic Tools: Intranodal-Tumor-Specific Antigen-Pulsed Dendritic Cell Vaccine Immunotherapy. Cancers (Basel) *14*. 10.3390/cancers14102438.

9. Engelhard, V.H., Strominger, J.L., Mescher, M., and Burakoff, S. (1978). Induction of secondary cytotoxic T lymphocytes by purified HLA-A and HLA-B antigens reconstituted into phospholipid vesicles. Proc Natl Acad Sci U S A *75*, 5688-5691. 10.1073/pnas.75.11.5688.

10. Latouche, J.B., and Sadelain, M. (2000). Induction of human cytotoxic T lymphocytes by artificial antigen-presenting cells. Nat Biotechnol *18*, 405-409. 10.1038/74455.

11. Altman, J.D., Moss, P.A., Goulder, P.J., Barouch, D.H., McHeyzer-Williams, M.G., Bell, J.I., McMichael, A.J., and Davis, M.M. (1996). Phenotypic analysis of antigen-specific T lymphocytes. Science *274*, 94-96. 10.1126/science.274.5284.94.

12. Maus, M.V., Riley, J.L., Kwok, W.W., Nepom, G.T., and June, C.H. (2003). HLA tetramer-based artificial antigen-presenting cells for stimulation of CD4+ T cells. Clin Immunol *106*, 16-22. 10.1016/s1521-6616(02)00017-7.

13. Litzinger, M.T., Foon, K.A., Sabzevari, H., Tsang, K.Y., Schlom, J., and Palena, C. (2009). Chronic lymphocytic leukemia (CLL) cells genetically modified to express B7-1, ICAM-1, and LFA-3 confer APC capacity to T cells from CLL patients. Cancer Immunol Immunother *58*, 955-965. 10.1007/s00262-008-0611-5.

14. Garnier, A., Hamieh, M., Drouet, A., Leprince, J., Vivien, D., Frébourg, T., Le Mauff, B., Latouche, J.B., and Toutirais, O. (2016). Artificial antigen-presenting cells expressing HLA class II molecules as an effective tool for amplifying human specific memory CD4(+) T cells. Immunol Cell Biol *94*, 662-672. 10.1038/icb.2016.25.

15. Sun, X., Han, X., Xu, L., Gao, M., Xu, J., Yang, R., and Liu, Z. (2017). Surface-Engineering of Red Blood Cells as Artificial Antigen Presenting Cells Promising for Cancer Immunotherapy. Small *13*. 10.1002/smll.201701864.

16. Shao, J., Xu, Q., Su, S., Wei, J., Meng, F., Chen, F., Zhao, Y., Du, J., Zou, Z., Qian, X., and Liu, B. (2018). Artificial antigen-presenting cells are superior to dendritic cells at inducing antigen-specific cytotoxic T lymphocytes. Cell Immunol *334*, 78-86. 10.1016/j.cellimm.2018.10.002.

17. Sun, L., Shen, F., Xiong, Z., Yang, H., Dong, Z., Xiang, J., Gu, Q., Ji, Q., Fan, C., and Liu, Z. (2022). DNA Engineered Lymphocyte-Based Homologous Targeting

Artificial Antigen-Presenting Cells for Personalized Cancer Immunotherapy. J Am Chem Soc *144*, 7634-7645. 10.1021/jacs.1c09316.

18. Mandal, S., Hammink, R., Tel, J., Eksteen-Akeroyd, Z.H., Rowan, A.E., Blank, K., and Figdor, C.G. (2015). Polymer-based synthetic dendritic cells for tailoring robust and multifunctional T cell responses. ACS Chem Biol *10*, 485-492. 10.1021/cb500455g.
19. Shen, C., Zhang, J., Xia, L., Meng, F., and Xie, W. (2007). Induction of tumor antigen-specific cytotoxic T cell responses in naïve mice by latex microspheres-based artificial antigen-presenting cell constructs. Cell Immunol *247*, 28-35. 10.1016/j.cellimm.2007.07.002.
20. Han, H., Peng, J.R., Chen, P.C., Gong, L., Qiao, S.S., Wang, W.Z., Cui, Z.Q., Yu, X., Wei, Y.H., and Leng, X.S. (2011). A novel system of artificial antigen-presenting cells efficiently stimulates Flu peptide-specific cytotoxic T cells in vitro. Biochem Biophys Res Commun *411*, 530-535. 10.1016/j.bbrc.2011.06.164.
21. Perica, K., De León Medero, A., Durai, M., Chiu, Y.L., Bieler, J.G., Sibener, L., Niemöller, M., Assenmacher, M., Richter, A., Edidin, M., et al. (2014). Nanoscale artificial antigen presenting cells for T cell immunotherapy. Nanomedicine *10*, 119-129. 10.1016/j.nano.2013.06.015.
22. Meyer, R.A., Sunshine, J.C., Perica, K., Kosmides, A.K., Aje, K., Schneck, J.P., and Green, J.J. (2015). Biodegradable nanoellipsoidal artificial antigen presenting cells for antigen specific T-cell activation. Small *11*, 1519-1525. 10.1002/smll.201402369.
23. Olden, B.R., Perez, C.R., Wilson, A.L., Cardle, II, Lin, Y.S., Kaehr, B., Gustafson, J.A., Jensen, M.C., and Pun, S.H. (2019). Cell-Templated Silica Microparticles with Supported Lipid Bilayers as Artificial Antigen-Presenting Cells for T Cell Activation. Adv Healthc Mater *8*, e1801188. 10.1002/adhm.201801188.
24. Jiang, Y., Krishnan, N., Zhou, J., Chekuri, S., Wei, X., Kroll, A.V., Yu, C.L., Duan, Y., Gao, W., Fang, R.H., and Zhang, L. (2020). Engineered Cell-Membrane-Coated Nanoparticles Directly Present Tumor Antigens to Promote Anticancer Immunity. Adv Mater *32*, e2001808. 10.1002/adma.202001808.

25. Xiao, P., Wang, J., Zhao, Z., Liu, X., Sun, X., Wang, D., and Li, Y. (2021). Engineering Nanoscale Artificial Antigen-Presenting Cells by Metabolic Dendritic Cell Labeling to Potentiate Cancer Immunotherapy. Nano Lett *21*, 2094-2103. 10.1021/acs.nanolett.0c04783.

26. Hwang, I., Shen, X., and Sprent, J. (2003). Direct stimulation of naive T cells by membrane vesicles from antigen-presenting cells: distinct roles for CD54 and B7 molecules. Proc Natl Acad Sci U S A *100*, 6670-6675. 10.1073/pnas.1131852100.

27. Kovar, M., Boyman, O., Shen, X., Hwang, I., Kohler, R., and Sprent, J. (2006). Direct stimulation of T cells by membrane vesicles from antigen-presenting cells. Proc Natl Acad Sci U S A *103*, 11671-11676. 10.1073/pnas.0603466103.

28. Markov, O., Oshchepkova, A., and Mironova, N. (2019). Immunotherapy Based on Dendritic Cell-Targeted/-Derived Extracellular Vesicles-A Novel Strategy for Enhancement of the Anti-tumor Immune Response. Front Pharmacol *10*, 1152. 10.3389/fphar.2019.01152.

29. Harvey, B.T., Fu, X., Li, L., Neupane, K.R., Anand, N., Kolesar, J.M., and Richards, C.I. (2022). Dendritic Cell Membrane-Derived Nanovesicles for Targeted T Cell Activation. ACS Omega *7*, 46222-46233. 10.1021/acsomega.2c04420.

30. Liu, C., Liu, X., Xiang, X., Pang, X., Chen, S., Zhang, Y., Ren, E., Zhang, L., Liu, X., Lv, P., et al. (2022). A nanovaccine for antigen self-presentation and immunosuppression reversal as a personalized cancer immunotherapy strategy. Nat Nanotechnol *17*, 531-540. 10.1038/s41565-022-01098-0.

31. Fearnley, D.B., Whyte, L.F., Carnoutsos, S.A., Cook, A.H., and Hart, D.N. (1999). Monitoring human blood dendritic cell numbers in normal individuals and in stem cell transplantation. Blood *93*, 728-736.

32. Derdak, S.V., Kueng, H.J., Leb, V.M., Neunkirchner, A., Schmetterer, K.G., Bielek, E., Majdic, O., Knapp, W., Seed, B., and Pickl, W.F. (2006). Direct stimulation of T lymphocytes by immunosomes: virus-like particles decorated with T cell receptor/CD3 ligands plus costimulatory molecules. Proc Natl Acad Sci U S A *103*, 13144-13149. 10.1073/pnas.0602283103.

33. Buzas, E.I. (2023). The roles of extracellular vesicles in the immune system. Nat Rev Immunol *23*, 236-250. 10.1038/s41577-022-00763-8.

34. Askenase, P. (2020). Artificial nanoparticles are not as good as the real thing. Nature *582*, S5-S5. 10.1038/d41586-020-01764-0.

35. Raposo, G., Nijman, H.W., Stoorvogel, W., Liejendekker, R., Harding, C.V., Melief, C.J., and Geuze, H.J. (1996). B lymphocytes secrete antigen-presenting vesicles. J Exp Med *183*, 1161-1172. 10.1084/jem.183.3.1161.

36. Kordelas, L., Rebmann, V., Ludwig, A.K., Radtke, S., Ruesing, J., Doeppner, T.R., Epple, M., Horn, P.A., Beelen, D.W., and Giebel, B. (2014). MSC-derived exosomes: a novel tool to treat therapy-refractory graft-versus-host disease. Leukemia *28*, 970-973. 10.1038/leu.2014.41.

37. Zhu, X., Badawi, M., Pomeroy, S., Sutaria, D.S., Xie, Z., Baek, A., Jiang, J., Elgamal, O.A., Mo, X., Perle, K., et al. (2017). Comprehensive toxicity and immunogenicity studies reveal minimal effects in mice following sustained dosing of extracellular vesicles derived from HEK293T cells. J Extracell Vesicles *6*, 1324730. 10.1080/20013078.2017.1324730.

38. Kamerkar, S., LeBleu, V.S., Sugimoto, H., Yang, S., Ruivo, C.F., Melo, S.A., Lee, J.J., and Kalluri, R. (2017). Exosomes facilitate therapeutic targeting of oncogenic KRAS in pancreatic cancer. Nature *546*, 498-503. 10.1038/nature22341.

39. Shi, X., Cheng, Q., Hou, T., Han, M., Smbatyan, G., Lang, J.E., Epstein, A.L., Lenz, H.J., and Zhang, Y. (2020). Genetically Engineered Cell-Derived Nanoparticles for Targeted Breast Cancer Immunotherapy. Mol Ther *28*, 536-547. 10.1016/j.ymthe.2019.11.020.

40. Muskan, M., Abeysinghe, P., Cecchin, R., Branscome, H., Morris, K.V., and Kashanchi, F. (2024). Therapeutic potential of RNA-enriched extracellular vesicles: The next generation in RNA delivery via biogenic nanoparticles. Mol Ther *32*, 2939-2949. 10.1016/j.ymthe.2024.02.025.

41. Shirmast, P., Shahri, M.A., Brent, A., Idris, A., and McMillan, N.A.J. (2024). Delivering therapeutic RNA into the brain using extracellular vesicles. Mol Ther Nucleic Acids *35*, 102373. 10.1016/j.omtn.2024.102373.

42. Kalluri, R., and LeBleu, V.S. (2020). The biology, function, and biomedical applications of exosomes. Science *367*. 10.1126/science.aau6977.

43. Wiklander, O.P.B., Mamand, D.R., Mohammad, D.K., Zheng, W., Jawad Wiklander, R., Sych, T., Zickler, A.M., Liang, X., Sharma, H., Lavado, A., et al. (2024). Antibody-displaying extracellular vesicles for targeted cancer therapy. Nat Biomed Eng *8*, 1453-1468. 10.1038/s41551-024-01214-6.

44. Cheng, L., and Hill, A.F. (2022). Therapeutically harnessing extracellular vesicles. Nat Rev Drug Discov *21*, 379-399. 10.1038/s41573-022-00410-w.

45. Carney, R.P., Mizenko, R.R., Bozkurt, B.T., Lowe, N., Henson, T., Arizzi, A., Wang, A., Tan, C., and George, S.C. (2025). Harnessing extracellular vesicle heterogeneity for diagnostic and therapeutic applications. Nat Nanotechnol *20*, 14-25. 10.1038/s41565-024-01774-3.

46. Sun, M.K., Passaro, A.P., Latchoumane, C.F., Spellicy, S.E., Bowler, M., Goeden, M., Martin, W.J., Holmes, P.V., Stice, S.L., and Karumbaiah, L. (2020). Extracellular Vesicles Mediate Neuroprotection and Functional Recovery after Traumatic Brain Injury. J Neurotrauma *37*, 1358-1369. 10.1089/neu.2019.6443.

47. Hoffmann, M.A.G., Yang, Z., Huey-Tubman, K.E., Cohen, A.A., Gnanapragasam, P.N.P., Nakatomi, L.M., Storm, K.N., Moon, W.J., Lin, P.J.C., West, A.P., Jr., and Bjorkman, P.J. (2023). ESCRT recruitment to SARS-CoV-2 spike induces virus-like particles that improve mRNA vaccines. Cell *186*, 2380-2391.e2389. 10.1016/j.cell.2023.04.024.

48. Chour, W. (2021). Molecular Technologies for Antigen-Based Immunity. Bioengineering (California Institute of Technology).

49. Chour, W., Choi, J., Xie, J., Chaffee, M.E., Schmitt, T.M., Finton, K., DeLucia, D.C., Xu, A.M., Su, Y., Chen, D.G., et al. (2023). Large libraries of single-chain trimer peptide-MHCs enable antigen-specific CD8+ T cell discovery and analysis. Commun Biol *6*, 528. 10.1038/s42003-023-04899-8.

50. Hein, Z., Uchtenhagen, H., Abualrous, E.T., Saini, S.K., Janßen, L., Van Hateren, A., Wiek, C., Hanenberg, H., Momburg, F., Achour, A., et al. (2014). Peptide-

independent stabilization of MHC class I molecules breaches cellular quality control. J Cell Sci *127*, 2885-2897. 10.1242/jcs.145334.

51. Mitaksov, V., Truscott, S.M., Lybarger, L., Connolly, J.M., Hansen, T.H., and Fremont, D.H. (2007). Structural engineering of pMHC reagents for T cell vaccines and diagnostics. Chem Biol *14*, 909-922. 10.1016/j.chembiol.2007.07.010.
52. Thayer, W.P., Dao, C.T., Ignatowicz, L., and Jensen, P.E. (2003). A novel single chain I-A(b) molecule can stimulate and stain antigen-specific T cells. Mol Immunol *39*, 861-870. 10.1016/s0161-5890(03)00010-5.
53. Diorio, C., Teachey, D.T., and Grupp, S.A. (2025). Allogeneic chimeric antigen receptor cell therapies for cancer: progress made and remaining roadblocks. Nat Rev Clin Oncol *22*, 10-27. 10.1038/s41571-024-00959-y.
54. Brudno, J.N., and Kochenderfer, J.N. (2024). Current understanding and management of CAR T cell-associated toxicities. Nat Rev Clin Oncol *21*, 501-521. 10.1038/s41571-024-00903-0.
55. Mulvey, A., Trueb, L., Coukos, G., and Arber, C. (2025). Novel strategies to manage CAR-T cell toxicity. Nat Rev Drug Discov. 10.1038/s41573-024-01100-5.
56. Wiklander, O.P.B., Brennan, M., Lötvall, J., Breakefield, X.O., and El Andaloussi, S. (2019). Advances in therapeutic applications of extracellular vesicles. Sci Transl Med *11*. 10.1126/scitranslmed.aav8521.
57. Uslu, U., and June, C.H. (2025). Beyond the blood: expanding CAR T cell therapy to solid tumors. Nat Biotechnol *43*, 506-515. 10.1038/s41587-024-02446-2.
58. Paul, S., Konig, M.F., Pardoll, D.M., Bettegowda, C., Papadopoulos, N., Wright, K.M., Gabelli, S.B., Ho, M., van Elsas, A., and Zhou, S. (2024). Cancer therapy with antibodies. Nat Rev Cancer *24*, 399-426. 10.1038/s41568-024-00690-x.
59. Fenis, A., Demaria, O., Gauthier, L., Vivier, E., and Narni-Mancinelli, E. (2024). New immune cell engagers for cancer immunotherapy. Nat Rev Immunol *24*, 471-486. 10.1038/s41577-023-00982-7.
60. Grakoui, A., Bromley, S.K., Sumen, C., Davis, M.M., Shaw, A.S., Allen, P.M., and Dustin, M.L. (1999). The immunological synapse: a molecular machine controlling T cell activation. Science *285*, 221-227. 10.1126/science.285.5425.221.

61. Choi, V.W., McCarty, D.M., and Samulski, R.J. (2006). Host cell DNA repair pathways in adeno-associated viral genome processing. J Virol *80*, 10346-10356. 10.1128/jvi.00841-06.

62. Berns, K.I., and Bohenzky, R.A. (1987). Adeno-associated viruses: an update. Adv Virus Res *32*, 243-306. 10.1016/s0065-3527(08)60479-0.

63. Issa, S.S., Shaimardanova, A.A., Solovyeva, V.V., and Rizvanov, A.A. (2023). Various AAV Serotypes and Their Applications in Gene Therapy: An Overview. Cells *12*. 10.3390/cells12050785.

64. Goertsen, D., Flytzanis, N.C., Goeden, N., Chuapoco, M.R., Cummins, A., Chen, Y., Fan, Y., Zhang, Q., Sharma, J., Duan, Y., et al. (2022). AAV capsid variants with brain-wide transgene expression and decreased liver targeting after intravenous delivery in mouse and marmoset. Nat Neurosci *25*, 106-115. 10.1038/s41593-021-00969-4.

65. Tabebordbar, M., Lagerborg, K.A., Stanton, A., King, E.M., Ye, S., Tellez, L., Krunnfusz, A., Tavakoli, S., Widrick, J.J., Messemer, K.A., et al. (2021). Directed evolution of a family of AAV capsid variants enabling potent muscle-directed gene delivery across species. Cell *184*, 4919-4938.e4922. 10.1016/j.cell.2021.08.028.

66. Lin, R., Zhou, Y., Yan, T., Wang, R., Li, H., Wu, Z., Zhang, X., Zhou, X., Zhao, F., Zhang, L., et al. (2022). Directed evolution of adeno-associated virus for efficient gene delivery to microglia. Nat Methods *19*, 976-985. 10.1038/s41592-022-01547-7.

67. Ghauri, M.S., and Ou, L. (2023). AAV Engineering for Improving Tropism to the Central Nervous System. Biology (Basel) *12*. 10.3390/biology12020186.

68. Au, H.K.E., Isalan, M., and Mielcarek, M. (2021). Gene Therapy Advances: A Meta-Analysis of AAV Usage in Clinical Settings. Front Med (Lausanne) *8*, 809118. 10.3389/fmed.2021.809118.

69. Klamroth, R., Hayes, G., Andreeva, T., Gregg, K., Suzuki, T., Mitha, I.H., Hardesty, B., Shima, M., Pollock, T., Slev, P., et al. (2022). Global Seroprevalence of Pre-existing Immunity Against AAV5 and Other AAV Serotypes in People with Hemophilia A. Hum Gene Ther *33*, 432-441. 10.1089/hum.2021.287.

70. Arjomandnejad, M., Dasgupta, I., Flotte, T.R., and Keeler, A.M. (2023). Immunogenicity of Recombinant Adeno-Associated Virus (AAV) Vectors for Gene Transfer. BioDrugs *37*, 311-329. 10.1007/s40259-023-00585-7.

71. Duan, D. (2023). Lethal immunotoxicity in high-dose systemic AAV therapy. Mol Ther *31*, 3123-3126. 10.1016/j.ymthe.2023.10.015.

72. Mingozzi, F., Chen, Y., Edmonson, S.C., Zhou, S., Thurlings, R.M., Tak, P.P., High, K.A., and Vervoordeldonk, M.J. (2013). Prevalence and pharmacological modulation of humoral immunity to AAV vectors in gene transfer to synovial tissue. Gene Ther *20*, 417-424. 10.1038/gt.2012.55.

73. Xiang, Z., Kuranda, K., Quinn, W., Chekaoui, A., Ambrose, R., Hasanpourghai, M., Novikov, M., Newman, D., Cole, C., Zhou, X., et al. (2022). The Effect of Rapamycin and Ibrutinib on Antibody Responses to Adeno-Associated Virus Vector-Mediated Gene Transfer. Hum Gene Ther *33*, 614-624. 10.1089/hum.2021.258.

74. Bertin, B., Veron, P., Leborgne, C., Deschamps, J.Y., Moullec, S., Fromes, Y., Collaud, F., Boutin, S., Latournerie, V., van Wittenberghe, L., et al. (2020). Capsid-specific removal of circulating antibodies to adeno-associated virus vectors. Sci Rep *10*, 864. 10.1038/s41598-020-57893-z.

75. Lee, G.K., Maheshri, N., Kaspar, B., and Schaffer, D.V. (2005). PEG conjugation moderately protects adeno-associated viral vectors against antibody neutralization. Biotechnol Bioeng *92*, 24-34. 10.1002/bit.20562.

76. Hoang Thi, T.T., Pilkington, E.H., Nguyen, D.H., Lee, J.S., Park, K.D., and Truong, N.P. (2020). The Importance of Poly(ethylene glycol) Alternatives for Overcoming PEG Immunogenicity in Drug Delivery and Bioconjugation. Polymers (Basel) *12*. 10.3390/polym12020298.

77. Meliani, A., Boisgerault, F., Fitzpatrick, Z., Marmier, S., Leborgne, C., Collaud, F., Simon Sola, M., Charles, S., Ronzitti, G., Vignaud, A., et al. (2017). Enhanced liver gene transfer and evasion of preexisting humoral immunity with exosome-enveloped AAV vectors. Blood Adv *1*, 2019-2031. 10.1182/bloodadvances.2017010181.

78. Hudry, E., Martin, C., Gandhi, S., György, B., Scheffer, D.I., Mu, D., Merkel, S.F., Mingozzi, F., Fitzpatrick, Z., Dimant, H., et al. (2016). Exosome-associated AAV

vector as a robust and convenient neuroscience tool. Gene Ther *23*, 380-392. 10.1038/gt.2016.11.

79. György, B., Fitzpatrick, Z., Crommentuijn, M.H., Mu, D., and Maguire, C.A. (2014). Naturally enveloped AAV vectors for shielding neutralizing antibodies and robust gene delivery in vivo. Biomaterials *35*, 7598-7609. 10.1016/j.biomaterials.2014.05.032.

80. Collins, L.T., Beatty, W., Moyo, B., Alves-Bezerra, M., Hurley, A., Lagor, W., Bao, G., Ponnazhagan, S., McNally, R., Rome, L., and Curiel, D.T. (2023). Encapsulation of AAVs into protein vault nanoparticles as a novel solution to gene therapy's neutralizing antibody problem. bioRxiv, 2023.2011.2029.569229. 10.1101/2023.11.29.569229.

81. Bing, S.J., Seirup, M., Hoang, T.T., Najera, S.S., Britten, C., Warrington, S.L., Chu, S.L., and Mazor, R. (2024). Rational immunosilencing of a promiscuous T-cell epitope in the capsid of an adeno-associated virus. Nat Biomed Eng *8*, 193-200. 10.1038/s41551-023-01129-8.

82. Guidance for Industry: Immunogenicity Assessment for Therapeutic Protein Products. (2014). In O.o.C. DoDI, ed.

83. Bing, S.J., Warrington, S., and Mazor, R. (2023). Low cross reactivity between wild type and deamidated AAV can lead to false negative results in immune monitoring T-cell assays. Front Immunol *14*, 1211529. 10.3389/fimmu.2023.1211529.

84. Becker, M.W., Peters, L.D., Myint, T., Smurlick, D., Powell, A., Brusko, T.M., and Phelps, E.A. (2023). Immune engineered extracellular vesicles to modulate T cell activation in the context of type 1 diabetes. Sci Adv *9*, eadg1082. 10.1126/sciadv.adg1082.

85. Chen, J.Y., Agrawal, S., Yi, H.P., Vallejo, D., Agrawal, A., and Lee, A.P. (2023). Cell-Sized Lipid Vesicles as Artificial Antigen-Presenting Cells for Antigen-Specific T Cell Activation. Adv Healthc Mater *12*, e2203163. 10.1002/adhm.202203163.

86. Tsai, S., Shameli, A., Yamanouchi, J., Clemente-Casares, X., Wang, J., Serra, P., Yang, Y., Medarova, Z., Moore, A., and Santamaria, P. (2010). Reversal of

autoimmunity by boosting memory-like autoregulatory T cells. Immunity *32*, 568-580. 10.1016/j.immuni.2010.03.015.

87. Wauters, A.C., Scheerstra, J.F., Vermeijlen, I.G., Hammink, R., Schluck, M., Woythe, L., Wu, H., Albertazzi, L., Figdor, C.G., Tel, J., et al. (2022). Artificial Antigen-Presenting Cell Topology Dictates T Cell Activation. ACS Nano *16*, 15072-15085. 10.1021/acsnano.2c06211.

88. Sunshine, J.C., Perica, K., Schneck, J.P., and Green, J.J. (2014). Particle shape dependence of CD8+ T cell activation by artificial antigen presenting cells. Biomaterials *35*, 269-277. 10.1016/j.biomaterials.2013.09.050.

89. Viola, A., Schroeder, S., Sakakibara, Y., and Lanzavecchia, A. (1999). T lymphocyte costimulation mediated by reorganization of membrane microdomains. Science *283*, 680-682. 10.1126/science.283.5402.680.

90. Lee, H.H., Elia, N., Ghirlando, R., Lippincott-Schwartz, J., and Hurley, J.H. (2008). Midbody targeting of the ESCRT machinery by a noncanonical coiled coil in CEP55. Science *322*, 576-580. 10.1126/science.1162042.

91. Yu, Y.Y., Netuschil, N., Lybarger, L., Connolly, J.M., and Hansen, T.H. (2002). Cutting edge: single-chain trimers of MHC class I molecules form stable structures that potently stimulate antigen-specific T cells and B cells. J Immunol *168*, 3145-3149. 10.4049/jimmunol.168.7.3145.

92. Arevalo, M.T., Wong, T.M., and Ross, T.M. (2016). Expression and Purification of Virus-like Particles for Vaccination. J Vis Exp. 10.3791/54041.

93. Jung, M.K., and Mun, J.Y. (2018). Sample Preparation and Imaging of Exosomes by Transmission Electron Microscopy. J Vis Exp. 10.3791/56482.

94. Renner, C., Wadle, A., Cerundolo, V., Stewart-Jones, G., and Jones, Y.E. (2010) High Affinity T-Cell Receptor-Like NY-ESO-1 Peptide Antibodies, Methods, And Uses Thereof. WIPO (PCT) patent PCT/IB2010/000597.

95. Cheng, Q., Dai, Z., Smbatyan, G., Epstein, A.L., Lenz, H.J., and Zhang, Y. (2022). Eliciting anti-cancer immunity by genetically engineered multifunctional exosomes. Mol Ther *30*, 3066-3077. 10.1016/j.ymthe.2022.06.013.

96. Dellgren, C., Nehlin, J.O., and Barington, T. (2015). Cell surface expression level variation between two common Human Leukocyte Antigen alleles, HLA-A2 and HLA-B8, is dependent on the structure of the C terminal part of the alpha 2 and the alpha 3 domains. PLoS One *10*, e0135385. 10.1371/journal.pone.0135385.

97. Uger, R.A., Chan, S.M., and Barber, B.H. (1999). Covalent linkage to beta2-microglobulin enhances the MHC stability and antigenicity of suboptimal CTL epitopes. J Immunol *162*, 6024-6028.

98. Fahnestock, M.L., Tamir, I., Narhi, L., and Bjorkman, P.J. (1992). Thermal stability comparison of purified empty and peptide-filled forms of a class I MHC molecule. Science *258*, 1658-1662. 10.1126/science.1360705.

99. Steć, A., Targońska, M., Karkosińska, E., Słowik, M., Płoska, A., Kalinowski, L., Wielgomas, B., Waleron, K., Jasiecki, J., and Dziomba, S. (2023). Protein overproduction alters exosome secretion in Chinese hamster ovary cells. Anal Bioanal Chem *415*, 3167-3176. 10.1007/s00216-023-04725-4.

100. Ge, Q., Stone, J.D., Thompson, M.T., Cochran, J.R., Rushe, M., Eisen, H.N., Chen, J., and Stern, L.J. (2002). Soluble peptide-MHC monomers cause activation of CD8+ T cells through transfer of the peptide to T cell MHC molecules. Proc Natl Acad Sci U S A *99*, 13729-13734. 10.1073/pnas.212515299.

101. Singha, S., Shao, K., Yang, Y., Clemente-Casares, X., Solé, P., Clemente, A., Blanco, J., Dai, Q., Song, F., Liu, S.W., et al. (2017). Peptide-MHC-based nanomedicines for autoimmunity function as T-cell receptor microclustering devices. Nat Nanotechnol *12*, 701-710. 10.1038/nnano.2017.56.

102. Clemente-Casares, X., Blanco, J., Ambalavanan, P., Yamanouchi, J., Singha, S., Fandos, C., Tsai, S., Wang, J., Garabatos, N., Izquierdo, C., et al. (2016). Expanding antigen-specific regulatory networks to treat autoimmunity. Nature *530*, 434-440. 10.1038/nature16962.

103. Rudensky, Y., Preston-Hurlburt, P., Hong, S.C., Barlow, A., and Janeway, C.A., Jr. (1991). Sequence analysis of peptides bound to MHC class II molecules. Nature *353*, 622-627. 10.1038/353622a0.

104. Samanta, D., Mukherjee, G., Ramagopal, U.A., Chaparro, R.J., Nathenson, S.G., DiLorenzo, T.P., and Almo, S.C. (2011). Structural and functional characterization of a single-chain peptide-MHC molecule that modulates both naive and activated CD8+ T cells. Proc Natl Acad Sci U S A *108*, 13682-13687. 10.1073/pnas.1110971108.

105. Krienke, C., Kolb, L., Diken, E., Streuber, M., Kirchhoff, S., Bukur, T., Akilli-Öztürk, Ö., Kranz, L.M., Berger, H., Petschenka, J., et al. (2021). A noninflammatory mRNA vaccine for treatment of experimental autoimmune encephalomyelitis. Science *371*, 145-153. 10.1126/science.aay3638.

106. Pear, W.S., Nolan, G.P., Scott, M.L., and Baltimore, D. (1993). Production of high-titer helper-free retroviruses by transient transfection. Proc Natl Acad Sci U S A *90*, 8392-8396. 10.1073/pnas.90.18.8392.

107. Nesterenko, P.A., McLaughlin, J., Tsai, B.L., Burton Sojo, G., Cheng, D., Zhao, D., Mao, Z., Bangayan, N.J., Obusan, M.B., Su, Y., et al. (2021). HLA-A(∗)02:01 restricted T cell receptors against the highly conserved SARS-CoV-2 polymerase cross-react with human coronaviruses. Cell Rep *37*, 110167. 10.1016/j.celrep.2021.110167.

108. Maude, S.L., Frey, N., Shaw, P.A., Aplenc, R., Barrett, D.M., Bunin, N.J., Chew, A., Gonzalez, V.E., Zheng, Z., Lacey, S.F., et al. (2014). Chimeric Antigen Receptor T Cells for Sustained Remissions in Leukemia. New England Journal of Medicine *371*, 1507-1517. doi:10.1056/NEJMoa1407222.

109. Schuster, S.J., Svoboda, J., Chong, E.A., Nasta, S.D., Mato, A.R., Anak, Ö., Brogdon, J.L., Pruteanu-Malinici, I., Bhoj, V., Landsburg, D., et al. (2017). Chimeric Antigen Receptor T Cells in Refractory B-Cell Lymphomas. New England Journal of Medicine *377*, 2545-2554. doi:10.1056/NEJMoa1708566.

110. Eckman, N., Nejatfard, A., Cavet, R., Grosskopf, A.K., and Appel, E.A. (2024). Biomaterials to enhance adoptive cell therapy. Nature Reviews Bioengineering *2*, 408-424. 10.1038/s44222-023-00148-z.

111. Lee, D.W., Kochenderfer, J.N., Stetler-Stevenson, M., Cui, Y.K., Delbrook, C., Feldman, S.A., Fry, T.J., Orentas, R., Sabatino, M., Shah, N.N., et al. (2015). T cells

expressing CD19 chimeric antigen receptors for acute lymphoblastic leukaemia in children and young adults: a phase 1 dose-escalation trial. The Lancet *385*, 517-528. 10.1016/S0140-6736(14)61403-3.

112. Porter, D.L., Levine, B.L., Kalos, M., Bagg, A., and June, C.H. (2011). Chimeric Antigen Receptor–Modified T Cells in Chronic Lymphoid Leukemia. New England Journal of Medicine *365*, 725-733. doi:10.1056/NEJMoa1103849.

113. June, C.H., Riddell, S.R., and Schumacher, T.N. (2015). Adoptive cellular therapy: a race to the finish line. Sci Transl Med *7*, 280ps287. 10.1126/scitranslmed.aaa3643.

114. Qi, Q., Liu, Y., Cheng, Y., Glanville, J., Zhang, D., Lee, J.Y., Olshen, R.A., Weyand, C.M., Boyd, S.D., and Goronzy, J.J. (2014). Diversity and clonal selection in the human T-cell repertoire. Proc Natl Acad Sci U S A *111*, 13139-13144. 10.1073/pnas.1409155111.

115. Eggermont, L.J., Paulis, L.E., Tel, J., and Figdor, C.G. (2014). Towards efficient cancer immunotherapy: advances in developing artificial antigen-presenting cells. Trends Biotechnol *32*, 456-465. 10.1016/j.tibtech.2014.06.007.

116. Turtle, C.J., and Riddell, S.R. (2010). Artificial antigen-presenting cells for use in adoptive immunotherapy. Cancer J *16*, 374-381. 10.1097/PPO.0b013e3181eb33a6.

117. Davis, M.M., Altman, J.D., and Newell, E.W. (2011). Interrogating the repertoire: broadening the scope of peptide-MHC multimer analysis. Nat Rev Immunol *11*, 551-558. 10.1038/nri3020.

118. Koo, D., Mao, Z., Dimatteo, R., Noguchi, M., Tsubamoto, N., McLaughlin, J., Tran, W., Lee, S., Cheng, D., de Rutte, J., et al. (2024). Defining T cell receptor repertoires using nanovial-based binding and functional screening. Proc Natl Acad Sci U S A *121*, e2320442121. 10.1073/pnas.2320442121.

119. de Rutte, J., Dimatteo, R., Archang, M.M., van Zee, M., Koo, D., Lee, S., Sharrow, A.C., Krohl, P.J., Mellody, M., Zhu, S., et al. (2022). Suspendable Hydrogel Nanovials for Massively Parallel Single-Cell Functional Analysis and Sorting. ACS Nano *16*, 7242-7257. 10.1021/acsnano.1c11420.

120. Abesekara, M.S., and Chau, Y. (2022). Recent advances in surface modification of micro- and nano-scale biomaterials with biological membranes and biomolecules. Front Bioeng Biotechnol *10*, 972790. 10.3389/fbioe.2022.972790.

121. Cheung, A.S., Zhang, D.K.Y., Koshy, S.T., and Mooney, D.J. (2018). Scaffolds that mimic antigen-presenting cells enable ex vivo expansion of primary T cells. Nat Biotechnol *36*, 160-169. 10.1038/nbt.4047.

122. Basu, S., Gohain, N., Kim, J., Trinh, H.V., Choe, M., Joyce, M.G., and Rao, M. (2023). Determination of Binding Affinity of Antibodies to HIV-1 Recombinant Envelope Glycoproteins, Pseudoviruses, Infectious Molecular Clones, and Cell-Expressed Trimeric gp160 Using Microscale Thermophoresis. Cells *13*. 10.3390/cells13010033.

123. Denisov, I.G., and Sligar, S.G. (2016). Nanodiscs for structural and functional studies of membrane proteins. Nat Struct Mol Biol *23*, 481-486. 10.1038/nsmb.3195.

124. Chen, L., Mou, S., Li, F., Zeng, Y., Sun, Y., Horch, R.E., Wei, W., Wang, Z., and Sun, J. (2019). Self-Assembled Human Adipose-Derived Stem Cell-Derived Extracellular Vesicle-Functionalized Biotin-Doped Polypyrrole Titanium with Long-Term Stability and Potential Osteoinductive Ability. ACS Appl Mater Interfaces *11*, 46183-46196. 10.1021/acsami.9b17015.

125. Antich-Rosselló, M., Forteza-Genestra, M.A., Calvo, J., Gayà, A., Monjo, M., and Ramis, J.M. (2021). Platelet-Derived Extracellular Vesicle Functionalization of Ti Implants. J Vis Exp. 10.3791/62781.

126. Pansani, T.N., Phan, T.H., Lei, Q., Kondyurin, A., Kalionis, B., and Chrzanowski, W. (2021). Extracellular-Vesicle-Based Coatings Enhance Bioactivity of Titanium Implants-SurfEV. Nanomaterials (Basel) *11*. 10.3390/nano11061445.

127. Shao, M., Lopes, D., Lopes, J., Yousefiasl, S., Macário-Soares, A., Peixoto, D., Ferreira-Faria, I., Veiga, F., Conde, J., Huang, Y., et al. (2023). Exosome membrane-coated nanosystems: Exploring biomedical applications in cancer diagnosis and therapy. Matter *6*, 761-799. 10.1016/j.matt.2023.01.012.

128. Jung, H., Jang, H.E., Kang, Y.Y., Song, J., and Mok, H. (2019). PLGA Microspheres Coated with Cancer Cell-Derived Vesicles for Improved Internalization into

Antigen-Presenting Cells and Immune Stimulation. Bioconjug Chem *30*, 1690-1701. 10.1021/acs.bioconjchem.9b00240.

129. Han, Z., Lv, W., Li, Y., Chang, J., Zhang, W., Liu, C., and Sun, J. (2020). Improving Tumor Targeting of Exosomal Membrane-Coated Polymeric Nanoparticles by Conjugation with Aptamers. ACS Appl Bio Mater *3*, 2666-2673. 10.1021/acsabm.0c00181.

130. Ukrainskaya, V., Rubtsov, Y., Pershin, D., Podoplelova, N., Terekhov, S., Yaroshevich, I., Sokolova, A., Bagrov, D., Kulakovskaya, E., Shipunova, V., et al. (2021). Antigen-Specific Stimulation and Expansion of CAR-T Cells Using Membrane Vesicles as Target Cell Surrogates. Small *17*, e2102643. 10.1002/smll.202102643.

131. Charoenviriyakul, C., Takahashi, Y., Morishita, M., Matsumoto, A., Nishikawa, M., and Takakura, Y. (2017). Cell type-specific and common characteristics of exosomes derived from mouse cell lines: Yield, physicochemical properties, and pharmacokinetics. Eur J Pharm Sci *96*, 316-322. 10.1016/j.ejps.2016.10.009.

132. Ferguson, S.W., and Nguyen, J. (2016). Exosomes as therapeutics: The implications of molecular composition and exosomal heterogeneity. J Control Release *228*, 179-190. 10.1016/j.jconrel.2016.02.037.

133. Sprent, J. (2005). Direct stimulation of naïve T cells by antigen-presenting cell vesicles. Blood Cells Mol Dis *35*, 17-20. 10.1016/j.bcmd.2005.04.004.

134. Olson, B.A., Huey-Tubman, K.E., Mao, Z., Hoffmann, M.A.G., Murray, R.M., and Mayo, S.L. (2025). Recruiting ESCRT to single-chain heterotrimer peptide-MHCI releases antigen-presenting vesicles that stimulate T cells selectively. bioRxiv, 2025.2001.2017.633600. 10.1101/2025.01.17.633600.

135. Mo, L.H., Luo, X.Q., Yang, G., Liu, J.Q., Yang, L.T., Liu, Z.Q., Wang, S., Liu, D.B., Liu, Z.G., and Yang, P.C. (2021). Epithelial cell-derived CD83 restores immune tolerance in the airway mucosa by inducing regulatory T-cell differentiation. Immunology *163*, 310-322. 10.1111/imm.13317.

136. Zhang, L.Z., Yang, J.G., Chen, G.L., Xie, Q.H., Fu, Q.Y., Xia, H.F., Li, Y.C., Huang, J., Li, Y., Wu, M., et al. (2024). PD-1/CD80(+) small extracellular vesicles from

immunocytes induce cold tumours featured with enhanced adaptive immunosuppression. Nat Commun *15*, 3884. 10.1038/s41467-024-48200-9.

137. Yu, Z.L., Liu, J.Y., and Chen, G. (2022). Small extracellular vesicle PD-L1 in cancer: the knowns and unknowns. NPJ Precis Oncol *6*, 42. 10.1038/s41698-022-00287-3.

138. Chen, G., Huang, A.C., Zhang, W., Zhang, G., Wu, M., Xu, W., Yu, Z., Yang, J., Wang, B., Sun, H., et al. (2018). Exosomal PD-L1 contributes to immunosuppression and is associated with anti-PD-1 response. Nature *560*, 382-386. 10.1038/s41586-018-0392-8.

139. Lees, R., Tempest, R., Law, A., Aubert, D., Davies, O.G., Williams, S., Peake, N., and Peacock, B. (2022). Single Extracellular Vesicle Transmembrane Protein Characterization by Nano-Flow Cytometry. J Vis Exp. 10.3791/64020.

140. Robbins, P.F., Li, Y.F., El-Gamil, M., Zhao, Y., Wargo, J.A., Zheng, Z., Xu, H., Morgan, R.A., Feldman, S.A., Johnson, L.A., et al. (2008). Single and dual amino acid substitutions in TCR CDRs can enhance antigen-specific T cell functions. J Immunol *180*, 6116-6131. 10.4049/jimmunol.180.9.6116.

141. Bethune, M.T., Li, X.H., Yu, J., McLaughlin, J., Cheng, D., Mathis, C., Moreno, B.H., Woods, K., Knights, A.J., Garcia-Diaz, A., et al. (2018). Isolation and characterization of NY-ESO-1-specific T cell receptors restricted on various MHC molecules. Proc Natl Acad Sci U S A *115*, E10702-e10711. 10.1073/pnas.1810653115.

142. Held, G., Matsuo, M., Epel, M., Gnjatic, S., Ritter, G., Lee, S.Y., Tai, T.Y., Cohen, C.J., Old, L.J., Pfreundschuh, M., et al. (2004). Dissecting cytotoxic T cell responses towards the NY-ESO-1 protein by peptide/MHC-specific antibody fragments. Eur J Immunol *34*, 2919-2929. 10.1002/eji.200425297.

143. Stewart-Jones, G., Wadle, A., Hombach, A., Shenderov, E., Held, G., Fischer, E., Kleber, S., Nuber, N., Stenner-Liewen, F., Bauer, S., et al. (2009). Rational development of high-affinity T-cell receptor-like antibodies. Proc Natl Acad Sci U S A *106*, 5784-5788. 10.1073/pnas.0901425106.

144. Lanier, L.L., O'Fallon, S., Somoza, C., Phillips, J.H., Linsley, P.S., Okumura, K., Ito, D., and Azuma, M. (1995). CD80 (B7) and CD86 (B70) provide similar

costimulatory signals for T cell proliferation, cytokine production, and generation of CTL. J Immunol *154*, 97-105.

145. Ghosh, R., Narasanna, A., Wang, S.E., Liu, S., Chakrabarty, A., Balko, J.M., González-Angulo, A.M., Mills, G.B., Penuel, E., Winslow, J., et al. (2011). Trastuzumab has preferential activity against breast cancers driven by HER2 homodimers. Cancer Res *71*, 1871-1882. 10.1158/0008-5472.Can-10-1872.

146. Gad, A.Z., Morris, J.S., Godret-Miertschin, L., Montalvo, M.J., Kerr, S.S., Berger, H., Lee, J.C.H., Saadeldin, A.M., Abu-Arja, M.H., Xu, S., et al. (2025). Molecular dynamics at immune synapse lipid rafts influence the cytolytic behavior of CAR T cells. Sci Adv *11*, eadq8114. 10.1126/sciadv.adq8114.

147. Zhang, W., Zhong, W., Wang, B., Yang, J., Yang, J., Yu, Z., Qin, Z., Shi, A., Xu, W., Zheng, C., et al. (2022). ICAM-1-mediated adhesion is a prerequisite for exosome-induced T cell suppression. Developmental Cell *57*, 329-343.e327. 10.1016/j.devcel.2022.01.002.

148. Hassan, R., Butler, M., O'Cearbhaill, R.E., Oh, D.Y., Johnson, M., Zikaras, K., Smalley, M., Ross, M., Tanyi, J.L., Ghafoor, A., et al. (2023). Mesothelin-targeting T cell receptor fusion construct cell therapy in refractory solid tumors: phase 1/2 trial interim results. Nat Med *29*, 2099-2109. 10.1038/s41591-023-02452-y.

149. Li, X.N., Wang, F., Chen, K., Wu, Z., Zhang, R., Xiao, C., Zhao, F., Wang, D., Zhao, H., Ran, Y., and Qu, C. (2025). XCL1-secreting CEA CAR-T cells enhance endogenous CD8(+) T cell responses to tumor neoantigens to confer a long-term antitumor immunity. J Immunother Cancer *13*. 10.1136/jitc-2024-010581.

150. Narayan, V., Barber-Rotenberg, J.S., Jung, I.Y., Lacey, S.F., Rech, A.J., Davis, M.M., Hwang, W.T., Lal, P., Carpenter, E.L., Maude, S.L., et al. (2022). PSMA-targeting TGFβ-insensitive armored CAR T cells in metastatic castration-resistant prostate cancer: a phase 1 trial. Nat Med *28*, 724-734. 10.1038/s41591-022-01726-1.

151. Jiang, N., Saftics, A., Romano, E., Ghaeli, I., Resto, C., Robles, V., Das, S., Van Keuren-Jensen, K., Seewaldt, V.L., and Jovanovic-Talisman, T. (2024). Multiparametric profiling of HER2-enriched extracellular vesicles in breast cancer

using Single Extracellular VEsicle Nanoscopy. J Nanobiotechnology *22*, 589. 10.1186/s12951-024-02858-x.

152. Hickey, J.W., Vicente, F.P., Howard, G.P., Mao, H.Q., and Schneck, J.P. (2017). Biologically Inspired Design of Nanoparticle Artificial Antigen-Presenting Cells for Immunomodulation. Nano Lett *17*, 7045-7054. 10.1021/acs.nanolett.7b03734.

153. Cheng, R.Y., de Rutte, J., Ito, C.E.K., Ott, A.R., Bosler, L., Kuo, W.Y., Liang, J., Hall, B.E., Rawlings, D.J., Di Carlo, D., and James, R.G. (2023). SEC-seq: association of molecular signatures with antibody secretion in thousands of single human plasma cells. Nat Commun *14*, 3567. 10.1038/s41467-023-39367-8.

154. Langerman, J., Baghdasarian, S., Cheng, R.Y.-H., James, R.G., Plath, K., and Di Carlo, D. (2025). Linking single-cell transcriptomes with secretion using SEC-seq. Nature Protocols. 10.1038/s41596-024-01112-w.

155. Udani, S., Langerman, J., Koo, D., Baghdasarian, S., Cheng, B., Kang, S., Soemardy, C., de Rutte, J., Plath, K., and Di Carlo, D. (2024). Associating growth factor secretions and transcriptomes of single cells in nanovials using SEC-seq. Nature Nanotechnology *19*, 354-363. 10.1038/s41565-023-01560-7.

156. Koo, D., Cheng, X., Udani, S., Baghdasarian, S., Zhu, D., Li, J., Hall, B., Tsubamoto, N., Hu, S., Ko, J., et al. (2024). Optimizing cell therapy by sorting cells with high extracellular vesicle secretion. Nat Commun *15*, 4870. 10.1038/s41467-024-49123-1.

157. Keener, A.B. (2020). How extracellular vesicles can enhance drug delivery. Nature *582*, S14-S15. 10.1038/d41586-020-01769-9.

158. Eisenstein, M. (2020). Inside the stem-cell pharmaceutical factory. Nature *582*, S16-S18. 10.1038/d41586-020-01770-2.

159. Zhang, Y., Ge, T., Huang, M., Qin, Y., Liu, T., Mu, W., Wang, G., Jiang, L., Li, T., Zhao, L., and Wang, J. (2023). Extracellular Vesicles Expressing CD19 Antigen Improve Expansion and Efficacy of CD19-Targeted CAR-T Cells. Int J Nanomedicine *18*, 49-63. 10.2147/ijn.S390720.

160. Guo, Y., Wang, H., Liu, S., Zhang, X., Zhu, X., Huang, L., Zhong, W., Guan, L., Chen, Y., Xiao, M., et al. (2025). Engineered extracellular vesicles with DR5

agonistic scFvs simultaneously target tumor and immunosuppressive stromal cells. Science Advances *11*, eadp9009. doi:10.1126/sciadv.adp9009.

161. Wang, L., Qi, C., Cao, H., Zhang, Y., Liu, X., Qiu, L., Wang, H., Xu, L., Wu, Z., Liu, J., et al. (2023). Engineered Cytokine-Primed Extracellular Vesicles with High PD-L1 Expression Ameliorate Type 1 Diabetes. Small *19*, e2301019. 10.1002/smll.202301019.
162. Rodenko, B., Toebes, M., Hadrup, S.R., van Esch, W.J., Molenaar, A.M., Schumacher, T.N., and Ovaa, H. (2006). Generation of peptide-MHC class I complexes through UV-mediated ligand exchange. Nat Protoc *1*, 1120-1132. 10.1038/nprot.2006.121.
163. Wagar, L.E., Salahudeen, A., Constantz, C.M., Wendel, B.S., Lyons, M.M., Mallajosyula, V., Jatt, L.P., Adamska, J.Z., Blum, L.K., Gupta, N., et al. (2021). Modeling human adaptive immune responses with tonsil organoids. Nat Med *27*, 125-135. 10.1038/s41591-020-01145-0.
164. Jenkinson, E.J., and Owen, J.J. (1990). T-cell differentiation in thymus organ cultures. Semin Immunol *2*, 51-58.
165. Robinson, J.H., and Owen, J.J. (1977). Generation of T-cell function in organ culture of foetal mouse thymus. II. Mixed lymphocyte culture reactivity. Clin Exp Immunol *27*, 322-327.
166. Alanio, C., Lemaitre, F., Law, H.K., Hasan, M., and Albert, M.L. (2010). Enumeration of human antigen-specific naive CD8+ T cells reveals conserved precursor frequencies. Blood *115*, 3718-3725. 10.1182/blood-2009-10-251124.
167. Hall, M.J., Schwartzman, A., Zhang, J., and Liu, X. (2017). Ambulatory Surgery Data From Hospitals and Ambulatory Surgery Centers: United States, 2010. Natl Health Stat Report, 1-15.
168. Mullard, A. (2025). 2024 FDA approvals. Nat Rev Drug Discov *24*, 75-82. 10.1038/d41573-025-00001-5.
169. Möller, A., and Lobb, R.J. (2020). The evolving translational potential of small extracellular vesicles in cancer. Nat Rev Cancer *20*, 697-709. 10.1038/s41568-020-00299-w.

170. Alvarez-Erviti, L., Seow, Y., Yin, H., Betts, C., Lakhal, S., and Wood, M.J. (2011). Delivery of siRNA to the mouse brain by systemic injection of targeted exosomes. Nat Biotechnol *29*, 341-345. 10.1038/nbt.1807.

171. Lajoie, M.J., Boyken, S.E., Salter, A.I., Bruffey, J., Rajan, A., Langan, R.A., Olshefsky, A., Muhunthan, V., Bick, M.J., Gewe, M., et al. (2020). Designed protein logic to target cells with precise combinations of surface antigens. Science *369*, 1637-1643. 10.1126/science.aba6527.

172. Banaszek, A., Bumm, T.G.P., Nowotny, B., Geis, M., Jacob, K., Wölfl, M., Trebing, J., Kucka, K., Kouhestani, D., Gogishvili, T., et al. (2019). On-target restoration of a split T cell-engaging antibody for precision immunotherapy. Nat Commun *10*, 5387. 10.1038/s41467-019-13196-0.

173. Dickopf, S., Buldun, C., Vasic, V., Georges, G., Hage, C., Mayer, K., Forster, M., Wessels, U., Stubenrauch, K.G., Benz, J., et al. (2022). Prodrug-Activating Chain Exchange (PACE) converts targeted prodrug derivatives to functional bi- or multispecific antibodies. Biol Chem *403*, 495-508. 10.1515/hsz-2021-0401.

174. Geis, M., Nowotny, B., Bohn, M.D., Kouhestani, D., Einsele, H., Bumm, T., and Stuhler, G. (2021). Combinatorial targeting of multiple myeloma by complementing T cell engaging antibody fragments. Commun Biol *4*, 44. 10.1038/s42003-020-01558-0.

175. Kofoed, C., Erkalo, G., Tay, N.E.S., Ye, X., Lin, Y., and Muir, T.W. (2025). Programmable protein ligation on cell surfaces. Nature. 10.1038/s41586-025-09287-2.

176. 3D Tissue Models Mimic the Human Immune System to Inform Drug Development. (2023). https://www.amgen.com/stories/2023/02/3d-tissue-models-mimic-the-human-immune-system-to-inform-drug-development.

177. Mock, M., Edavettal, S., Langmead, C., and Russell, A. (2023). AI can help to speed up drug discovery - but only if we give it the right data. Nature *621*, 467-470. 10.1038/d41586-023-02896-9.

178. Chen, P., Liu, X., Gu, C., Zhong, P., Song, N., Li, M., Dai, Z., Fang, X., Liu, Z., Zhang, J., et al. (2022). A plant-derived natural photosynthetic system for improving cell anabolism. Nature *612*, 546-554. 10.1038/s41586-022-05499-y.

179. Banks, I.M. (2008). Use of Weapons, reprint Edition (Orbit).

180. Khullar, D. (2023). Burnout, Professionalism, and the Quality of US Health Care. JAMA Health Forum *4*, e230024. 10.1001/jamahealthforum.2023.0024.

181. Zhao, Z., and Zlokovic, B.V. (2020). Therapeutic TVs for Crossing Barriers in the Brain. Cell *182*, 267-269. 10.1016/j.cell.2020.06.041.

182. Sweeney, M.D., Zhao, Z., Montagne, A., Nelson, A.R., and Zlokovic, B.V. (2019). Blood-Brain Barrier: From Physiology to Disease and Back. Physiol Rev *99*, 21-78. 10.1152/physrev.00050.2017.

183. Banks, W.A. (2016). From blood-brain barrier to blood-brain interface: new opportunities for CNS drug delivery. Nat Rev Drug Discov *15*, 275-292. 10.1038/nrd.2015.21.

184. Pulgar, V.M. (2018). Transcytosis to Cross the Blood Brain Barrier, New Advancements and Challenges. Front Neurosci *12*, 1019. 10.3389/fnins.2018.01019.

185. Terstappen, G.C., Meyer, A.H., Bell, R.D., and Zhang, W. (2021). Strategies for delivering therapeutics across the blood-brain barrier. Nat Rev Drug Discov *20*, 362-383. 10.1038/s41573-021-00139-y.

186. Cho, C.F., Wolfe, J.M., Fadzen, C.M., Calligaris, D., Hornburg, K., Chiocca, E.A., Agar, N.Y.R., Pentelute, B.L., and Lawler, S.E. (2017). Blood-brain-barrier spheroids as an in vitro screening platform for brain-penetrating agents. Nat Commun *8*, 15623. 10.1038/ncomms15623.

187. Bergmann, S., Lawler, S.E., Qu, Y., Fadzen, C.M., Wolfe, J.M., Regan, M.S., Pentelute, B.L., Agar, N.Y.R., and Cho, C.F. (2018). Blood-brain-barrier organoids for investigating the permeability of CNS therapeutics. Nat Protoc *13*, 2827-2843. 10.1038/s41596-018-0066-x.

188. Moreira, R., Nóbrega, C., de Almeida, L.P., and Mendonça, L. (2024). Brain-targeted drug delivery - nanovesicles directed to specific brain cells by brain-targeting ligands. J Nanobiotechnology *22*, 260. 10.1186/s12951-024-02511-7.

189. Gao, J., Gunasekar, S., Xia, Z.J., Shalin, K., Jiang, C., Chen, H., Lee, D., Lee, S., Pisal, N.D., Luo, J.N., et al. (2024). Gene therapy for CNS disorders: modalities, delivery and translational challenges. Nat Rev Neurosci *25*, 553-572. 10.1038/s41583-024-00829-7.

190. Shay, T.F., Sullivan, E.E., Ding, X., Chen, X., Ravindra Kumar, S., Goertsen, D., Brown, D., Crosby, A., Vielmetter, J., Borsos, M., et al. (2023). Primate-conserved carbonic anhydrase IV and murine-restricted LY6C1 enable blood-brain barrier crossing by engineered viral vectors. Sci Adv *9*, eadg6618. 10.1126/sciadv.adg6618.

191. Yom-Tov, N., Guy, R., and Offen, D. (2022). Extracellular vesicles over adeno-associated viruses: Advantages and limitations as drug delivery platforms in precision medicine. Adv Drug Deliv Rev *190*, 114535. 10.1016/j.addr.2022.114535.

192. Gurung, S., Perocheau, D., Touramanidou, L., and Baruteau, J. (2021). The exosome journey: from biogenesis to uptake and intracellular signalling. Cell Commun Signal *19*, 47. 10.1186/s12964-021-00730-1.

193. Dietz, L., Oberländer, J., Mateos-Maroto, A., Schunke, J., Fichter, M., Krämer-Albers, E.M., Landfester, K., and Mailänder, V. (2023). Uptake of extracellular vesicles into immune cells is enhanced by the protein corona. J Extracell Vesicles *12*, e12399. 10.1002/jev2.12399.

194. Liam-Or, R., Faruqu, F.N., Walters, A., Han, S., Xu, L., Wang, J.T., Oberlaender, J., Sanchez-Fueyo, A., Lombardi, G., Dazzi, F., et al. (2024). Cellular uptake and in vivo distribution of mesenchymal-stem-cell-derived extracellular vesicles are protein corona dependent. Nat Nanotechnol *19*, 846-855. 10.1038/s41565-023-01585-y.

195. Alvarez, V.A., Ridenour, D.A., and Sabatini, B.L. (2006). Retraction of synapses and dendritic spines induced by off-target effects of RNA interference. J Neurosci *26*, 7820-7825. 10.1523/jneurosci.1957-06.2006.

196. Faure, M.P., Alonso, A., Nouel, D., Gaudriault, G., Dennis, M., Vincent, J.P., and Beaudet, A. (1995). Somatodendritic internalization and perinuclear targeting of neurotensin in the mammalian brain. J Neurosci *15*, 4140-4147. 10.1523/jneurosci.15-06-04140.1995.

197. Vita, N., Laurent, P., Lefort, S., Chalon, P., Dumont, X., Kaghad, M., Gully, D., Le Fur, G., Ferrara, P., and Caput, D. (1993). Cloning and expression of a complementary DNA encoding a high affinity human neurotensin receptor. FEBS Lett *317*, 139-142. 10.1016/0014-5793(93)81509-x.

198. Rädler, J., Gupta, D., Zickler, A., and Andaloussi, S.E. (2023). Exploiting the biogenesis of extracellular vesicles for bioengineering and therapeutic cargo loading. Mol Ther *31*, 1231-1250. 10.1016/j.ymthe.2023.02.013.

199. Hobor, F., Dallmann, A., Ball, N.J., Cicchini, C., Battistelli, C., Ogrodowicz, R.W., Christodoulou, E., Martin, S.R., Castello, A., Tripodi, M., et al. (2018). A cryptic RNA-binding domain mediates Syncrip recognition and exosomal partitioning of miRNA targets. Nat Commun *9*, 831. 10.1038/s41467-018-03182-3.

200. Zietzer, A., Hosen, M.R., Wang, H., Goody, P.R., Sylvester, M., Latz, E., Nickenig, G., Werner, N., and Jansen, F. (2020). The RNA-binding protein hnRNPU regulates the sorting of microRNA-30c-5p into large extracellular vesicles. J Extracell Vesicles *9*, 1786967. 10.1080/20013078.2020.1786967.

201. Villarroya-Beltri, C., Gutiérrez-Vázquez, C., Sánchez-Cabo, F., Pérez-Hernández, D., Vázquez, J., Martin-Cofreces, N., Martinez-Herrera, D.J., Pascual-Montano, A., Mittelbrunn, M., and Sánchez-Madrid, F. (2013). Sumoylated hnRNPA2B1 controls the sorting of miRNAs into exosomes through binding to specific motifs. Nat Commun *4*, 2980. 10.1038/ncomms3980.

202. Ma, L., Singh, J., and Schekman, R. (2023). Two RNA-binding proteins mediate the sorting of miR223 from mitochondria into exosomes. Elife *12*. 10.7554/eLife.85878.

203. Shurtleff, M.J., Temoche-Diaz, M.M., Karfilis, K.V., Ri, S., and Schekman, R. (2016). Y-box protein 1 is required to sort microRNAs into exosomes in cells and in a cell-free reaction. Elife *5*. 10.7554/eLife.19276.

204. Kossinova, O.A., Gopanenko, A.V., Tamkovich, S.N., Krasheninina, O.A., Tupikin, A.E., Kiseleva, E., Yanshina, D.D., Malygin, A.A., Ven'yaminova, A.G., Kabilov, M.R., and Karpova, G.G. (2017). Cytosolic YB-1 and NSUN2 are the only proteins recognizing specific motifs present in mRNAs enriched in exosomes. Biochim Biophys Acta Proteins Proteom *1865*, 664-673. 10.1016/j.bbapap.2017.03.010.

205. Shurtleff, M.J., Yao, J., Qin, Y., Nottingham, R.M., Temoche-Diaz, M.M., Schekman, R., and Lambowitz, A.M. (2017). Broad role for YBX1 in defining the small noncoding RNA composition of exosomes. Proc Natl Acad Sci U S A *114*, E8987-e8995. 10.1073/pnas.1712108114.

206. England, C.G., Ehlerding, E.B., and Cai, W. (2016). NanoLuc: A Small Luciferase Is Brightening Up the Field of Bioluminescence. Bioconjug Chem *27*, 1175-1187. 10.1021/acs.bioconjchem.6b00112.

207. Martinko, A.J., Simonds, E.F., Prasad, S., Ponce, A., Bracken, C.J., Wei, J., Wang, Y.H., Chow, T.L., Huang, Z., Evans, M.J., et al. (2022). Switchable assembly and function of antibody complexes in vivo using a small molecule. Proc Natl Acad Sci U S A *119*. 10.1073/pnas.2117402119.

208. Borcoman, E., Kanjanapan, Y., Champiat, S., Kato, S., Servois, V., Kurzrock, R., Goel, S., Bedard, P., and Le Tourneau, C. (2019). Novel patterns of response under immunotherapy. Ann Oncol *30*, 385-396. 10.1093/annonc/mdz003.

209. Westcott, P.M.K., Sacks, N.J., Schenkel, J.M., Ely, Z.A., Smith, O., Hauck, H., Jaeger, A.M., Zhang, D., Backlund, C.M., Beytagh, M.C., et al. (2021). Low neoantigen expression and poor T-cell priming underlie early immune escape in colorectal cancer. Nat Cancer *2*, 1071-1085. 10.1038/s43018-021-00247-z.

210. Pi, F., Binzel, D.W., Lee, T.J., Li, Z., Sun, M., Rychahou, P., Li, H., Haque, F., Wang, S., Croce, C.M., et al. (2018). Nanoparticle orientation to control RNA loading and ligand display on extracellular vesicles for cancer regression. Nat Nanotechnol *13*, 82-89. 10.1038/s41565-017-0012-z.

211. Wiklander, O.P.B., Brennan, M.Á., Lötvall, J., Breakefield, X.O., and EL Andaloussi, S. (2019). Advances in therapeutic applications of extracellular vesicles. Science Translational Medicine *11*, eaav8521. doi:10.1126/scitranslmed.aav8521.

212. Shackelford, S., Eastridge, B.J., and Spinella, P.C. (2020). Epidemiology of Prehospital and Hospital Traumatic Deaths from Life-Threatening Hemorrhage. In (Springer International Publishing), pp. 31-40. 10.1007/978-3-030-20820-2_2.

213. Eastridge, B.J., Mabry, R.L., Seguin, P., Cantrell, J., Tops, T., Uribe, P., Mallett, O., Zubko, T., Oetjen-Gerdes, L., Rasmussen, T.E., et al. (2012). Death on the battlefield

(2001-2011): implications for the future of combat casualty care. J Trauma Acute Care Surg *73*, S431-437. 10.1097/TA.0b013e3182755dcc.

214. Epstein, A., Lim, R., Johannigman, J., Fox, C.J., Inaba, K., Vercruysse, G.A., Thomas, R.W., Martin, M.J., Konstantyn, G., and Schwaitzberg, S.D. (2023). Putting Medical Boots on the Ground: Lessons from the War in Ukraine and Applications for Future Conflict with Near-Peer Adversaries. J Am Coll Surg *237*, 364-373. 10.1097/xcs.0000000000000707.

215. Hong, C., He, Y., Bowen, P.A., Belcher, A.M., Olsen, B.D., and Hammond, P.T. (2023). Engineering a Two-Component Hemostat for the Treatment of Internal Bleeding through Wound-Targeted Crosslinking. Adv Healthc Mater *12*, e2202756. 10.1002/adhm.202202756.

216. Sekhon, U.D.S., Swingle, K., Girish, A., Luc, N., de la Fuente, M., Alvikas, J., Haldeman, S., Hassoune, A., Shah, K., Kim, Y., et al. (2022). Platelet-mimicking procoagulant nanoparticles augment hemostasis in animal models of bleeding. Sci Transl Med *14*, eabb8975. 10.1126/scitranslmed.abb8975.

217. Nellenbach, K., Mihalko, E., Nandi, S., Koch, D.W., Shetty, J., Moretti, L., Sollinger, J., Moiseiwitsch, N., Sheridan, A., Pandit, S., et al. (2024). Ultrasoft platelet-like particles stop bleeding in rodent and porcine models of trauma. Sci Transl Med *16*, eadi4490. 10.1126/scitranslmed.adi4490.

218. Chan, L.W., Wang, X., Wei, H., Pozzo, L.D., White, N.J., and Pun, S.H. (2015). A synthetic fibrin cross-linking polymer for modulating clot properties and inducing hemostasis. Sci Transl Med *7*, 277ra229. 10.1126/scitranslmed.3010383.

219. Gao, Y., Sarode, A., Kokoroskos, N., Ukidve, A., Zhao, Z., Guo, S., Flaumenhaft, R., Gupta, A.S., Saillant, N., and Mitragotri, S. (2020). A polymer-based systemic hemostatic agent. Sci Adv *6*, eaba0588. 10.1126/sciadv.aba0588.

220. Yang, P.P., Zhang, K., He, P.P., Fan, Y., Gao, X.J., Gao, X., Chen, Z.M., Hou, D.Y., Li, Y., Yi, Y., et al. (2020). A biomimetic platelet based on assembling peptides initiates artificial coagulation. Sci Adv *6*, eaaz4107. 10.1126/sciadv.aaz4107.

221. Kuhn, B.J., Swanson, A., Cherupalla, A.S., Booth, L., Dickerson, W.M., Fitzpatrick, G.M., Alexander, W.A., and Moskowitz, K.A. (2024). Mechanisms of action of an

investigational new freeze-dried platelet-derived hemostatic product. J Thromb Haemost *22*, 686-699. 10.1016/j.jtha.2023.11.022.

222. Maisha, N., Kulkarni, C., Pandala, N., Zilberberg, R., Schaub, L., Neidert, L., Glaser, J., Cannon, J., Janeja, V., and Lavik, E.B. (2022). PEGylated Polyester Nanoparticles Trigger Adverse Events in a Large Animal Model of Trauma and in Naïve Animals: Understanding Cytokine and Cellular Correlations with These Events. ACS Nano *16*, 10566-10580. 10.1021/acsnano.2c01993.

223. Ding, Y.F., Huang, Q., Quan, X., Cheng, Q., Li, S., Zhao, Y., Mok, G.S.P., and Wang, R. (2022). Supramolecularly functionalized platelets for rapid control of hemorrhage. Acta Biomater *149*, 248-257. 10.1016/j.actbio.2022.07.007.

224. Cazes, N., Corcostegui, S.P., Lovi, S., Romary, E., Desrobert, V., Lidzborski, L., and Derkenne, C. (2024). Should soldiers take oral tranexamic acid before going into battle? J Trauma Acute Care Surg *97*, S24-s26. 10.1097/ta.0000000000004343.

225. Leung, J., Strong, C., Badior, K.E., Robertson, M., Wu, X., Meledeo, M.A., Kang, E., Paul, M., Sato, Y., Harashima, H., et al. (2023). Genetically engineered transfusable platelets using mRNA lipid nanoparticles. Sci Adv *9*, eadi0508. 10.1126/sciadv.adi0508.

226. Mini fat particles help to turn platelets into protein factories. (2023). Nature. 10.1038/d41586-023-03753-5.

227. Chen, H., Liu, D., Guo, J., Aditham, A., Zhou, Y., Tian, J., Luo, S., Ren, J., Hsu, A., Huang, J., et al. (2025). Branched chemically modified poly(A) tails enhance the translation capacity of mRNA. Nat Biotechnol *43*, 194-203. 10.1038/s41587-024-02174-7.

228. Martinko, A.J., Tran, H.L., Simonds, E.F., Cooke, A.L., Huang, Z., Raguveer, S., Agullet, J.P., Prasad, S., Going, C., Marshall, L., et al. (2023). A bioorthogonal antibody-based chemically-induced-dimerization switch for therapeutic application. bioRxiv, 2023.2004.2011.536272. 10.1101/2023.04.11.536272.

229. Wu, C.Y., Roybal, K.T., Puchner, E.M., Onuffer, J., and Lim, W.A. (2015). Remote control of therapeutic T cells through a small molecule-gated chimeric receptor. Science *350*, aab4077. 10.1126/science.aab4077.

230. Zajc, C.U., Dobersberger, M., Schaffner, I., Mlynek, G., Pühringer, D., Salzer, B., Djinović-Carugo, K., Steinberger, P., De Sousa Linhares, A., Yang, N.J., et al. (2020). A conformation-specific ON-switch for controlling CAR T cells with an orally available drug. Proc Natl Acad Sci U S A *117*, 14926-14935. 10.1073/pnas.1911154117.

231. Hill, Z.B., Martinko, A.J., Nguyen, D.P., and Wells, J.A. (2018). Human antibody-based chemically induced dimerizers for cell therapeutic applications. Nat Chem Biol *14*, 112-117. 10.1038/nchembio.2529.

232. Butler, F.K., Jr., Hagmann, J., and Butler, E.G. (1996). Tactical combat casualty care in special operations. Mil Med *161 Suppl*, 3-16. 10.1007/978-3-319-56780-8_1.

233. Clifford, C.C. (2004). Treating traumatic bleeding in a combat setting. Mil Med *169*, 8-10, 14. 10.7205/milmed.169.12s.8.

234. Alarhayem, A.Q., Myers, J.G., Dent, D., Liao, L., Muir, M., Mueller, D., Nicholson, S., Cestero, R., Johnson, M.C., Stewart, R., et al. (2016). Time is the enemy: Mortality in trauma patients with hemorrhage from torso injury occurs long before the "golden hour". Am J Surg *212*, 1101-1105. 10.1016/j.amjsurg.2016.08.018.

235. Butler, F.K., Jr., Holcomb, J.B., Shackelford, S.A., Barbabella, S., Bailey, J.A., Baker, J.B., Cap, A.P., Conklin, C.C., Cunningham, C.W., Davis, M.S., et al. (2018). Advanced Resuscitative Care in Tactical Combat Casualty Care: TCCC Guidelines Change 18-01:14 October 2018. J Spec Oper Med *18*, 37-55. 10.55460/yjb8-zc0y.

236. Shakur, H., Roberts, I., Bautista, R., Caballero, J., Coats, T., Dewan, Y., El-Sayed, H., Gogichaishvili, T., Gupta, S., Herrera, J., et al. (2010). Effects of tranexamic acid on death, vascular occlusive events, and blood transfusion in trauma patients with significant haemorrhage (CRASH-2): a randomised, placebo-controlled trial. Lancet *376*, 23-32. 10.1016/s0140-6736(10)60835-5.

237. collaborators, C.-t. (2019). Effects of tranexamic acid on death, disability, vascular occlusive events and other morbidities in patients with acute traumatic brain injury (CRASH-3): a randomised, placebo-controlled trial. Lancet *394*, 1713-1723. 10.1016/s0140-6736(19)32233-0.

238. Hong, S., Leroueil, P.R., Majoros, I.J., Orr, B.G., Baker, J.R., Jr., and Banaszak Holl, M.M. (2007). The binding avidity of a nanoparticle-based multivalent targeted drug delivery platform. Chem Biol *14*, 107-115. 10.1016/j.chembiol.2006.11.015.

239. Reulen, S.W., Dankers, P.Y., Bomans, P.H., Meijer, E.W., and Merkx, M. (2009). Collagen targeting using protein-functionalized micelles: the strength of multiple weak interactions. J Am Chem Soc *131*, 7304-7312. 10.1021/ja807723p.

240. Tassa, C., Duffner, J.L., Lewis, T.A., Weissleder, R., Schreiber, S.L., Koehler, A.N., and Shaw, S.Y. (2010). Binding affinity and kinetic analysis of targeted small molecule-modified nanoparticles. Bioconjug Chem *21*, 14-19. 10.1021/bc900438a.

241. Anselmo, A.C., Modery-Pawlowski, C.L., Menegatti, S., Kumar, S., Vogus, D.R., Tian, L.L., Chen, M., Squires, T.M., Sen Gupta, A., and Mitragotri, S. (2014). Platelet-like nanoparticles: mimicking shape, flexibility, and surface biology of platelets to target vascular injuries. ACS Nano *8*, 11243-11253. 10.1021/nn503732m.

242. Haji-Valizadeh, H., Modery-Pawlowski, C.L., and Sen Gupta, A. (2014). A factor VIII-derived peptide enables von Willebrand factor (VWF)-binding of artificial platelet nanoconstructs without interfering with VWF-adhesion of natural platelets. Nanoscale *6*, 4765-4773. 10.1039/c3nr06400j.

243. Sinauridze, E.I., Kireev, D.A., Popenko, N.Y., Pichugin, A.V., Panteleev, M.A., Krymskaya, O.V., and Ataullakhanov, F.I. (2007). Platelet microparticle membranes have 50- to 100-fold higher specific procoagulant activity than activated platelets. Thromb Haemost *97*, 425-434.

244. Scott, B., and Dara, M. (2017). The Russian Way of Warfare: A Primer. https://policycommons.net/artifacts/4828938/the-russian-way-of-warfare/.

245. Fazal, T.M. (2023). Ukraine's Military Medicine Is a Critical Advantage. Foreign Policy, 17-19.